SISSA
Scuola
Internazionale
Superiore di
Studi Avanzati

Neuroscience Area – PhD course in

Molecular Biology

Generation and validation of a preclinical model of hypermutated lung cancer to study ICB resistance and DC Therapy

Candidate:

Lucía Inés López Rodríguez

Advisor:

Dr. Federica Benvenuti, PhD

Academic Year 2021-22

Index

This is thesis is dedicated to my Grandparents

Abstract

Immune checkpoint inhibitors have emerged as a mainstay of treatment for NSCLC; however, the number of patients responding to the treatment is still limited. Hence, understanding the factors that regulate the responses and mechanism of resistance is a key objective. The tumor mutational burden (TMB) correlates with T cell infiltration and with clinical responses to Immune checkpoint blockade (ICB) in lung cancer. In parallel, several studies evidenced a critical role of type 1 conventional dendritic cells (cDC1) for cross-presentation of tumor antigens, induction of anti-tumoral $CD8^+$ T cells immunity and response to checkpoint blockade. However, the relevance of cDC1 for programming $CD8^+$ T cells to *bona-fide* neoantigens (neoAgs) in lung tumors with increased TMB remains unexplored.

To address this question, we generated a mismatch deficient variant of the poorly immunogenic KP (*Kras*$^{G12D/Wt}$; $p53^{-/-}$) model of lung cancer to enhance the TMB. MLH1 deficient KP cells (KP^{neo}) accumulated SNVs and frameshift that translated into novel predicted neoantigens that were sequenced and classified by expression and predicted binding affinity for MHCI. *In vivo* experiments in both subcutaneous and orthotopic lung models showed an induction of neoantigen specific CD8 T cells responses and tumor growth control in KP^{neo} tumors. Notably, these responses were lost in a cDC1-deficient background, indicating that cDC1 cross presentation is required for neoantigens immunogenicity. Despite mild spontaneous immunogenicity, however, KP^{neo} tumors remained refractory to anti-PD-L1 antibodies. A combinatorial therapy including anti-PD-L1 plus FMS-like tyrosine kinase 3 ligand (a growth factor essential for DCs development and maintenance) and Polyinosinic:Polycytidylic acid (Poly (I:C), a stimulus for DC maturation) largely enhanced CD8 T cell activation and achieved control of progressing KP^{neo} tumors. Interestingly, the combinatorial treatment was ineffective in parental KP cells, indicating that a certain level of neoantigens is a prerequisite for the response.

Moreover, in the lung orthotopic setting we found that DC therapy is necessary and sufficient to induce proliferation and activation of CD8 T cell and to inhibit the

progression of tumor growth. To understand the cellular and molecular network underlying the efficacy on DC therapy we performed single-cell RNA sequencing (scRNA-seq) of immune cells from KP^{neo} tumor bearing lungs. scRNA-seq uncovered the molecular pathways induced by DCs therapy in lung tumor tissues, which include enhancement of cellular proliferation and upregulation of metabolic pathways in lung resident cDC1. Moreover, DC-based therapy reduced an immunoregulatory program in DC subsets and strongly modified proliferation and effector functions/cytotoxicity across multiple T cell states. We conclude that boosting DC activity in ICB-resistant mutated lung tumors is critical to leverage neoantigen content for therapeutic advantage.

Acknowledgments

The work presented in this thesis is the culmination of more than four years of intellectual and physical effort. This is the conclusion of the collective effort of a large number of people without their help this final report would not be possible. I would like to thank:

The researchers present in my thesis committee, they have provided their time and experienced to guide and enrich my work.

ICGEB, that during these thirty years have made bridges between a reference center and developing countries through fellowship programs, meeting and courses and short-term internship.

The Arturo Falaschi program that through scholarships provides real opportunities for people like me. This program reduces the gap by providing access to people from developing countries to reference centers in the world, to have an experience that would be impossible for them in their current conditions.

I owe an immense debt of gratitude to my thesis advisor Dr. Federica Benvenuti. She welcomes me in her lab and expended countless hours of mentoring and support. She dedicates her laboratory not only to transcending the frontier of knowledge; she also is dedicated to breaking the invisible glass ceiling over the heads of women in science.

Cellular Immunology Laboratory, we are an authentic team that supports each other with the same strength that someone can experience in a family. I would like to thank to the current members but also to the people that was part on the past.

The bioexperimental facilities carry out silent work that impacts on the quality of our most precious reagent, which is the well-being of the mice, day by day.

My circle of friends who supported me during these four years even though we have a long ocean in between.

I owe an immense debt of gratitude to my family. I have upset completely our situation by deciding to a PhD so far from home. However, they have received this decision with

joy and happiness, and they have given me unconditional support. The cross the ocean every time that I have a hard time to bring me support and love.

Elia: thank you for your immense patient and love. You decided to start this process with me knowing very well that it requires total dedication. You supported me every weekend that I had experiments, every night that the experiments ended late, always with a big smile. You are the greatest partner that I can imagine!

List of figures

List of abbreviations

APCs: Antigen presenting cells.
BMDCs: Bone marrow dendritic cells,
$CD8^+$ TSTEM: Stem-like $Tcf1^+CD8^+$.
cDC1: Type 1 conventional dendritic cells.
CTLA-4: Cytotoxic T lymphocyte antigen 4.
DAMPs: Danger-associated molecular patterns.
DEGs: Differentially expressed genes.
DTA: Diphtheria toxin subunit A.
Flt3L: FMS-like tyrosine kinase 3 ligand.
GEMMs: Genetically engineered mouse models.
GzmB: Granzyme B.
ICB: Immune checkpoint blockade.
IFNγ: Interferon-γ.
In/Del: Insertions and deletions.
KLRG1: Killer cell lectin like receptor G1.
KP: $Kras^{G12D/Wt}$;$p53^{-/-}$.
LUAD: Lung adenocarcinoma.
LUSC: Lung squamous cell carcinoma.
MHCI: Major histocompatibility complex class I.
MHCII: Major histocompatibility complex class II.
MMR: Mismatch repair.
MMRd: Deficient DNA mismatch repair.
mregDCs: Mature DCs enriched in immunoregulatory molecules.
MSI: Microsatellite instability.
neoAgs: Neoantigens.
NES: Normalized expression score.
NSCLC: Non-small cell lung carcinoma.
PAMPs: Pathogen-associated molecular patterns.
PD-1: Programmed death 1.
PD-L1: Programmed death 1 ligand.
poly(I:C): Polyinosinic:polycytidylic acid.
Prf1: Perforin 1.
SCLC: Small cell lung carcinoma.
scRNAseq: Single cell RNA-sequencing.
SNVs: single nucleotide variants.
TAAs: Tumor-associated antigens.
TCF-1: T cell factor 1.
TCR: T cell receptor.
TFs: Transcription factors.

TLRs: Toll-like receptors.
TMB: Tumor mutational burden.
TME: Tumor microenvironment.
TSAs: Tumor-specific antigens.
UMAP: Uniform manifold approximation and projection.
WES: Whole exome sequencing.

1. Introduction

Cancer is one of the leading causes of death worldwide, and lung cancer is one of the most common cases, with an estimated 2.21 million deaths each year[1]. Historically, lung cancer has been classified as non-small cell lung carcinoma (NSCLC) and small cell lung carcinoma (SCLC)[2], and approximately 85% of patients have been diagnosed as NSCLC (group of histological subtypes), of which lung adenocarcinoma (LUAD) and lung squamous cell carcinoma (LUSC) are the most common subtypes[3,4].

The most common etiology for lung cancer is smoking tobacco[1] and the World Health Organization created a Framework Convention on Tobacco Control for Governments, to reduce the prevalence of tobacco use and exposure to tobacco smoke. By implementing these measures, governments reduce the heavy burden of disease and death that is attributable to tobacco use or exposure[3]. Even though tobacco prevention strategies are a crucial component in the fight against lung cancer, development of sophisticated therapies is required to meaningfully improve clinical outcomes for patients.

1.1 Cancer and immune system

1.1.1 Immunosurveillance

The immune system acts as a sentinel detecting aberrant antigens in the body through a process called immunosurveillance[5,6]. During this process, immune cells can recognize a transformed cell and following different steps can efficiently eliminate it. The generation of immunity to cancer is a cyclic process that Chen and Mellman called as the cancer-immunity cycle[7] (Figure 1.1).

In the initial step of the cycle, tumor-associated antigens (TAAs) or tumor-specific antigens (TSAs) are released from the tumor to the tumor microenvironment (TME) by apoptosis or cell death (Step 1). These TAAs or TSAs are captured by antigen presenting cells (APCs) for processing (Step 2). This step must be accompanied by immunogenic signal such as proinflammatory cytokines[7]. Then, the APCs mature and migrate to the lymph node to present tumor antigens resulting in priming and activation of T cells (Step 3). For this step, it is critical that T cells recognize the antigen as foreign or against which central tolerance has been incomplete. The activated T cells traffic (step 4) and infiltrate the tumor nodules (Step 5), they specifically recognize and bind to cancer cells through

the interaction between its T cell receptor (TCR) and its cognate antigen bound to major histocompatibility complex class I MHCI (step 6) and kill their target cancer cell (step 7).

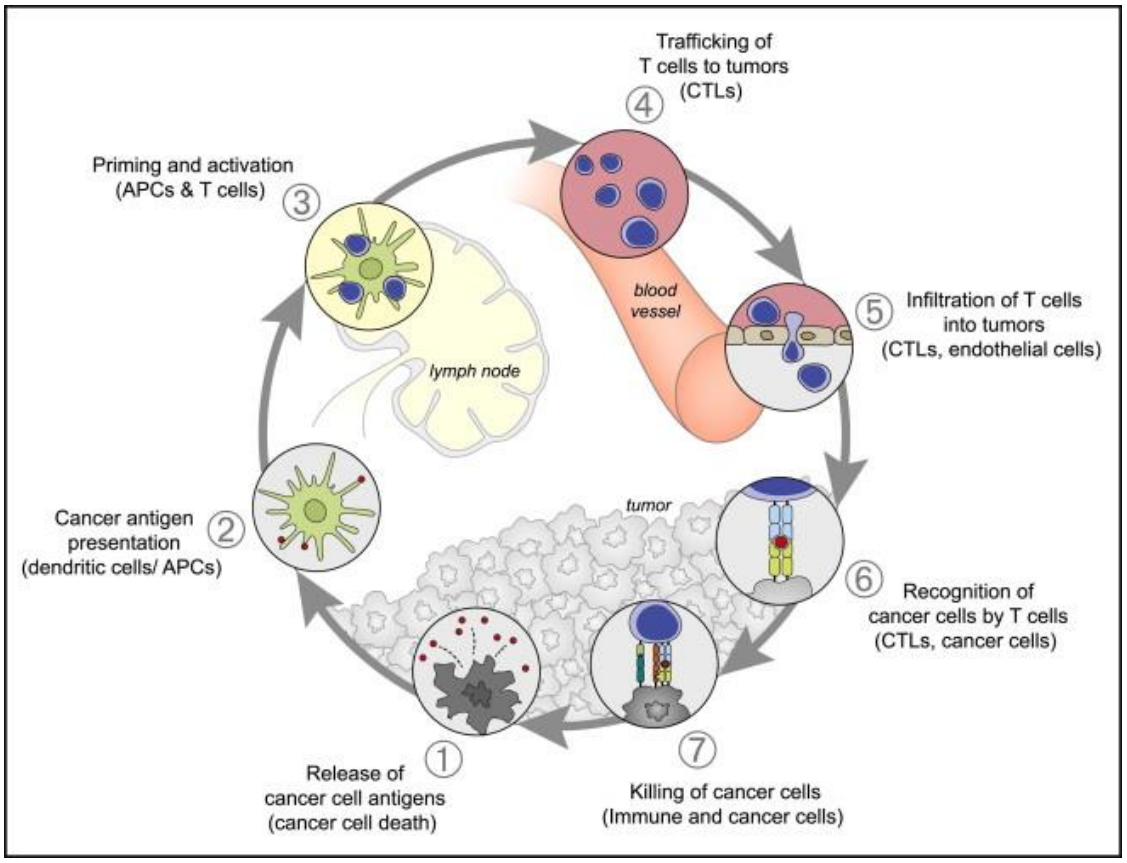

Figure 1.1| Cancer-immunity cycle. Cancer cells release TAAs or TSAs that are captured by APCs and presented to T cells in the draining lymph node. Activated-specific T cells traffic and infiltrate the tumor where they can recognize the cancer cell based on the presentation of the antigen in the MHCI complex. Once the T cell recognize the tumor cell, they can eliminate it.

The cycle outlined above is an active process that continuously patrols the body for nascent cancer cells to be eliminated. Consequently, the immune system sculpts tumors by removing more immunogenic clones leading to sub-clonal populations less immunogenic, resulting in a selection of the antigen repertoire present in a tumor[8]. This process is known as immunoediting[9]. This process leads to an equilibrium phase, in which residual tumor cells not removed in the elimination phase are held in a state of dormancy. Then, the last phase of immunoediting is the “escape”, in which edited tumors are no longer recognized by immune processes, begin to grow progressively, induce an immunosuppressive TME, and then emerge as clinically apparent cancers[10,11].

In this context, understanding the mechanisms that generate TAAs and TSAs in tumor cells and, in particular, understanding the role of immunogenic antigens during the

initiation of cancer immunity cycle would allow the development of more effective strategies to enhance the cancer-immunity.

1.1.2 Immune checkpoint blockade therapies to treat cancer

Over the past decade there has been a revolution in cancer treatments, by moving from treatments that eliminated the tumor cell directly (for example, chemotherapy or radiation), towards therapies that enhance or reinvigorate the own T cell–mediated immune response against cancer[1213]. Nowadays, therapies targeting the immune checkpoint molecules have changed the landscape of therapies available to treat solid tumors[14].

The original observation that blocking the prototypical immune checkpoint receptor cytotoxic T lymphocyte antigen 4 (CTLA-4) could mediate tumor regression in murine models[15] led to the clinical development and approval of anti-CTLA-4 as a treatment for patients. Later, antibodies against checkpoints Programmed death 1 (PD-1) and its major ligand PD-L1 have shown great promise in treating many diverse cancer types, including NSCLC[16]. Although more than 25 years have passed since the first observations in murine models on the benefits of ICB, only few studies have addressed the molecular mechanisms behind this effect. These antibodies block the interaction of the immune checkpoint molecules with their ligands on antigen presenting cells, tumor cells, or T cells[12]. Data from *in vitro* experiments have shown that using antibodies against PD-L1 disrupt the PD-L1/B7.1 cis interaction on dendritic cells. The disruption of this interaction allows CD28 costimulation by increased B7.1/CD28 interaction leading to an antitumor T cell immunity[17].

Despite the unprecedented successes of ICBs only 20% of patients with NSCLC derive clinical benefit[18,19]. This is partially due to the fact that NSCLC is a heterogeneous group of diseases[3,4], but also due to intratumoral heterogeneity[20], the quality of the immune response generated[21] and the characteristics of the tumor microenvironment[22].

1.1.3 Factors determining long-term antitumor responses by ICB

The key parameters that correlate with the efficacy of ICB therapies in NSCLC patients are[23]: 1) PD-L1 expression in tumor and immune cells[24]; 2) infiltration and localization[25] of immune cell (particularly, cytotoxic lymphocytes) generating an inflamed tumor

microenvironment ; 3) increased mutational burden or neoantigen load in tumor cells[16]. All these parameters are the characteristics of hot tumors. By contrast, cold tumors are resistant to ICB and are poorly infiltrated by the immune cells or directly exclude the immune system.

Clinical evidence correlates PD-L1 positive staining in human biopsies and ICB outcome in NSCLC[26,27]. PD-L1 expression within the tumor microenvironment is indicative of T cell function because PD-L1 is induced by interferon-γ (IFNγ)[28]. Patients with PD-L1$^+$ tumors and T cell–infiltrated tumors comprise about 40% of the ICB-treated patients with NSCLC and are the group most likely to respond to ICB[29,30]. In addition, data from a clinical trial (NCT01903993) shown that the presence of tumor-associated PD-L1$^+$ DCs is associated with improved clinical benefit from PD-L1 blockade with atezolizumab (anti PD-L1 mAb)[17].

A second parameter associated with outcome to ICB is infiltration of cytotoxic T cells in tumors [31] and the presence of molecular signatures of immune activation[32], introducing the notion of ‘‘hot’’ (inflamed and highly infiltrated) tumors[13,22]. Understanding the mechanisms regulating T cell phenotype are therefore crucial to improve T cell-based therapies and patient outcomes.

A third key feature that correlates with better outcomes to ICB is the mutational burden in tumors. There is large variability in the prevalence of somatic mutation across the cancer types, ranging from 10 to 1000 mutations per Mb[20]. This range is particularly broad in NSCLCs because tumors in non-smokers generally have few somatic mutations compared with tumors in smokers where mutations are abundant[33]. Documented correlation between the mutational load in tumor cell and ICB sensitivity was published by Rizvi *et al.*, for patients with NSCLC[16]. The authors have shown a significant correlation between improved percent of free survival and high mutational burden. They hypothesized that increase in somatic mutation generated neoAgs that can be a target of the tumor immune response. Recent studies performed by independent groups have confirmed the correlation between high mutational burden and better outcomes to ICB, using different cohorts of patients with NSCLC[34–36].

Mouse preclinical model of cancers have provided invaluable insights related to the mechanisms of the immune response against cancer[37]. Genetically engineered mouse models (GEMMs) of cancer recapitulate histopathological and genetics features of human adenocarcinomas[38]. The KP (*Kras*$^{G12D/Wt}$; p53$^{-/-}$) mouse model of lung cancer mimics the oncogenic transformation processes observed in human, where mutations in oncogenes, such as KRAS, are thought to occur early, followed by inactivation of the p53 pathway[39]. In this model the tumor evolves from hyperplasia during the early stage to adenocarcinoma in the later stages[40] and provides an invaluable tool to study the cancer immunity. This model has been modified to express surrogate antigens as antigens from ovalbumin[41] or neoAgs identified in melanoma[42]. From these models, tumor cells have been isolated and used as transplantable cell lines. During the course of this thesis, the KP model was further modified by removing a mismatch repair component (*Msh2*), thus generating lung tumors with microsatellite instability and subsequent accumulation of somatic mutations[43]. However, at the beginning of this study there were no preclinical models carrying multiple and diverse bona fide neoAgs that could be used to study how the immune system sculpts the tumor.

During the next section, the T-cell response to cancer and the role of neoAgs during immunity to cancer are further explored.

1.1.4 T cell response to neoantigens

As described in the second section of this thesis, T cells play an important role during tumor control and, together with NK cells, are directly responsible for tumor cell destruction mediated by the immune system.

Within the T cell compartment, CD8 T cells that differentiate into effector cytotoxic CD8 T cells is the main cellular subset endowed with the ability to directly kill tumors cells and that correlates with anti-tumoral responses[16]. Emerging evidence are shedding light on the role of CD4 T cells to provide help during anti-tumor immunity. There are many mechanisms by which CD4 T cells contribute to anti-tumor immunity, these mechanisms included CD4-mediated cytotoxicity, activation of myeloid cells as macrophages, inducing tumor cell senesce and helping to prime CD8 T cells[44,45]. Recently, this last point has been extended and Ferris *et al.*, have demonstrated that CD4 T cells directly engage

cDC1 via antigen-MHCII interactions to induce cDC1-specific signaling required for optimal CD8 T cell responses[46,47].

The third T lymphocyte subset that has an impact during anti-tumor immunity is the γδ T cells. This subset represents a minor population within the lymphocytes infiltrating human tumors and shares innate and adaptive immune properties. Moreover, γδ T cells activates and recognizes antigens in a MHCI-independent manner. Activation of this subset in the TME leads to secretion of perforin 1 (PRF1) and granzyme B (GzmB), leading to pore formation, entry of granzyme proteases, and subsequent apoptosis of tumor cells[48]. Furthermore, it has been reported that γδ T cells target tumor cells through antibody-dependent cellular cytotoxicity, thus, the Fcγ receptor expressed on γδ T cells binds to the Fc region of antibodies bound to target cells, leading to the death of tumor cells[49]. However, the role of γδ T cells has been debated and paradoxical data have been published[50–53]. In particular, using a preclinical mouse model of NSCLC was demonstrated that γδ T cells promote cancer development[54].

Cross-priming by DCs is critical to induce anti-tumoral CD8 T cells. The process of activation leads to a differentiation process in which CD8 T cells can become effector, memory or exhausted cells. These three states have different roles during the cancer immunity. The process of CD8 T cell differentiation will be further explore in the next section.

1.1.4.1 CD8 T cell differentiation after antigen recognition

Upon antigen recognition, activated CD8 T cells in the tumor microenvironment undergo a complex pathway of differentiation that carries analogies with anti-viral T cell responses and traits specific of the anti-tumoral response. This differentiation process is guided by the TME and also by changes in the activity of transcription factors (TFs) and chromatin dynamics[55–57].

Activated T cells expand clonally and begin to express specific functional and distinct gene programs. During lineage commitment, activated T cells gradually lose their plasticity while acquiring effector specific functions and differentiation markers[55]. This process is orchestrated by the fine activity of lineage- specific TFs which induce cell-type- specific gene expression patterns guiding memory, effector and exhausted T cell

specifications[58]. Within TFs guiding the differentiation, T-bet, Blimp-1, Id2, IRF4 and Zeb2 have been described to be associated with effector T cells[59,60], for memory T cells were described T cell factor 1 (TCF-1), Eomes, Id3, E proteins, B-cell lymphoma 6 (Bcl-6) and Forkhead Box O1 (FOXO1)[61] and for exhaustion Nuclear Receptor Subfamily 4 Group A Member 1 (Nr4a1) and Thymocyte Selection Associated High Mobility Group Box (Tox)[62–64]. However, the expression of some these TFs do not change across the differentiation states suggesting that additional mechanisms contribute to their activity in promoting cell fate commitment[64]. Thus, the role of epigenetics emerged as mechanism to contribute to TFs activity during the T differentiation process. Chromatin dynamics can regulate gene expression through different mechanism such as: histone variants, post-transcriptional histone tail modifications, DNA methylation, nucleosome re-positioning and modifying the chromosome 3D architecture[55,65]. After antigenic stimulation, Histone methyltransferases actively alter the epigenetic landscapes of genes involved in reprogramming of effector or memory differentiation. For example, acquisition of effector functions correlates with epigenetic changes of poised enhancers (characterized by methylation of the lysin in the histone 3, $H3K4me1^{+}H3K4me2^{+}H3K27me3^{+}$) into active enhancers (characterized by methylation and acetylation in the histone 3, $H3K4me1^{+}$ $H3K4me2^{+}$ $H3K27ac^{+}$)[55,66]. Moreover, the perforin, IFNγ, granzymes loci acquire a permissive chromatin state and are decorated with active histone marks during the development of cytotoxic effectors[67].

Regarding the surface markers and function of the $CD8^{+}$ T cells flow cytometry analysis and recent studies using single cell RNA-sequencing (scRNAseq) have shown that effector-cytotoxic $CD8^{+}$ T cells are characterized by short live and the expression of cytotoxic molecules as Killer Cell Lectin Like Receptor G1 (KLRG1), granzymes and perforin molecules[68]. This subset is involved in the direct killing of tumor cells.

Following tumor cell or pathogen clearance, terminally differentiated effector $CD8^{+}$ T cells die, whereas a small subset of long-lived memory cells with unique features of stemming and plasticity survives for long periods of time[55]. This subset can be subdivided based on the surface markers into central memory ($CD44^{+}CD62L^{+}CD127^{+}$), effector memory ($CD44^{+}CD62L^{+}CD127^{+}$) and tissue resident ($CD69^{+}CD103^{+}$) in non-lymph-tissues[69]. Similar to chronic viral infections, the constant exposure of $CD8^{+}$ T cells

to TAAs or TSAs can induce the expression of immune-checkpoint molecules, which characterizes a dysfunctional state called T-cell exhaustion[70,71]. It is defined by the loss of effector function, sustained expression of inhibitory receptors and a transcriptional state distinct from that of functional effector $CD8^+$ T cell[70].

Exhaustion is not a binary state that comes from effector functions to an exhausted phenotype, instead is a gradual process[72]. Thus, the loss of functions occurs in a hierarchical manner, where $CD8^+$ T cells start losing some functions as the capacity to produce IL-2[73] or their proliferative capacity[74]. In an intermediate state, $CD8^+$ T cell maintain the expression of the transcription factor TCF-1 but fail to produce interferons as IFNγ and to degranulate[68]. During this stage $CD8^+$ T cell expressed intermediate levels of inhibitory molecules as PD-1 and Lymphocyte-activation gene 3 (LAG3). Single- cell transcriptome analyses of $CD8^+$ T cells in colorectal cancer[75], breast cancer[76], melanoma[77] and NSCLC[68] have identified this stage of intermediate dysfunction. In more advanced stages T cells express different checkpoint or inhibitory molecules such as T-cell immunoglobulin mucin 3 (TIM3), CTLA4, Lag3, CD39 and 4-1BB, and variable surface levels of PD-1 (reviewed in [60]). This subset is involved in the direct killing of the tumor cell[78].

The intratumoral status of $CD8^+$ T cells described above were summarized by Van der Leun et al[72]. in the figure 1.2. The naïve-like $CD8^+$ T cells that arrive to the tumor acquire effector functions according to the tumor microenvironment and the exposure to the antigens differentiated into the different dysfunctional states. The naïve $CD8^+$ T cells are characterized by the expression of C-C chemokine receptor type 7 (CCR7), interleukin 7 (IL7) and the transcription factor TCF-1. Since the cytotoxic state found in tumors is also found in healthy tissues, the authors described differentiation in this subset as a TME-independent process. This state is characterized by the expression of cytolytic molecules such as killer cell lectin like receptor G1 (KLRG1), PRF1, Fc gamma receptor IIIa (FCGR3A) and C-X3-C Motif Chemokine Receptor 1 (CX3CR1), and low expression of checkpoint molecules. They propose that the development of (pre)dysfunctional cell states is predominantly driven by antigen exposure and the TME. During the pre-dysfunctional state $CD8^+$ T cells express granzymes and intermediate levels of inhibitory molecules. The early to late dysfunctional states are characterized by the loss of effector functions

(granzymes) and proliferation capacity and an increase in the expression and number of inhibitory and checkpoint molecules such as PD-1, CTLA-4, TIM3 and LAG3.

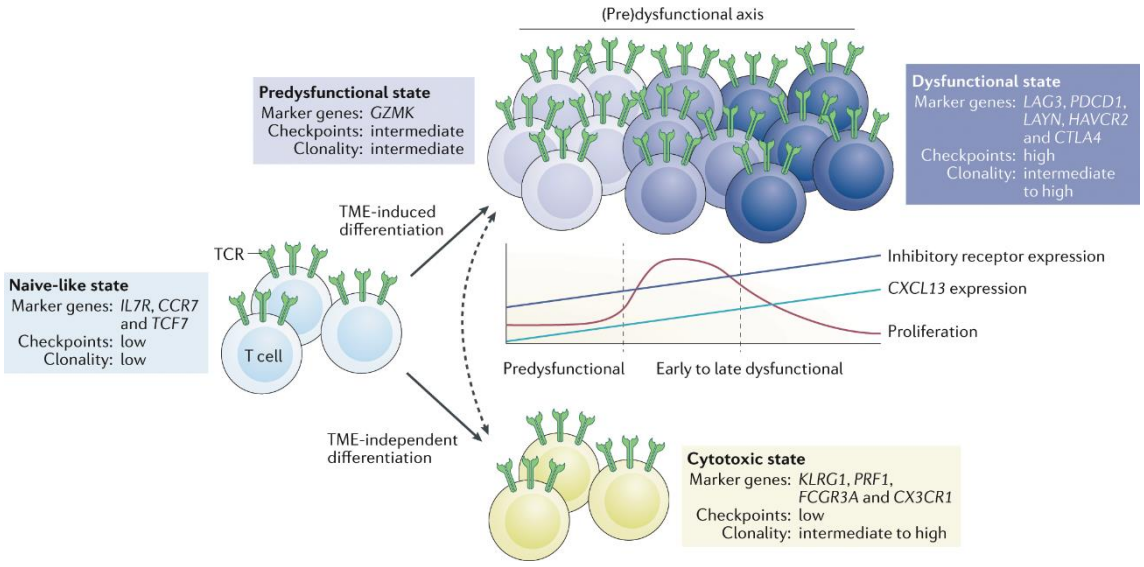

Figure 1.2| Model of intratumoral states of CD8⁺ T cells. The scheme represents the main characteristic and the major CD8⁺ T cells states in tumors. Data from human samples with NSCLC, colorectal cancer, hepatocellular carcinoma, and melanoma showed common states across the adaptive immunity against cancer. In brief the CD8⁺ T cells show a naïve-like state characterized by the expression of CCR7, IL7 and the transcription factor TCF-1. Since the cytotoxic state found in tumors is also found in healthy tissues, the authors described differentiation in this subset as a TME-independent process. This state is characterized by the expression of cytolytic molecules and low expression of checkpoint molecules. They propose that the development of (pre)dysfunctional cell states is predominantly driven by antigen exposure and the TME. These states are characterized by the loss of effector functions, proliferation capacity and an increase in the expression and number of inhibitory and checkpoint molecules such as PD-1, CTLA-4, TIM3 and LAG3.

1.1.4.2 Immunotherapy with immune checkpoint blockade targets progenitor exhausted CD8⁺ T cells

The early and intermediate states of dysfunction offer a therapeutic opportunity by using monoclonal antibodies that block PD-1 or CTLA4. The precise mechanisms supporting the efficacy of immune checkpoint blockade have not been fully elucidated yet[79].

Spencer *et al.*, have demonstrated using a preclinical model of colorectal cancer (M38) that ICB induces the expansion of specific tumor-infiltrating T cell subsets. In particular, PD-1 blockade primarily induces expansion of exhausted-like tumor-infiltrating CD8 T cells and CTLA-4 blockade induces expansion of ICOS⁺ Th1-like CD4 effector as well as exhausted-like CD8 T cells[80]. In addition, it was demonstrated in MC38 model that the

CXCR3 chemokine system enhanced the proliferation and function of intratumoral $CD8^+$ T cells during anti-PD-1 treatment and that $CD103^+$-dendritic cells-derived secreting CXCL9 played a pivotal role in this process[81]. D'Alise *et al.*, have demonstrated in MC38 model that a therapy containing anti-PD-1 combined with Adenovirus–vectored vaccines encoding tumor neoAgs eradicate large tumors. They showed that the therapy increased generated the accumulation of stem-like $Tcf1^+CD8^+$ ($CD8^+$ T_{STEM}) T cell progenitors in the draining lymph node and effector $CD8^+$ T cells intratumorally. In this context the combinatorial therapy enhances the magnitude of neoantigen-specific $CD8^+$ T cells and promotes their differentiation into $CD8^+$ T_{STEM}[82].

In sarcoma, a combination of PD-1 and CTLA-4 blockade targeted the exhaustion/dysfunctional phenotype of intratumoral tumor-specific $CD8^+$ T cells producing unique effects not obtained with the monotherapies[83]. The combinatorial ICB targets intratumoral $CD8^+$ T cells population changing from one showing characteristics of exhaustion/dysfunction to one showing signs of reactivation[83,84].

Besides, in B16 melanoma model Siddiqui *et al.*, showed that PD-1 blockade reinvigorates intratumoral tumor-reactive $CD8^+$ T cells $TCF\text{-}1^+$ $PD\text{-}1^+$ with stem-like properties and promote tumor control after the therapy[85].

Recently, Spranger *et al.*, have described a subset of tumor reactive CD8 T cells with a dysfunctional phenotype that infiltrated nodules. This subset does not show the same molecular signatures that of the dysfunctional phenotype described before, and it is exclusive for lung tumor tissues. This subset failed to produce IFNγ (a critical feature of antitumor immune response), expressed low levels of GzmB, and didn´t show cytotoxicity *in vivo*. This study provided evidence that not all tumor-reactive T cells are functionally interchangable and that not all tumor-specific $CD8^+$ T cells will react to ICB[86]. Clinical data demonstrate that there is a fraction of patients with tumors infiltrated by T cells; but these T cells fail to up-regulate effector molecules and PD-L1 in response to ICB, remaining refractory to these therapies[4].

A common factor that emerges from the evidence mentioned above is the importance of intratumoral T cell infiltration during ICB efficacy. Therefore, the role of the density and location of T cells in the tumor will be explored in the next section.

1.1.4.3 T cell infiltration in tumors

It has been observed in colorectal cancer that the density and location of immune cells within the tumor site could predict survival in patients[87]. In particular, $CD8^+$ T cell density has been shown as a predictor of immunotherapy response[88]. By analyzing the T cell localization within the tumor, studies from 2013 have demonstrated the importance of T cell infiltration into the tumor nodules relative to the adjacent tissue[4,7,89].

Based on this evidence a robust, consensus and standardized scoring system has been developed to quantify lymphocytes, either in the tumor nodule or the invasive margin, called Immunoscore. This system classifies tumors from I0 (immune dessert tumors, "cold" tumors) to I4 (high immune cell densities in both tumor and adjacent tissue, "hot" inflamed tumors) introducing the idea of the immune context in the TME[90]. Hot and inflamed tumors are characterized by the infiltration of cytotoxic T cells expressing PD-1 and tumor cells expression the PD-L1. In colorectal cancer with microsatellite instability high (the role of microsatellite instability will be explored in the next section) harboring a higher rate of nonsynonymous single-nucleotide polymorphisms showed higher responses to ICBs[13,91]. Contrary, cold tumors were described to be poorly infiltrated by T cells and to have scarce expression PD-L1 cells. Also, tumors are characterized by high proliferation with low mutational burden and low expression of genes related to the antigen presentation machinery such as MHC class-I[92].

Later, in 2019 Galon *et al.*, have added two middle categories under the name "altered". The altered phenotype includes the "excluded" and "immunosuppressed" tumors[87]. In the first case immune cells are found at the edge of tumor nodules and do not infiltrate. This reflects the intrinsic ability of the host immune system to effectively mount a T cell-mediated immune response and the ability of the tumor to escape such response by physically hindering T cell infiltration. Recently, the role of two fibroblast subsets during the exclusion of cytotoxic T cells has been shown; fibroblasts promote the generation of a compact extracellular matrix that avoid T cell infiltration[25]. In the immunosuppressed tumors there is a low degree of immune cell infiltration but in absence of physical barriers. Here the presence of an immunosuppressive TME limits the recruitment and expansion of immune cells[93]. The four tumor types are summarized in the scheme presented in the figure 1.3.

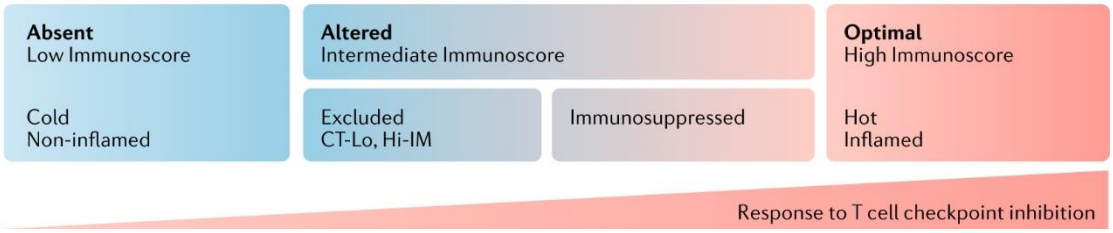

Figure 1.3| Defining hot, altered, and cold tumors and their response to ICB. Galon *et al.*, have proposed in 2019 four types of tumors according to the level of infiltration by T cell in tumors. Cold tumors are poorly immunogenic and poorly infiltrate by T cells. Tumors that exclude T cells or in which the T cells show an immunosuppressed phenotype are summarized by the name "altered". Hot tumors are chatacterized to be highly infiltrate by T cells and patients have better outcomes to ICB[87].

1.2 Neoantigens

Cancer is a genetic disease characterized by the accumulation of genetic alterations[7]. Gene mutations caused by genetic instability during carcinogenesis can occur in the coding region causing changes in the amino acid sequence[94]. These changes produce proteins that are not found in normal cells that can be recognized by the immune system [10,21]. These aberrant antigens are named neoantigens[11] as they are foreign to the immune system. In the tumor microenvironment neoAgs can be released and captured by DCs and presented in the MHC class-I or -II to T cells (reviewed on [7]).

The sources for the accumulation of somatic mutations that generate neoAgs are variable; in some tumors they can be physical or chemical agents, such as ultraviolet radiation in melanoma or smoke in lung cancer[10]. Also, errors during the DNA replication coupled with deficiencies in the DNA repair system represent an important source of neoAgs[95]. The processes involved during the neoantigen generation include single nucleotide variants, insertion or deletions, changes in the splicing, translocations, or post-translational modifications[96]. All these mutational processes can lead to the generation of aberrant proteins that can be recognized by the immune system (Figure 1.4).

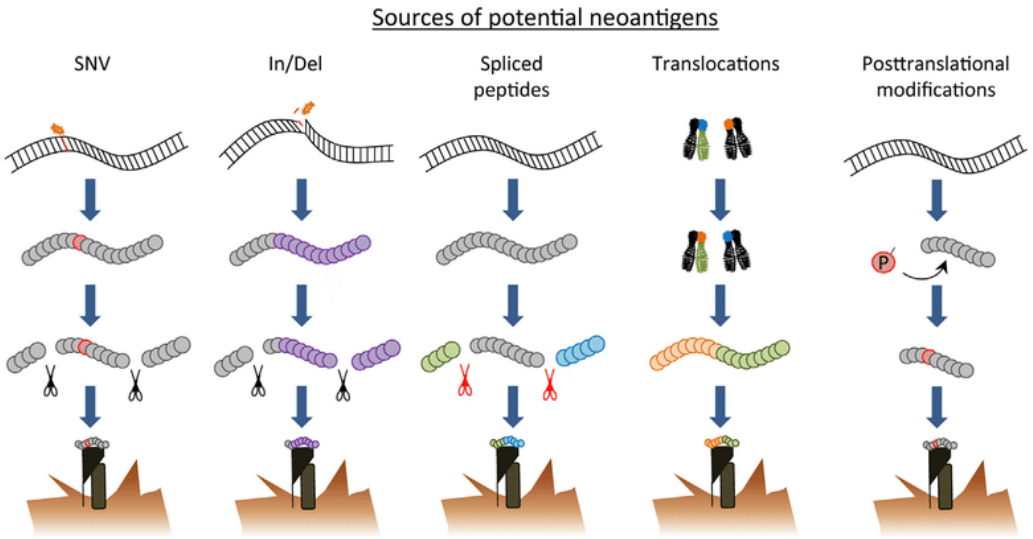

Figure 1.4| Different sources for potential neoantigens in the cancer cell. Mutational processes such as single nucleotide variants (SNV), insertions and deletions (In/Del), spliced peptides, translocations and posttranslational modifications lead to the generation of aberrant peptides that can be recognize by the immune system. The scheme was modified from Bräunlien *et al.*,[96].

1.2.1 Deficiencies in DNA repair system and neoantigens

The integrity of genetic information depends on the fidelity of DNA replication and on the efficiency of several different DNA repair processes. The mismatch repair (MMR) system is one of the key guardians of genomic integrity[97], and this pathway is responsible for correcting base substitution mismatches and insertion-deletion mismatches generated during DNA replication in organisms from bacteria to mammals[98]. Deficient DNA mismatch repair (MMRd) may be caused by germline or somatic mutations in mismatch repair genes (MLH1, MSH2, MSH3, MSH6, and PMS2), or through epigenetic silencing of MLH1[99]. Loss of MMR function induces a hypermutated phenotype, identified clinically by a genomic scar known as microsatellite instability (MSI)[100]. The frequency of MSI is variable across the different cancer types and its signatures may differ among them[101]. Previous studies made in Lung adenocarcinoma, Lung squamous cell carcinoma and Lung small cell cancer revealed that 1% of the patients presented MSI[102–106].

Loss of MMR function can also drive a hypermutator phenotype in cancer cells generating non-synonymous mutation in other regions in the genome outside from microsatellites[107]. A study published in 2017 shows that alterations in DNA repair pathways are known to increase the mutational burden of cancers. In particular, patients with lung adenocarcinoma whose tumor's harbored a high clonal neoantigen

burden exhibited improved relapse-free survival[108]. Rizvi *et al.,* showed that although carcinogens in tobacco smoke are largely responsible for the mutagenesis in lung cancers; as well as deleterious mutations in a number of genes that are important in DNA repair and replication. For example, in patients with high mutational burden, considered as responders to immune-checkpoint inhibitors, they identified deleterious mutations in POLD1, POLE, and MSH2 (enzymes involved in the mismatch repair system)[16]. Subsequent studies have delved into the role of MLH1 (another MMR component) in NSCLC in different cohorts, showing that methylation in the *mlh1* promoter is higher in malignant lung tissue compared to adjacent healthy tissue and its methylation is negatively correlated with levels of MLH1 in the malignant lung tissue[109].

Mismatch repair is a highly conserved process from prokaryotes to eukaryotes and many of its components are orthologous between them; however, the proteins involved in the repair pathway in eukaryotes can differ depending on the nature of the mismatch and the substrate for excision[98].

The main components are MutS, in charge of mismatch recognition and binding, and MutL (complex formed by 1 out of the 5 homologues which presents in eukaryotes MLH1, MLH2, MLH3, and PMS1 or PMS2). MutL complex binds MutS and they destabilize the DNA helix, so endonuclease can introduce a nick and removes the strand with the mismatch. The missing DNA is polymerized by DNA polymerase δ or ε and a DNA ligase ligates the bases (reviewed in [98]).

1.2.1.1 MLH1

As previously mentioned, MLH1 homologs are essential components of MMR and are conserved across all domains of life[64]. Human MLH1 (hMLH1) is a 756-amino-acid, 84 kDa protein that can be split into two main parts: an N-terminal domain, where the ATPase activity resides, and a C-terminal domain, which is the site of dimerization with MLH1 paralogs[65]. MLH1 and PMS2 paralogs form a heterodimeric complex, MutLα. Since the mismatch is identified and isolated by the MutS mismatch-recognition complex, MutLα is recruited[66] and, via its C-terminal endonuclease activity[67], generates strand breaks in the heteroduplex 30 and 50 to the mismatch that facilitate the repairing[67,68].

Few studies address MLH1 mutations and their impact on mismatch repair; however, these papers clearly showed the phenotype generated *in vitro* and *in vivo*. Wu *et al*. have shown that mutations at the N-terminus of MLH1 correlate with Lynch syndrome in patients[69]. Furthermore, the MLH1 knockout mouse represents a preclinical model that resembles the characteristics of the human MMRd counterpart. These mice developed many different neoplasias with a heterogeneous mutational landscape[70]. Germano *et al*., generated a colorectal cancer cell line (MC38) knocked out for *mlh1*. The inactivation of *mlh1* increased the mutational burden and led to dynamic mutational profiles, which resulted in the persistent renewal of neoAgs *in vitro* and *in vivo*, correlated with tumor growth control by the immune system. In addition, the authors showed that even in CT26, a non- immunogenic cell line neoAgs are generated after MLH1 deletion, and mice treated with immunotherapies (α-CTLA4 and α-PD1) controlled the tumor growth[10].

Although the active role of MLH1 deficiency during neoantigen loading has been well characterized, mutations in its gene are not the only source of neoantigen generation and, in particular, MLH1 deficiencies are not found in all biopsies of NSCLC.[110–112]. However, Mlh1 deletion offers a specific and validated tool to investigate the role of increased neoantigen load during cancer immunity.

In summary, during the previous sections, several pieces of evidence were presented that support the importance of high mutational load in tumors and high immune infiltrate in tumor nodules during the generation of anticancer immunity and ICB responsiveness. Currently, the cellular determinants of neoAgs immunogenicity in mutated tumor are not fully understood. In particular, the quantitative and qualitative threshold of neoAgs that generates an effective immune response against cancer is an important unresolved issue.

1.3 Role of conventional type 1 dendritic cell during tumor progression

1.3.1 Dendritic cells

DCs are professional antigen-presenting cells (APCs) that recognise antigens from different microenvironments in the body and present antigens and co-stimulatory signals to cells of the adaptive immune system (reviewed on [113]). Through the

presentation of exogenous antigens on both MHC class I and II, DCs are capable of inducing a potent immune response[114].

In steady state, DCs reside in the periphery and show an immature phenotype characterized by the high capacity to engulf antigens, low expression of co-stimulatory molecules, such as CD80, CD86 and CD40, and limited secretion of cytokines[115,116].

Different stimuli associated with danger-associated molecular patterns (DAMPs) and pathogen-associated molecular patterns (PAMPs) can induce the activation and maturation of DCs. Activated DCs are characterized by a reduced or lower antigen capture activity, an increased expression of major histocompatibility complex II (MHC class II) and other co-stimulatory molecules mentioned before, a high ability to produce cytokines and an active migration to draining lymph nodes to activate T cells[117,118]. DCs in active state are potent inducers of T cell responses and are long considered as a critical component of antitumor immunity (reviewed on [119]). T cell priming predominantly occurs in tumor-draining lymph nodes, although some naïve T cells might also be primed within the tumor microenvironment. Even if antigen-carrying tumor cells can reach lymph nodes by themselves in certain experimental setups or, naturally, during metastasis, priming of T cells in tumor-draining lymph nodes from progressively growing non-invasive tumors requires the delivery of tumor antigens to tumor-draining lymph nodes by migratory cDCs[120].

1.3.1.1 DCs subsets

Since the initial identification of DC by Ralph Steinman[121] in the mouse spleen, methodological advances have revealed the heterogeneity of this subsets. Historically, DCs have been classified based on their location (migratory and resident, or Langerhans specialized in skin); based on their phenotype (flow cytometry analysis allowed to identify several subsets)[122]; or based on their ontology[123]. Recently, transcriptome signatures based on scRNAseq have increased the resolution among subsets and also the heterogeneity inside the DC subsets[83,124–126]. Currently there is no consensus regarding the number and phenotype's characteristics for all DCs subsets. Some authors proposed that classification based on scRNAseq could generate a misleading classification because this technique captured a snapshot of the DCs' transcriptional

state which is dynamic in myeloid cells[127]. Also, the transcriptional state could be modified between healthy and disease conditions.

For this reason, classification based on combined techniques would allow a better understanding regarding the heterogeneity of DCs subsets. In the next paragraphs a classification based on ontology and recent data from scRNAseq and flow cytometry in healthy conditions in mice will be presented. There is a unanimity regarding two major DC subsets: plasmacytoid and conventional (or classical) DCs[123,124,127–129]. However, there is no consensus regarding the nomenclature and features of DC3, mono-derived DCs or CCR7$^+$ DCs[124,125,130].

- Plasmacytoid DC

pDCs represent a small fraction of DCs that share the origin with the classical DCs[131]. They are considered as resident DCs in lymphoid tissues but they can also move to the blood circulation and be recruited to peripheral tissues during inflamation[132]. pDCs express low levels of the integrin CD11c and MHC class II[128], and express high levels of endosomal nucleic acid-sensing Toll-like receptors (TLRs) TLR7 and TLR9, which recognize single-stranded RNA and unmethylated CpG motif-containing DNA, respectively. pDCs specialize in the recognition of virus-derived products as viral nuclei acids and they respond by producing high amount of type I and III interferons[133]. Similar to classical DCs, pDCs express flt3 receptor and are strictly dependent on its ligand to develop[134].

- Mono-derived DC

moDCs are dendritic cells that differentiate from monocytes during inflammation. Monocytes are able to migrate into the inflammatory site and differentiate into DC with the capacity to produce IL-12[135]. In mice, moDCs share expression of CD11c conventional DCs but uniquely express FcγR1 (CD64) as well as the protein tyrosine kinase MerTK and CD88[136]. In melanoma, mo-DCs can migrate to the TME and act as antigen-presenting cells and activating T cells[137]. Tumor cells secrete CCL2 that plays a chemotactic role during moDCs recruitment. However, moDCs can differentiate in an immunosuppressive subset expressing PD-L1 in the TME due to the presence of stromal TGF-β1 and IL-6.

Upon lipopolysaccharide stimulation moDCs produce more IL-10 than IL-12, failing during antigen presentation an suppressing T cell proliferation[135].

- Conventional DC

cDCs is a heterogeneous subset that can be also subdivided into many subsets. The exact number of subsets in each tissue is largely dependent on the ‘‘standard’’ practice for that tissue[138]. They can be found in lymphoid and non-lymphoid tissues. cDCs have a superior capacity to sense tissues from injuries, allografts, pathogens, cancer cells and to capture antigens from the environment; in addition, they have a major role during self-tolerance[139]. This subset has an enhanced capacity to migrate to the lymph node where they excel in the antigen presentation to T cells[140]. A common feature that all cDC subsets share is that they depend on the growth factor FMS-like tyrosine kinase 3 ligand (FLT3L) to develop[141] and in the expression of the transcription factor Zbtb46[142]. In lymph nodes resident cDCs express lower levels of MHC-II and higher levels of CD11c than migratory cDCs. Similarly, in peripheral tissues, cDCs presumed to be ready to migrate can be distinguished from their resting counterparts by increased levels of activations markers such as CD80, CD86, and CCR7[143]. The conventional DCs divided in two main subsets: type 1 conventional DCs (cDC1) and type 2 conventional DCs (cDC2); additionally, a third subset has been described in many reports, under different names (DC3, mregDC, migDCs) according to the tissue or the transcriptional signatures under healthy or disease conditions.

1. cDC1

cDC1s excel at cross-presenting exogenous antigens (including tumor antigens) to $CD8^+$ T cells and are key cells for the generation of cytotoxic effector T cell responses. cDC1 abundance has been recently associated with increased survival in human cancer as renal cell cancer and NSCLC[17] and in different preclinical models[144–147]. cDC1 is a critical subset for the spontaneous rejection of immunogenic cancers and for the success of T cell-based immunotherapies[148]. Beyond the role of antigen presenting cells, cDC1s have the ability to enhance the local cytotoxic effect of T cells and NK through the secretion of cytokines and chemoattractants[149,150].

The differentiation into cDC1 depends on the transcription factors BATF3, IRF8, and ID2[151]. cDC1s exclusively express the chemokine receptor XCR1 and the C-type lectin receptor DNGR-1/CLEC9A[148]. Expression of the integrin αE (CD103) is also commonly used as an additional marker to identify cDC1 in mouse tumors[152]; however, the expression of this marker has been reported also in tumor-reactive $CD8^+$ T cells[153]. cDC1s express higher amounts of Flt3 than cDC2 and have lower expression of CD11b, Sirpα[122].

2. cDC2

cDC2 represents the second major subset of conventional DCs and is more heterogeneous than cDC1. This subset depends on IRF4 as transcriptional factor for its development. They are characterized by the expression of $CD11b^+$ and $CD172^{+}$[124,154], and they primarily present antigens through MHC class II to $CD4^+$ T cells[155]. cDC2s in tumor comprise a significantly larger portion[156] but the role during tumor control is less explored. Binnewies *et al.*, have shown using the melanoma preclinical model B16 that a subset of cDC2 targets Treg suppression and it is a necessary population for directing antitumor $CD4^+$ T cell immunity. Additionally, cDC2 abundance in the human TME may act as a biomarker for ICB responsiveness[157]. Recently, it was shown that cDC2 expressing interferon stimulated genes are able to cross-dress tumor-derived antigens-MHC class I complex and cross-present tumor antigens to $CD8^+$ T cells[158].

3. Debated subsets

In the last years many studies from clinical data and using mouse preclinical model have reported new DCs subsets. Zilionis *et al.*, described a third subset of DC that called DC3 found in human and mice. This subset has an exclusive gene signature that shows an "activated" state and shares genes with monocytes and macrophages[124]. This subset has also been described in human samples as antigen presenting cells that activates $CD8^+$ T cells[159]. Maier *et al.*, have described a third subset of DC called as 'mature DCs enriched in immunoregulatory molecules' (mregDCs), owing to their expression of immunoregulatory genes and maturation genes[125]. Gerhard *et al.*, have proposed that DC3 and mregDCs are the same subset of tumor infiltrating DCs[160]. Dixon *et al.*,

described a DC subset expressing CCR7 with high migratory capacity as a responsible for the tumor control after TIM3 ablation[161].

In the last section, the bibliography and current knowledge on DC subsets have been reviewed. A common factor among them is their importance during the orchestration of an effective immune response against tumors. The role of conventional DCs in the tumor microenvironment will be covered in the next section.

1.3.1.2 Role for DCs in the TME

The TME is composed of non-neoplastic cells that include blood vessels, immune cells, fibroblasts, extracellular matrix, cytokines, chemokines, and other active compounds[162,163]. In particular, tumor-infiltrating myeloid cells consist of granulocytes and mononuclear phagocytes, which have been shown to contribute to tumor control, immunoediting and response to treatment[164,165]. DCs represent one of subset of tumor infiltrating mononuclear phagocytes.

Particularly, cDC1s are professional antigen presenting cells that are crucial for T cell priming during the antitumor adaptive immunity[148]. cDC1s are necessary for tumor antigen trafficking to draining LNs, antigen cross-presentation, and $CD8^+$ T cell activation[122,166]. cDC1s have also been shown to recruit $CD8^+$ T cells into the TME through the secretion of chemoattractant as CXCL9 and CXCL10[150].

The impact of cDC1 on anti-tumor immunity has been directly demonstrated using transgenic mice strain in which this subset is absent. Mice deficient in cDC1 (*Batf3*$^{-/-}$) or lung cDC1 deficient mice (*irf8*$^{\Delta DC}$) showed an increased tumor burden and reduced number of $CD8^+$ T cells producing interferon IFNγ and tumor necrosis factor TNFα, in KP model[111]. At the same time, models with mutated *Pten* in $CD207^+$ cells[114] led to a threefold expansion of cDC1 number in lung and a lower tumor burden, associated with higher numbers of $TNF\alpha^+$ $IFN\gamma^+$ $CD8^+$ T cells[111].

Presence of human cDC1 equivalent correlates with an increased overall survival in human tumors[167–170]. Preclinical studies support that elevating cDC1 numbers in tumors by expansion or recruitment leads to accelerated anti-tumor immunity, even in absence of added stimuli to promote cDC1 activation[17,144,148].

In the TME there are several molecules that activate cDC1. In particular, therapies targeting the tumor cell as chemotherapy or radiotherapy produced the cell elimination through immunogenic cell death. This type of cell death generates the accumulation of several molecules in the TME such as tumor-derived DNA, ATP, or high mobility group box 1 (HMGB1) that are able to activate cDC1. In brief, tumor-derived DNA can activate cGAS-STING pathway in cDC1 leading the induction of type I interferon[171]. ATP can activate cDC1 by the activation of NOD-receptors family[172] and HMGB1 activates DCs through TLR4 pathway[173]. All these processes lead to the activation of cDC1 with the subsequent IL-12 production, that has a major role in NK and T cell recruitment and activation[174]. Activated cDC1 also secrete CXCL9 and CXCL10 that recruit tumor-specific $CXCR3^+$ $CD8^+$ T cells[126] that contributes to the tumor control.

1.3.1.3 cDC1 recruitment in tumors

Despite the major role of cDC1 during the orchestration of the immune response against cancer, this subsets is under-represented in solid tumor and constitutes a minority across the intratumoral immune cells[122,144]. The mechanisms that determine cDC1 abundance in tissue can involve chemotaxis for the recruitment and retention in the TME.

The main source for chemokines in the TME is the tumor cells themselves. They produce, CCL2[175], CXCL1[176], CCL20[177] and CXCL5[178] and other chemokines that recruit various stromal cells into the tumor that support tumor growth; some immune subsets recruited by these chemokines are monocytes, neutrophils, macrophages and Tregs[179]. Preferential production by tumor cells of chemokines that attract pro-tumorigenic immune cells and the activation of oncogenic signaling might be one reason for the low cDC1 abundance observed in progressing tumors. In this sense, Spranger *et al.*, have shown that in BRAF tumors deficient for the WNT/β-catenin signaling pathway, tumor cells start producing CCL4 that increase the recruitment of cDC1 in the tumor[180].

However, tumor cells are not the only subset involved during the recruitment of cDC1, immune cells also play an important role. Two independent groups have shown that CCL5 and XCL1 produced by NK cells lead to the accumulation and positioning of cDC1 in the tumor creating clusters of cDC1-NK cells. [149,168]. Studies on melanoma and head

and neck squamous cell carcinoma provided evidence that link the levels of Flt3L in the TME produced by NK cells, and the abundance of cDC1[168,181].

Regarding NSCLC, Lavin *et al.*, showed that numbers of cDC1 are reduced in lesions compared with adjacent healthy lung tissues[162] in patients, and in mouse preclinical models[146]. Recent studies performed in the preclinical NSCLC mouse model, KP (mice with mutations in *Kras* and *p53* spontaneously develop lung lesions with features of NSCLC[41]), showed that cDC1 abundance declines in the tumor TME[182].

Based on the data presented above, cDC1 mobilization might represent a strategy to generate an efficient immune response against cancer.

1.3.2 Immunoregulatory signals from the TME thar impair cDC1 function

The TME consist in a challenging environment for immune cells. In solid tumors hypoxia[183], competition for nutrients[184] and regulatory soluble molecules generate an adverse environment where the survival and activated phenotypes in cDC1 are dampened (Figure 1.5).

Immune cells present in the TME often include cells that have acquired immunosuppressive phenotypes[185]. In a melanoma preclinical mouse model intratumoral DCs appeared to be immature and they did not present tumor-derived antigen, as they were unable to induce the proliferation of tumor-specific $CD4^+$ and $CD8^+$ T cells[186]. DCs exposed to IL10 produced by macrophages lost the capacity to produce IL-12 in breast cancer[187]. Previous data from our lab showed that DC-tumor cell co-culture impaired the DCs' functions through lactic acid[188]. In addition, prostaglandin E2 produced by tumor cells acts on both NK cells and cDC1s suppressing production of cDC1 chemoattractants[149]. Studies on cDC1 derived from PBMC in patients with NSCLC showed that cDC1 co-cultured with tumor cells modulated the expression of pro- and anti-inflammatory cytokines. The co-culture between cDC1 and tumor cells leads to an increase in IL-6, IL-27 and IL-10, and the decrease of IL-12 and IL-23[116]. Further, the co-culture leads to the downregulation of the expression of activation molecules, such as CD40, CD80, CD86, and HLA-DR, on cDC1[116].

In TME the metabolic competition and glucose restriction are predominant and have been shown to cause major bioenergetic deficiencies in T cells[189]. However, the potential consequences of nutrient limitation in cDC1 metabolism and function remain not fully understood. The fact that DCs undergo substantial metabolic reprogramming during activation is well established[189], and this process demands high amounts of glucose for protein synthesis and secretion, characterized by an increase in glucose uptake and enhanced glycolysis[190]. Therefore, competition for glucose in the TME might dampen the capacity of cDC1 to secrete chemokines and cytokines after activation in tumors[148]. Further studies addressing the impact of metabolic reprogramming in cDC1 on TME are needed to elucidate its role during the orchestration of antitumor immunity.

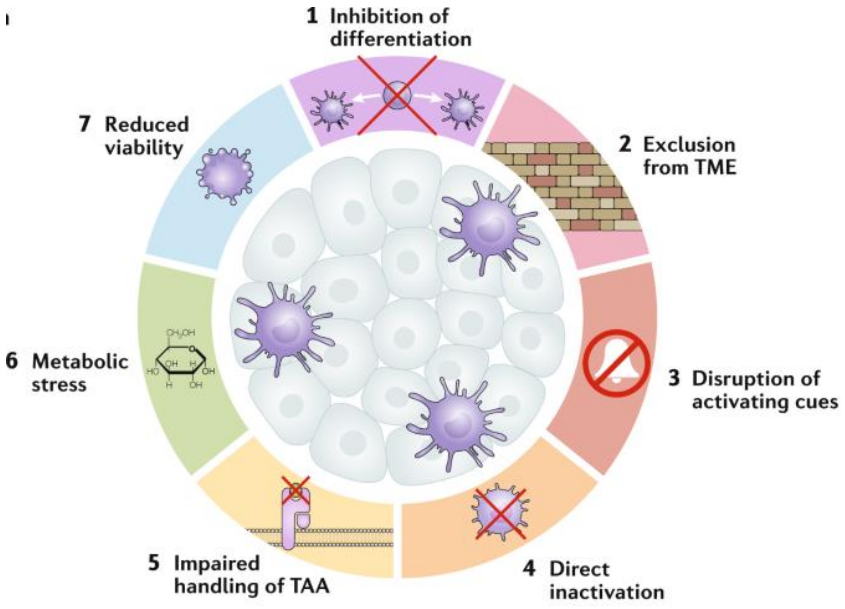

Figure 1.5| Immunoregulatory signals from the TME that impair cDC1 function. Key DC-features that tumor cells develop to perturb DC functions, resulting in insufficient T cell activation. (1) Inhibition of differentiation due to the decrease in specific growth factor for cDCs. (2) Physical exclusion from the tumor or by reducing the secretion of chemoattractant as CCL4. (3) Disruption of activating cues, for example by inhibiting the recognition of HMGB1 in dying cells. (4) Direct inactivation of cDCs by cytokines as IL-10 which inhibit the production of IL-12. (5) The handling, presentation, and cross-presentation of TAAs by DCs is impaired by tumors. (6) The TME change the nutrient availability producing a competition for glucose that generates metabolic stress in immune cells. (7) Tumors can also modify the immune cells viability by affecting some factors such *a*s hypoxia. The scheme was modified from Wculek *et al.*, [191].

Altogether, these results suggest that expansion of intra-tumoral DC may provide a key strategy for the induction of potent anti-tumor immunity[162]. So, therapies enhancing DC may offer a road to be explored to boost the tumor control by the immune system.

1.3.3 Enhancing DCs in tumors

DC therapy aims at eliciting a tumor-specific immune response, by loading DCs *in vitro* with tumor antigens and additional maturation stimuli.

Initial approaches to DC therapies were based on *in vitro* loading of tumor-associated antigens on DCs[192]. In first- and second-generation DC therapies, moDCs were differentiated with granulocyte-macrophage colony-stimulating factor (GM-CSF) and IL-4 and loaded with tumor neoAgs. Although DCs were able to promote T-cell differentiation and $CD8^+$ T-cell activation, without the correct maturation stimuli, this strategy showed unsatisfactory clinical results[185]. This first approach was improved using maturation cocktails, including IL-6, TNF, IL-1b, PGE2, and polyinosinic:polycytidylic acid (poly(I:C))[193], leading to FDA approval.

Next generation therapies targeted DCs *in vivo* using: Toll-like receptor ligands as LPS, Imiquimod, CpG or Poly (I:C)[194]; intra-tumoral injection of TriMix (CD40L, CD70, constitutive active TLR4) and mRNA encoding for tumor antigens in patients with stage III and IV melanoma mRNA[195], or attenuated viral agents[196–198]. Anguilles *et al.*, have reviewed the objective response of these therapies in patients with melanoma, prostate cancer, renal cell cancer and malignant glioma and they found that only 8.5% of patients had an objective response[199].

The new approaches used in preclinical studies include ICB and therapies enhancing DC[114]. It has been shown that immune checkpoint inhibitors, such as monoclonal antibodies targeting PD-1, CTLA-4 can restore tumor-specific T cell activity[16]. In addition, monoclonal antibodies targeting PD-L1 in tumor cells[200] or in dendritic cells[201,202] have shown success in treating colorectal cancer and NSCLC in mouse models[203]. Particularly, monoclonal antibodies blocking PD-L1 on DCs release B7 sequestration in cis by PD-L1, which allows the B7-CD28 interaction to enhance T cell priming[203].

1.3.3.1 Boosting and activation of cDC1 by FLT3L administration

Therapies that included the growth factor FLT3L have shown promising results improving tumor control by the immune system[144–147,204,205].

FLT3L is a DC growth factor that promotes the expansion of $Flt3^+$ primitive hematopoietic stem cells[206]. FLT3 is expressed in DC progenitor such as common myeloid progenitors and the macrophage DC progenitors[207] and remains present in terminally differentiated cDC and pDCs[152]; which suggests that Flt3-FLT3L pathway could have a functional impact on mature DCs[208]. FLT3L therapy increases and activates cDC1 infiltrating tumor and also increases the number of precursors[152].

The administration of FLT3L as a single agent was demonstrated to control the growth of some tumors as: methylcholanthrene-induced fibrosarcoma[209], C3L5 breast tumor[210], B16 melanoma, and lymphoma[211]. However, daily administration of FLT3L to treat pancreatic tumor in mice led to a 2.5-fold increase in cDC1 in the tumors, but did not impact on the tumor growth[147]. The same approach was used in healthy volunteers generating a 130-fold increase in cDC1 numbers[212].

Expanding and activating cDC1 with FLT3L, in combination with adjuvants, checkpoint inhibitors and radiotherapy was shown to improve control of genetically induced melanoma[144,213] and of various ectopic murine cancer models[214]. A synergistic effect of FLT3L and Toll-like receptor agonists[215] improves the effect of PD-1 and PD-L1 therapies[144,216].

In highly suppressive and poorly infiltrated pancreatic cancer in mouse model, the administration of FLT3L in combination with αCD40 rescued cDC1 abundance and potentiated their maturation. This boosts $CD8^+$ T cell activation and improves response to vaccination and immune control of tumor outgrowth[146,217].

Recently, Schenkel *et al.*, have tested a combinatorial therapy including FLT3L and anti-CD40 in a preclinical mouse model of lung cancer[218]. They have observed that the therapy increased the number of migratory cDC1 in the draining lymph node 10-fold more in comparison with control group. Moreover, the therapy produced an increase in the CD86 expression but not in PD-L1 expression in migratory cDC1; suggesting that the therapy restores the number and boosts the quality of migratory cDC1. In addition, the authors evaluated whether the increased number of migratory cDC1 improved the anti-tumor $CD8^+$ T response. They have shown that combinatorial therapy increased the number of tumor-specific $CD8^+$ T cells in the draining lymph node and a 3-fold increase

in the number of SlamF6^{+}TCF1^{+} tumor-specific CD8^{+} T cells in tumor-bearing lungs. Interestingly, they observed that the therapy reduced in 50% the tumor area in tumor bearing lungs in comparison with the control group[218].

Interestingly, a proof of concept has been also provided that CD8^{+} cell specific for a model antigen and engineered to express Flt3L potentiate activation of bystander antigens by epitope spreading[219]. A study in a colorectal model illustrated the potential of enhancing DC therapy in low mutational burden tumors and indicated the importance of orthotopic models for preclinical immunotherapy testing[220].

Currently, there are 45 clinical trials that involve FLT3L to treat cancer of which three are focused on treating NSCLC. These studies combine FLT3L with radiotherapy or in combination with anti-CD40 agonists[221].

The dynamic of cDC1s in tumor microenvironment is still not fully understood; especially how their phenotype affects neoantigen presentation to lymphocytes to activate an effective tumor immune response. Besides, there are few studies combining DCs therapies with ICB; however, these few demonstrated that even in cold tumors such as glioblastoma, by boosting DCs, tumors become more infiltrated by T cells and respond well to ICB therapies[222,223]. Therefore, it is essential to characterize the role of DCs in neoantigen presentation in the tumor microenvironment; and particularly to analyze the effect of boosting DCs on tumor burden and anti-tumor immune response.

2. State of art

Taken together, the concepts summarized above provided evidence for the active role of cDC1 during the orchestration of the immune response against tumors. Furthermore, it has been shown in murine ectopic tumor models that enhancing cDC using FLT3L allowed the induction of potent antitumor immunity.

However, this evidence has been obtained using preclinical models harboring surrogate antigens that do not reflect the heterogeneity and multiplicity of tumor-associated antigens. In particular, many studies used a single, strong antigen such as ovalbumin that elicits a potent response and does not reveal the complexity behind the immune response against a repertoire of varied neoAgs in tumors.

Here I aimed to fill this gap by generating a hypermutated variant of the KP model, with a broad tumor neoantigen content, and we used this model to study how cDC1s regulate responses to multiple neoAgs. In addition, I wanted to explore the molecular changes that occurred due to DC therapy in lung tissues. Particularly, how the DC therapy modified immune subsets that populate the lung and their impact in the clinical progression of the disease.

The question was addressed by following specific aims as mentioned below:

- Characterization of neoantigen content in parental KP cells and in *Mlh1 depleted* KP cells.
- *In vivo* characterization of the immunogenicity of neoAgs expressed in lung tumors in wild type and cDC1 deficient animals.
- Studying the responsiveness to ICB in a neoantigen-enriched lung cancer model.
- Exploring the role of cDC1 mobilization by a therapy containing FLT3L to the tumor microenvironment, during the generation of antitumor immune responses
- Characterization of changes in the composition of the tumor microenvironment after DC-enhancing therapy by scRNAseq.

3. Material and methods

3.1 Mice

Mice were housed at the ICGEB animal house facility. Wild type C57BL/6JOlahsd were purchased from ENVIGO and kept in our facility under inbreeding conditions. Batf3$^{-/-}$ mice were kindly donated by Dr. Christian Lehmann (Erlangen university hospital) and maintained in our facility on a pure C57BL/6J background. XCR1^{Venus} mice were generated as described in [224], and kindly provided by Professor Kastenmuller, (Wurzburg Institute of system Immunology). XCR1^{DTA} mice were generated by Mattiuz *et al.,* [225] and kindly provided by Dr. Marc Dalod. The study was approved by International Centre for Genetic Engineering and Biotechnology (ICGEB) board for animal welfare and authorized by the Italian Ministry of Health (approval number 1133/2020-PR, issued on 12/11/2020). Animal care and treatment were conducted with national and international laws and policies (European Economic Community Council Directive 86/609; OJL 358; December 12, 1987). All experiments were performed in accordance with the Federation of European Laboratory Animal Science Association (FELASA) guidelines institutional guidelines and the Italian law.

3.2 Tumor cell lines

The KP line has been isolated from primary lung tumors of C57BL/6 KP mice (K-ras$^{LSLG12D/+}$; p53$^{fl/fl}$ mice)[226]. The line was kindly provided by Dr. Tyler Jacks (Massachusetts Institute of Technology, Cambridge, USA), and used previously[178,182]. All cell lines were maintained under standard conditions.

3.3 Genome editing

Mlh1 knockout cell were generated by Crispr Cas9 using two single guide RNAs (sgRNA) targeting *Mlh1* exon 5 as described by Germano *et al.,* [107]. sgRNAS were cloned into pZac2.1-U6sgRNA-CMV-ZsGreen with *BsbI* restriction enzyme to allow cloning of the guide under the control of U6 promoter. KP cells were transiently transfected with the plasmid containing the sgRNA sequences and a second plasmid coding for Cas9 (pSpCas9(BB)(PX458)) using Lipofectamine 3000 (Invitrogen), following the manufacturer´s instructions. ZsGreen^{+} cells were cell sorted and single clones were tested for Mlh1 expression. KP^{ctrl} cells derive from cells transiently transfected with only (pSpCas9(BB)(PX458).

3.4 Western Blot

Cellular proteins were obtained by whole cell lysis using radioimmunoprecipitation assay buffer (50 mM Tris HCl, 150 mM NaCl, 1.0% (v/v) NP-40, 0.5% (w/v) Sodium Deoxycholate, 1.0 mM EDTA, 0.1% (w/v) SDS and 0.01% (w/v) sodium azide at a pH of 7.4), containing proteinase inhibitor (Sigma-Aldrich). Protein concentration was measured by BCA assay (Pierce). Proteins from KP, KP^{ctrl} and KP KO lysates were analysed by SDS-PAGE. Membranes were blocked with 3% BSA-TBS for 2 hours and were incubated with an appropriate primary antibody anti-MLH1 (EPR3894, Abcam) or anti-Tubulin (Clone 11H10, Cell signaling), overnight at 4°C. After rinsing, the membranes were incubated with HRP-conjugated secondary antibodies for 45 minutes. Finally, membranes with incubated with chemiluminescent signal was developed using ECL and imaged by ChemiDoc Imaging System (Biorad).

3.5 In vitro cell line proliferation rate

To test the proliferation rate of the edited cells, crystal violet assay[227] was performed. For this, $3x10^3$ cells from KP, KP^{ctrl} ($Mlh1^{wt}$) and KP KO clones were seeded in 96-well plates and kept for 6, 24 and 48 hours. Cells were fixed with 1% paraformaldehyde and stained with crystal violet following the manufacturer´s instructions. Cells were washed, and the dye was solubilized by adding 1% sodium dodecyl sulphate (Sigma-Aldrich). Optical density was measured at 570 nm using microplate reader (Biorad). Proliferation rate was calculated as fold change of the optical density found after 6 hours, consider as day 0.

3.6 Whole Exome Sequencing data analysis

Genomic DNA (gDNA) was extracted from C57 spleen and KP, KP^{ctrl} and KP KO cell lines using DNA Blood and cell culture kit (Qiagen) following the manufacturer´s instructions. Whole-exome sequencing (WES) was performed at Macrogen Europe as follow: Next Generation Sequencing (NGS) libraries were prepared using SureSelectXT Library Prep Kit and sequenced on Illumina platform as paired-end 151bp reads. FastQ files provided by Macrogene Europe were analyzed using a bioinformatics pipeline previously published[228]. On average, we obtained 99% of the exome region covered by at least one read and a median depth of 98x on sequencing data. Mutational calling was performed using the comparison strategy: mouse germline alterations were subtracted by using

normal DNA sequenced from the spleen of C57 mice. We selected only variants supported by 5 or more altered reads.

3.7 RNA sequencing analysis

RNA was extracted from KP, KP^{ctrl} and KP^{neo} cells using RNeasy Mini kit (Qiagen) and sent to Macrogen Europe that generated sequencing data: TruSeq Stranded mRNA LT Sample Prep Kit was used for generating NGS library which were then sequenced on Illumina platform as paired-end 101bp reads. FastQ files produced by Macrogene Europe were analyzed as previous published[229]. In brief, data was aligned using MapSplice2[230] and mm10 assembly as reference genome. The generated BAM files were post-processed to translate genomic to transcriptomic coordinates and used as input to RSEM[231] for gene expression quantification employing GENCODE vM9 as transcript annotation.

3.8 Neoantigen prediction analysis

The neoantigen prediction analysis was performed using a previous published bioinformatic pipeline[232] setting C57 mouse haplotypes: H2-Kb and H2-Db. Briefly, the mutational calling data, i.e., SNVs and indels, was used for generating mutated peptides of length 8-11 and then employed as input of NetMHC 4.0 software[233]. Only peptides with predicted strong binding affinity (%rank <= 0.5) were considered. To further filter out predicted neoAgs based on expression level we performed the mutational calling also on the BAM files generated from RNA sequencing data. We set 3 as the minimum number of altered allele and matched the results with those obtained by WES.

3.9 Pathway enrichment analysis

GSEA was used to compare KP^{ctrl} and KP^{neo} cell lines. Log_2FC-ordered gene list was used to retrieve gene set enrichment using fgsea package in R. Gene sets representing relevant biological processes were selected from Reactome and Hallmarks from MsigDB database.

3.10 Heterotopic and orthotopic tumor growth studies

To establish subcutaneous tumors, 5×10^5 cells were injected in the right flank of 8-12 weeks female mice. For the orthotopic model cells, 5×10^4 cells were injected intravenously. To assess growth in the subcutaneous model, measurements were collected at day 0, 10, 12, 15, 18 and 21 according to the experiment using a caliper. Tumor size was calculated as V=d2×D/2 (where, d = minor tumor axis and D = major

tumor axis) and reported as tumor mass volume (mm^3 of individual tumor volume). Lungs were harvested at two time points corresponding to early lesions (9-12 days post tumor induction, tumor area < 10% total lung area) or advanced tumors (21-25 days post tumor induction, tumor area > 10% total lung area). To evaluate tumor burden in lung tissues, organs were harvested, fixed in formaldehyde 10% and paraffin embedded following standard procedure. Consecutive sections every 200 µm were dewaxed and rehydrated and stained with the H&E (Bio-Optica, Milano Spa). Ilastik software was trained to automatically detect and segmentate tumor nodules. The area of tumor nodules was quantified over consecutive sections and averaged (3 sections/sample). Measurements and automatic thresholding were performed using Image J. The area occupied by tumor nodules was expressed as a function of the total lung lobe area.

3.11 Mouse treatments

3.11.1 Immune checkpoint blockade

For subcutaneous tumors, mice were treated intratumorally with either 20 µg α-PD-L1 (clone 10F.9G2, Bioxcell) or with 20 µg of rat IgG2a isotype control antibody (clone 2A3, Bioxcell) every four days post tumor inoculation. In the orthotopic KP model, mice were treated intraperitoneally with α-PD-L1 (200 µg) every three days, for early endpoints starting from day 3 and for late endpoint starting from day 7. For control, mice were injected with rat IgG2a isotype control antibody.

3.11.2 CD8 T cell depletion

Mice were injected intraperitoneally with either 200 µg of α-CD8 (YTS169.4, Bioxcell) or rat IgG2a control antibody (LTF-2, Bioxcell) every three days post tumor implantations subcutaneously or intravenously. Tumors were harvested after 21 days and tumor-bearing lungs after 14 days after injection.

3.11.3 Intratumoral therapy for subcutaneous tumors

Tumor-bearing mice were treated with a combination of 10 µg of rhuFLT3L (Celldex), 50 µg high molecular weight Poly (I:C) and 20 µg α-PD-L1 mAb. A control group of tumor-bearing mice were injected with 20 µg rat IgG2a isotype control (clone 2A3, Bioxcell). Both groups were injected intratumorally every three days post tumor injection.

3.11.4 Treatments for lung tumor-bearing mice

Mice harbouring KP^{neo} lung-tumors were divided into four groups that were treated intraperitoneally as follows: the first group with 100 µg rat IgG2a control isotype (clone 2A3 and LTF-2, Bioxcell), second group received 200 µg anti-PD-L1 (clone 10F.9G2), the third group received FL/αCD40 that combines 100 µg αCD40 (clone FGK4.5FGK45, Bioxcell) and 30 µg of rhuFLT3L (Celldex), and the last group received a combinatorial therapy that includes FL/αCD40 and αPD-L1. The schedule for the administration of the therapies are summarizes in the scheme (Figure 3.1).

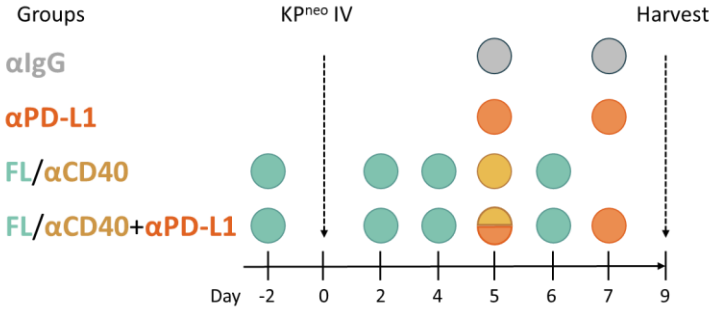

Figure 3.1| Treatment schedule for mice bearing KP^{neo} tumors. Wt mice were intravenously injected with KP^{neo} tumors and treated with control isotype (αIgG), anti-PD-L1 (αPD-L1), FLT3L and αCD40 (FL/αCD40), or FL/α-CD40 and α-PD-L1 (FL/αCD40+αPD-L1) following the scheme.

3.12 Tissue processing

Tumor bearing lungs were harvested from mice after cardiac perfusion with PBS. Subcutaneous tumors were collected from mice and weighed. Both tumor tissues were physically dissociated and digested with a mix containing 0.1% Collagenase II and 250 U/mL DNAseI. Enzymatic digestion was stopped by adding 10 mM EDTA and pieces of tissues were smashed in a 70 µm cell strainer to obtain a single cell suspension. Red blood cells were lysed using ACK Buffer and single cell suspension were resuspended in the appropriate buffer according to the experiment.

For histological analysis, tumors were harvested and fixed in 4% paraformaldehyde (PFA), lungs were intratracheally perfused with 1% PFA, fixed in 4% PFA, both tissues cryopreserved in 30% sucrose in PBS overnight. Tissues were embedded in a frozen tissue matrix following standard procedure and sectioned in 5 µm sections in cryostat. To assess tumor burden, lung tissues were harvested, fixed in formaldehyde 10% and paraffin embedded following standard procedure.

3.13 Immunofluorescence staining

Before staining, tumor tissues were fixed in 4% PFA for 10' at room temperature (RT). Washed twice with PBS and incubated in blocking buffer containing 5% mouse normal serum for 30' at RT in a humidified chamber. Sections were incubated with a primary antibody rat anti-mouse CD8 (4SM15, Invitrogen) in blocking buffer, overnight at 4°C. After staining, primary antibodies were detected using chicken anti-rat conjugated with Alexa488 (940882, Invitrogen) secondary antibody for 1 hour at RT and nuclei were stained with Hoescht 33342 (H3570, Invitrogen) for 15' at RT. Sections were washed between steps with PBS.

Images were acquired using a confocal microscope Zeiss LSM 880. Images were analyzed using ImageJ software.

3.14 Immunohistochemistry staining

To assess tumor burden, paraffin embedded tissues were sectioned every 200 µm in 5 µm slices. Sections were dewaxed and stained with hematoxylin and eosin using the Bio-optica kit, following the manufacturer´s instructions. Images were acquired using Leica microscope. Ilastik software was trained to automatically detect and segmentate tumor nodules. The segmented images were analyzed using ImageJ software and tumor burden was normalized with the total lung area.

For $CD8^+$ quantification, sections were dewaxed and rehydratated. Tissues were incubated with 10 mM Citrate Buffer for 10´ at 96°C to perform antigen retrieval. Slices were incubated with H_2O_2 for 10´ at RT to block endogenous peroxidases and then blocked in 10% rat normal serum for 30' at RT. The tissue sections were staining overnight with rat anti-mouse CD8 (4SM15, Invitrogen) in 0.1% Tween-PBS. Sections were washed with PBS and incubated with a rat anti-mouse HRP. Detection was performed using the ImmPRESS polymer detection system (Vector Laboratories), according to manufacturer's instructions. Tissues were counterstained with hematoxylin. Images were acquired using a Leica DFC450 C microscope and $CD8^+$ T cells quantification was done using ImageJ software and the number of CD8 was normalized with the tumor area.

3.15 Flow cytometry and cell sorting

Single cell suspension was washed in FACS Buffer (1% BSA in PBS) and incubated with αCD16/CD32 (BioLegend) to block the FcR binding sites, for 10´ on ice. Viability of cells was assessed by staining with Live/Dead Fixable Aqua Staining (Life technologies), 30´ in PBS on ice. For cell surface staining cells were resuspended in antibody-containing staining buffer for 45´ on ice. The primary antibodies used are listed in the table 1. Cells were fixed in 1% PFA in PBS, or in Cytofix/ Cytoperm solution (BD Biosciences) following manufacturer's instructions. For intracellular staining, cells were incubated with anti-IFNγ, anti-TNFα, anti-GzmB in permwash buffer for 1 hour. For intranuclear staining cells were fixed using FoxP3 staining Buffer (eBiosciences) following the manufacturer´s instructions and cells were stained with anti-Ki-67 for 1 hour at 4°C. Cells were washed and incubated with anti-rabbit Alexa 488 antibody for 30´ at 4°C.

Table 1. List of fluorescent-conjugated primary antibodies used in flow cytometry staining.

Antibodies Flow cytometry		Source	Identifier
B220	FITC	BioLegend	103206
CD11b	BV421	BioLegend	101251
CD11c	BV785	BioLegend	117335
CD19	FITC	BioLegend	115505
CD3	PercPCy5.5	BioLegend	100328
CD3	FITC	BioLegend	100305
CD4	BV785	BioLegend	100453
CD44	PE	BioLegend	103007
CD44	FITC	BioLegend	103005
CD45	APC/Fire™ 750	BioLegend	103154
CD62L	BV650	BioLegend	104453
CD8	APC	BioLegend	100712
CD8	BV605	BioLegend	100743
GzmB	Alexa fluor 647	BioLegend	515405
IFNγ	PE	Biolegend	505808
Ki-67	Clone D3B5	Cell Signaling	12202s
MHCI	PE	BioLegend	116607
MHCII	Alexa fluor 700	BioLegend	107622
NK1.1	FITC	BioLegend	108705
PD1	BV421	BioLegend	135221
SiglecF	PercPCy5.5	BD	565526
TCF-1	PE	Cell Signaling	14456S
TNFα	FITC	BioLegend	506303
XCR1	BV650	BioLegend	148220

Absolute cell count was performed by adding TrueCount Beads (Biolegend) to the samples following manufacturer's instructions, or by multiplying the frequencies into the number of viable cells. Viable cells number was obtained by counting cells with trypan blue (Invitrogen). All data was acquired using FACS Celesta (BD) and analyzed using FlowJo (Tree Start, Inc).

Cells were gated on their size and granularity; doublets and dead cells were excluded. For lung and tumor tissue cells were gated on $CD45^+$ and different populations were defined as follows:

- T cells: $CD3^+$
- $CD8^+$ T cells: $CD3^+$ $CD8^+$ $CD4^-$.
  Effector memory: $CD44^+CD62L^-$.
  Activated: PD-1^+ or IFNγ^+ or TNFα^+.
  TCF-1^+PD-1^+.
  Proliferating: Ki-67^+.
  Effectors: $GzmB^+$.
  TCF1^-GzmB^+.
- Myeloid cells: Lin^-(including CD3, CD19, NK1.1, B220, Ly6C, Ly6G and F4/80).
  cDC1: $CD11c^+$ $MHCII^{high}$ $Xcr1^+$ $CD11b^-$.
- Tumor cells: CD45-.

For total tdLN cells, the same markers described above were used with the exception of CD45.

For cell sorting, single cells suspension was incubated with α-CD45-APCFire as described before. Live/Dead Fixable Aqua Staining (Life technologies) to assessed cell viability. $CD45^+$ cells were isolated using ARIA Cell Sorter (BD) and number of cells were counted with trypan blue before processing for scRNAseq analysis.

For cell sorting, single cells suspension was incubated with α-CD45-APCFire as described before. Live/Dead Fixable Aqua Staining (Life technologies) to assessed cell viability. $CD45^+$ cells were isolated using ARIA Cell Sorter (BD) and number of cells were counted with trypan blue before processing for scRNAseq analysis.

3.16 CD8⁺ T cell isolation

Single cells suspension from tumour-bearing lungs described previously were used for $CD8^+$ T cells sorting using immunomagnetic sorting using $CD8\alpha^+$ T cell isolation kit (Milteny) following the manufacturer's instruction. Purity was checked by flow cytometry. Isolated $CD8^+$ T cells were resuspended in Trizol (Ambion) and RNA extraction was performed.

3.17 Gene expression analysis by RT-qPCR

Tumor-bearing lungs or tumor masses were disrupted and homogenised using a homogenizer. RNA extraction was performed with Trizol (Gibco) following the manufacturer´s instructions. cDNA synthesis was performed using SuperscriptII and random hexamers (Invitrogen), and gene expression was determinate by qPCR using EVA Green according with the manufacturer´s instruction and specific primers. The list and sequences of the specific primers is listed in table 2. The levels of gene expression were normalized using the expression of *Gapdh* or *Gusb* as housekeeping genes.

Raw qPCR data was analyzed in excel. Briefly, the average of the median threshold cycle (Ct) for reference genes (Ct reference) or for the gene of interest (Ct GOI) was calculated for each sample in duplicate. For normalizing, the Ct reference was subtracted from the Ct GOI (ΔCt), and the ΔCt from the control condition (for example, KP^{ctrl} or KP^{neo} in WT) was subtracted from the ΔCt of the sample of interest (for example, KP^{neo} or KP^{neo} in $XCR1^{DTA}$), obtaining the ΔΔCt. When the primer efficiency was 1 the expression level (FC) of the GOI was calculated as 2^-ΔΔCt. Due to the expression levels value behave as log normal Log_2FC was plotted.

Table 2. List of specific primers used to quantify by qPCR the expression of cytokines, chemokines, and cytotoxic molecules.

Primers qRT-PCR	Sequence (5'—3')
IFNγ Forward	ATG AAC GCT ACA CAC TGC ATC
IFNγ Reverse	CCA TCC TTT TGC CAG TTC CTC
Cxcr3 Forward	GCCATGTACCTTGAGGTTAGTGA
Cxcr3 Reverse	ATCGTAGGGAGAGGTGCTGT
GzmB Forward	ACAAGGACCAGCTCTGTCCTT
GzmB Reverse	TGTCAGTTGGGTTGTCACAGC
Eomes Forward	ACCGGCACCAAACTGAGA
Eomes Reverse	AAGCTCAAGAAAGGAAACATGC
Ccl4 Forward	CTCAGCCCTGATGCTTCTCAC
Ccl4 Reverse	AGAGGGGCAGGAAATCTGAAC
Cxcl9 Forward	CCTAGTGATAAGGAATGCACGATG
Cxcl9 Reverse	CTAGGCAGGTTTGATCTCCGTTC
Il-12 Forward	TGGTTTGCCATCGTTTTGCTG
Il-12 Reverse	ACAGGTGAGGTTCACTGTTTCT
Ccl22 Forward	AAGACAGTATCTGCTGCCAGG
Ccl22 Reverse	GATCGGCACAGATATCTCGG
Ccl3 Forward	TGAAACCAGCAGCCTTTGCTC
Ccl3 Reverse	AGGCATTCAGTTCCAGGTCAGTG
Cx3cl1 Forward	GCTATCAGCTAAACCAGGAGTC
Cx3cl1 Reverse	AGAAGCGTCTGTGCTGTGTC
Cd40 Forward	ACCAGCAAGGATTGCGAGGCAT
Cd40 Reverse	GGATGACAGACGGTATCAGTGG
GusB Forward	ACTGACACCTCCATGTATCCCAAG
GusB Reverse	CAGTAGGTCACCAGCCCGATG
GAPDH Forward	AGAAGGTGGTGAAGCAGGCAT
GAPDH Reverse	CGAAGGTGGAAGAGTGGGAGT

3.18 Neoantigen- specific T cell response

Bone marrow dendritic cells (BMDCs) were obtained by bone marrow differentiation in FLT3L-containing medium for 7 days and were loaded with 2 µM peptides (Neo1, Neo3, Neo5, Neo8, Neo11, Neo16 or SIINFEKL) in the presence of 0.1 µg/mL LPS for three hours. 1 x10^4 loaded-BMDCs were co-cultured with 1 x10^5 total tdLN cells from tumor bearing mice or healthy mice. After 5 days IFNγ levels was measured by ELISPOT or in the supernatant by ELISA. For ELISA, Max Standard sets (BioLegend) were used following the manufacturer's instructions.

3.19 ELISpot assay

ELISpot-plates were activated with 35% ethanol for 2´ and coated with anti-IFNγ (4 µg/mL, BioLegend), overnight at 4°C. Plated were washed with PBS- 0.1% Tween and

blocked with RPMI for 2 hours at 37°C. BMDCs were loaded with 2 µg of selected peptides (Neo1, Neo3, Neo5, Neo8, Neo11 or Neo16) in presence of LPS (0.1 µg/mL) for three hours at 37°C. Total cells from tdLN were obtained as described above. Cells were then plated across control and peptide stimulation conditions at a concentration of $1x10^5$ total tdLN cells and $1x10^4$ loaded-BMDCs per well and gently mixed before incubation for 20 h. After overnight incubation, cells were removed, and the plates were washed and IFNγ spots detected using biotin α-IFNγ (2 µg/mL, Biolegend). Then, plates were incubated with Streptavidin-ALP (Mabtech) and spots were developed using BCIP/NBT plus (Mabtech).

3.20 Single-cell sequencing

Sample preparation. Lungs from tumor-bearing mice treated with either FLT3L and αCD40, or rat IgG2a control isotype were harvested 9 days after tumor injection. Single cell suspension was obtained using gentle MACS dissociator (Milteny), filtered using 70 µm cell strainer. Samples were incubated with α-CD45-APCFire and Live/Dead Fixable Aqua Staining (Life technologies) to assessed cell viability.

$CD45^+$ cells were isolated using ARIA Cell Sorter (BD). Single cells were prepared using Chromium Next GEM Single Cell 3' Reagent Kits v3.1 (Dual Index) (10X Genomics), following the manufacturer's instructions. In brief, 10.000 cells were loaded onto each channel and partitioned into Gel Beads in Emulsion in the Chromium instrument. Cell lysis and barcoding occur, followed by amplification, fragmentation, adaptor ligation and index library PCR. Libraries were sequenced on an NextSeq500 High 150.

3.20.1 scRNA-seq data processing and analysis

After demultiplexing, fastq files were processed employing the Cell Ranger (v 4.0.0)[234] workflow using default parameters. Reads alignment was performed to reference genome mm10 (reference version 2020-A, 10X Genomics). Gene expression matrices, containing the number of unique molecular identifiers (UMIs) for every cell and gene, were computed retaining only confidently mapped reads, non-PCR duplicates, with valid barcodes and UMIs. All downstream analyses were carried out in R environment (v 4.0.3) by the Seurat package (v 4.0.3)[235]. Gene counts were imported as a Seurat object, filtering out genes expressed in less than 3 cells. For each sample, putative doublets were identified using scDblFinder R package (v 1.4.0)[236], setting the expected doublet

rate at 5%, following 10X Genomics estimates according to the number of loaded cells. Sample count matrices were then merged and cells expressing less than 200 genes, or less than 1000 unique gene counts were discarded, along with cells with a ratio of mitochondrial versus endogenous genes expression exceeding 10% and with doublets. Raw expression data were normalized applying log2 transformation with NormalizeData function and scaled using ScaleData function, regressing on the percentage of mitochondrial gene expression and cell cycle scores, previously computed using CellCycleScoring function. Top 2000 genes with the highest standardized variance were computed using FindVariableFeatures function (selection.method = "vst"). Principal component analysis (PCA) was computed using RunPCA function with default parameters.

PCA embedding was corrected for sample batch were through the Seurat Wrapper package (v 0.3.0). When analyzing the whole immune compartment, batch effect was removed by matching mutual nearest neighbor (MNN) algorithm[237], implemented with the RunFastMNN function using default parameters. For the analysis of dendritic cells and T cells, batch correction was achieved with the Harmony algorithm (v 0.1.0)[238], by running the RunHarmony function on the first 20 PCA dimensions and theta=2. Shared Nearest Neighbor (SNN) graph was computed using the FindNeighbors function, taking as input the first 20 corrected PCA dimensions. Cell clusters were defined using Louvain algorithm with the FindCluster function. For visualization in 2 dimensions uniform manifold approximation and projection (UMAP)[239] was used. Cluster-specific genes were identified using FindAllMarkers function with option only.pos = TRUE, pseudocount.use=0.1 and logfc.threshold=1, setting a cut-off of FDR < 0.01.

3.21 Statistical analysis

All graphs and statistical analyses were conducted using GraphPad Prism (GraphPad) and R packages. All data represent mean ± SEM.

The number of biological replicates and statistical test are indicated in the figure legend. Comparison between two groups was tested by parametric Student t-test. For multiple comparison, parametric one-way analysis of variance (ANOVA) was performed followed by Tukey´s posttest. When two variables were analysed among two or more groups two-

ways ANOVA was performed, followed by Sidak´s posttest, only during the *in vitro* growth of KP KO clones Tukey´s posttest was used. *p<0.05, **p<0.01, ***p<0.001, ****p<0.0001.

4. Results

Chapter 1. Tumors with low neoantigen burden are resistant to ICB.

Nowadays ICB therapies are included in the treatments for cancer patients. These treatments provided durable responses in around 20% of patients with NSCLC. There are key parameters that correlate with the efficacy of ICB therapies; in particular, PD-L1 expression in tumor and immune cells, infiltration of immune cell generating an inflamed tumor microenvironment, and an increased mutational burden or neoantigen load in tumor cells. These parameters characterized hot tumors. By contrast, cold tumors are resistant to ICB and are poorly infiltrated by the immune cells or directly exclude the immune system[240].

Experimental models of lung cancer are instrumental to understand mechanism underlying resistance to therapy and to identify novel targets for the clinics. A valuable preclinical model of lung cancer has emerged in recent year derived from GEMMs of NSCLC that mimic the genetic and histopathological features of the human disease, the KP model[241]. These mice encode an oncogenic variation in the *Kras* gene, in which the glycine in the codon 12 was changed to aspartic acid and they are knock out for *p53*. Both genomic modifications are conditional mutations and are activated by a Cre recombinase, once these mutations are activated the mouse start to develop a hyperplasia in the lung that derives into *in situ* adenocarcinomas. Tumor cells were isolated from tumor bearing lungs, generating a transplantable cell line that generates orthotopic tumor and faithfully recapitulates the histological and genetic features of human lung adenocarcinoma[226]. KP is considered to be poorly immunogenic; however, the mutational burden and neoantigen content of KP are unknown.

To assess the basal mutational burden in KP cells we have performed whole exome sequencing (WES) and RNA-seq. We identified single nucleotide variants (median 42.51 SNVs/Mb), and 10 frameshifts present in the KP genome (Table 4.1). These mutations generated 156 neoantigens; of which, 23 are expressed epitopes predicted to bind to MHC class-I (Figure 4.1). These values mirrored those found in human samples with NSCLC[20].

Table 4.1| Mutational status of KP cell line. The mutational burden was assessed using WES and RNA-seq and single nucleotides variants and frameshifts were found. These mutations generate 156 predicted neoantigens of which 22 were expressed by the KP cell line.

	KP
SNV/Mb	42,51
Frameshifts	10
Predicted neoantigens	156
Expressed neoantigens	Aurkb-R44W-SALALVNWF
	Chst14-I172V-AGVLNNVDV
	Casc5-R950S-SAVEINNETSL
	Eif3h-F84I-LEITNCFPI
	Glod4-K14R-FKVRNRFQTV
	Glod4-K14E-FKVENRFQTV
	Hebp1-V86L-VSFALFPNE
	Lyrm5-D28G-AGYFKRRL
	Naip2-N540Y-LLYRFQLV
	Nlgn2-V210A-AAYGNVIVA
	Ovca2-T32A-KALRGRAEL
	Rnf130-V198L-LSISFIVL
	Slc30a4-G64R-VNRAHPAL
	Spg11-L217W-WIYIFNTM
	Sppl2a-A74P-LSLMNLTGTPL
	Tmem87a-F145L-FSGDLTHRLPL
	Ttc28-A616R-AAPYYEQYLRL
	Ubr3-L1686F-SVFASCLGL
	Zfp106-I1257N-SSVYPANPAVI
	Zfp106-I1257F-SVYPAFPAV
	Zfp106-C659R-ASPRNSTVL
	Zfp106-A656T-STSPCNSTVL
	Arntl2-I164M-LMGQNLFDFL

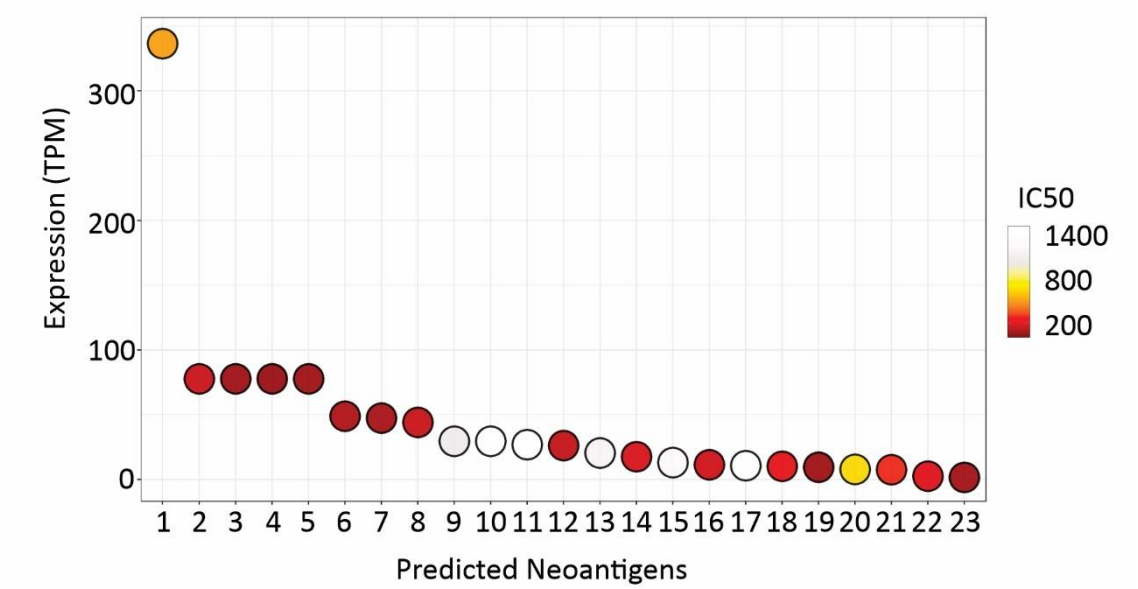

Figure 4.1| Expressed neoantigens in the KP cell line. Non-synonymous mutations were filtered by expression using RNA-seq and used to predict neoantigens using NetMHCI 4.0 package. Expressed neoantigens were plotted according to their expression levels (TPM), and color depicts the predicted IC_{50} value for each peptide-MHC class-I complex (n=3).

To investigate the impact of ICB on KP expressing this amount of putative neoantigens animals were challenged with KP intravenously and treated with anti-PD-L1 or with rat IgG2a control isotype at two different end points. The size of tumor nodules measured at two consecutive time points showed that tumors grew progressively in both treated and non-treated group (Figure 4.2 A). Analysis of the $CD8^+$ infiltrate, frequencies of effector memory T cells and IFNγ production by $CD8^+$ T cells after *ex vivo* stimulation were measured in early lung lesions. We observed similar numbers of CD8 T cells in tumor bearing lungs treated with anti-PD-L1 or isotype. The fraction of $CD44^+CD62L^-$ CD8 representing tissue memory cells were slightly modified by therapy, however the increase was not significant (Figure 4.2 B). *Ex-vivo* restimulation of total draining lymph node cells with PMA/iono followed by intracellular staining with antibodies to IFNγ showed a fraction (10% of total lung $CD8^+$ T cells) of positive cells, equally in control and anti-PD-L1 treated animals (Figure 4.2. D). Thus, the basal predicted neoantigen content in KP is not sufficient to confer responsiveness to checkpoint (Figure 4.2 B-D), indicating that predicted neoantigens expressed by the parental line are not sufficient to trigger a tumor specific response.

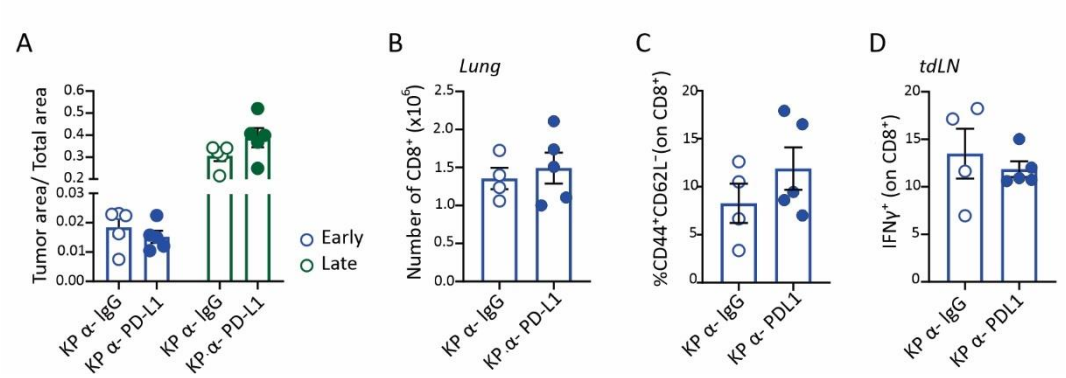

Figure 4.2| Orthotopic KP tumors harboring 22 neoantigens are resistant to ICB. KP tumor were injected intravenously and tumor bearing lungs were harvested at early and late time points. Tumor bearing mice were treated with either anti rat control isotype (α-IgG) or a monoclonal antibody anti-PD-L1 (αPD-L1). **A)** Quantification of lung tumor area at early and late time points (n=5). **B)** Quantification of $CD8^+$ T cells in tumor bearing lungs at early time points (n=5). **C)** Frequencies of effector $CD8^+$ T cells ($CD44^+CD62L^-$) in tumor bearing lungs at early end points (n=5). **D)** Frequencies of $CD8^+$ T cells from tdLN producing IFNγ after PMA/Iono stimulation (n=5).

Chapter 2. Induction of bona-fide neoantigens in KP lung tumors.

Dynamics of anti-tumoral T cell responses and checkpoint blockade efficacy in the KP model were previously investigated by introducing expression of surrogate neoantigens in cancer cells. Here, we wanted to increase the immunogenicity of KP cells through the induction of *bona-fide* neoantigens.

To this goal, we have used a strategy already published by Germano *et al.*, based on deletion of *Mlh1* which was shown allow accumulations of somatic mutations and immunogenicity in a colon cancer line (CT26). To induce deletion in KP we thus transiently transfected cells with sgRNA guides specific for *Mlh1*, targeting the exon 5 and a second vector encoding for the Cas9 protein. sgRNA guides were cloned into a vector under the U6 promoter control and upstream of the sequence encoding for ZsGreen protein. The expression of ZsGreen allowed to detect the cells that were effectively transfected and also, to sort them. $ZsGreen^+$ sorted cells followed by single cell cloning were amplified in culture and deletion of Mlh1 was evaluated by western blot.

Thus, two $Mlh1^{ko}$ clones (KP KO) were selected by western blot (Figure 4.3 A) and cells derived from mock Cas9 transfection were used as control KP^{ctrl} (Figure 4.3 A).

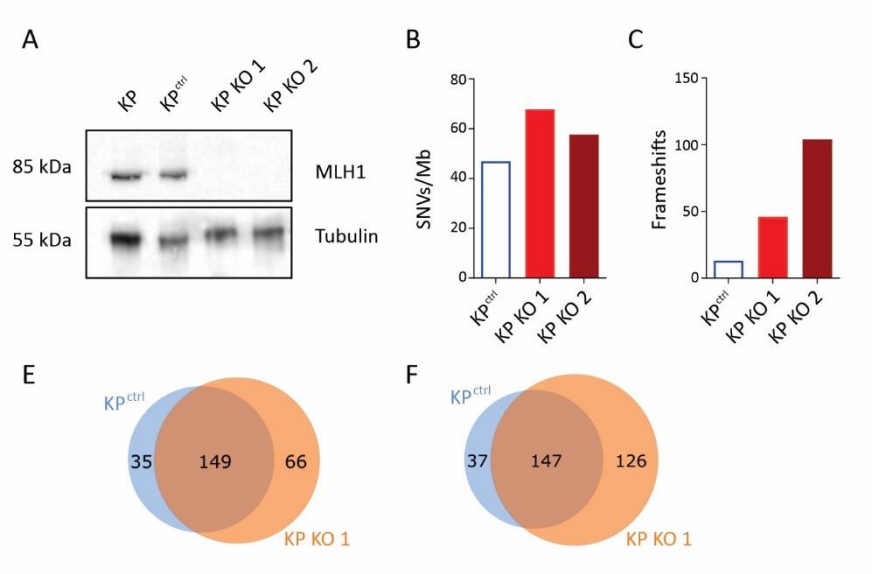

Figure 4.3| *Mlh1* deletion led to the accumulation of somatic mutations that impact on the neoantigen burden in KP KO clones. A) MLH1 expression in the parental cell line KP, in KP^{ctrl} and KP KO clones. **B)** Number of single nucleotide variants per mega base (SNV/Mb) in the indicated cell lines. **C)** Number of frameshifts in the indicated cell lines. **D-E)** Whole exome data from the indicated cells were compared. Unique events were defined as predicted neoantigens that were present exclusively in one cell type, shared neoantigens were present in both cell type. Venn diagrams show the numbers of predicted unique and shared neoantigens. Predicted neoantigens of KP^{ctrl}, KP KO 1 and KP KO 2 were calculated in comparison with C57 genome (1 replicate per each sample).

In order to accumulate somatic mutations after Mlh1 deletion, the two selected clones $Mlh1^{ko}$ (KP KO 1 and KP KO 2) and KP^{ctrl} were expanded *in vitro* for several generations (100 days). After this period in culture, the genome of KP KO 1, KP KO 2 and KP^{ctrl} were sequenced by WES in order to establish their mutational burden. Thus, the whole exome data from the cell lines were aligned and compared with the mouse reference genome.

This approach showed that the KP KO clones showed an accumulation of mutations compared to the Mlh1 competent cell line. The number of single nucleotide variants per megabase (SNVs/Mb) increased ~1.5-fold in KP KO cell lines (Figure 4.3 B), and the number of frameshifts increased 3- to 7-fold after MLH1 deletion. (Figure 4.3C).

Then, non-synonymous mutations were filtered from SNVs and frameshifts, and the peptides generated from these mutations were used to predict their putative affinity for MHCI. Non-synonymous mutations resulted in 66 and 126 predicted novel MHCI epitopes for KP KO 1 and 2, respectively (Figure 4.3 D-E); showing that MLH1 deletion contributed to the generation of somatic mutations.

Moreover, we wondered whether the maintenance of KP cells in culture could lead to the spontaneous accumulation of mutations due to the genomic instability inherent of

p53^{ko} cell line. Thus, the predicted neoantigens obtained from the KP^{ctrl} and the parental line KP were further filtered by expression. To this aim, RNA sequencing (RNA-seq) analysis was performed and only expressed putative neoantigens were maintained and compared between the two cell lines. We observed gain in one single expressed neoantigen in KP^{ctrl} with respect to the KP parental line, concluding that *in vitro* cell passages did not significantly affect neoantigen burden (Figure 4.4).

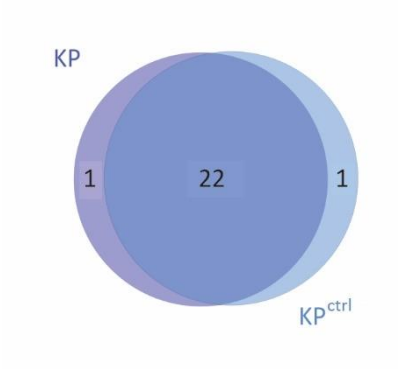

Figure 4.4| Expressed neoantigens in KP and KP^{ctrl} cell lines. Coding variants identified by whole exome sequencing were sorted by expression levels. Venn diagram from RNA-seq data shows the number of expressed neoantigens in KP^{ctrl} and KP cell line. Data represent mean from three RNA-seq replicates.

To evaluate whether the genome editing procedure or the deletion of *Mlh1* altered cellular features as the proliferative capacity, *in vitro* growth rate was carefully evaluated by plating an identical number of cells and counting cell numbers every 24 hr by crystal violet staining. The proliferation rate in the 2 selected KP KO clones and KP^{ctrl} was comparable to the parental line KP, and no statistical differences were found (Figure 4.5 A). This result shows that the intrinsic proliferation capacities were not affected by the deletion of *Mlh1*.

Neoantigen presentation on MHCI complex on cancer cells is essential to be target of CD8 T cell responses and its downregulation represents one of the immune evasion strategies developed by tumor cells[242]. Therefore, we examined expression of MHC class I molecules on the surface of KP^{ctrl} and KP KO clones to ensure that the increase mutational rate had not affected its expression (Figure 4.5 B). KP, KP^{ctrl} and KP KO clones were incubated with 0.2 ng/mL recombinant IFNγ to induce expression and MHCI levels were measured by flow cytometry. KP, KP^{ctrl} and KP KO 2 showed high expression of MHCI; however, KP KO 1 downregulated MHC class-I expression. Thus, KP^{ctrl} and KP KO 2 (named KP^{neo} hereafter) were retained for further analysis.

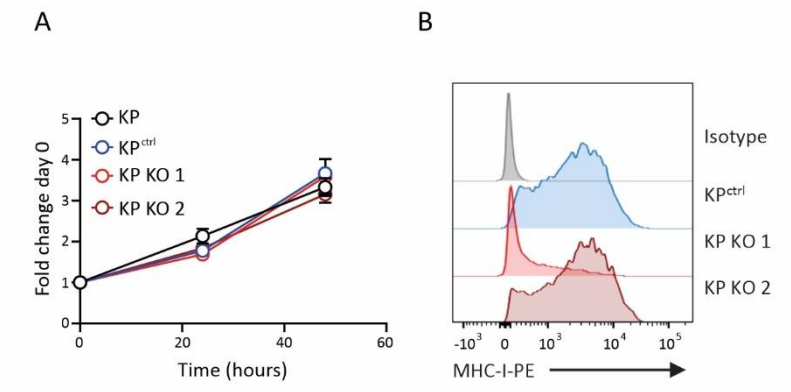

Figure 4.5| Selection of KP^{neo} clone. A) *In vitro* growth curves for the indicated clones were measured using the crystal violet assay at three time points. Fold change was calculated with respect to day 0. Data are represented as mean ± SEM of three replicates in the same experiment. No significant differences were found in two-ways ANOVA followed by Tukey´s possttest. **B)** MHC class-I levels were measured in the indicated clones by flow cytometry. An isotype antibody was used as a control.

Next, we evaluated expression of predicted neoAgs emerged from genomic analysis in KP^{neo} cells. Thus, the putative neoantigens predicted from WES were further filtered by expression and compared to those from KP^{ctrl} cell line. This analysis established that 26 of the mutant variants in KP^{neo} corresponded to expressed novel peptides (Figure 4.6 A). The 26 expressed neoantigens in KP^{neo} were distributed across a range of expression levels and predicted binding affinities for MHCI (Figure 4.6 B), creating a specific array of neoantigens which combines high and low expression with different affinities for MHCI.

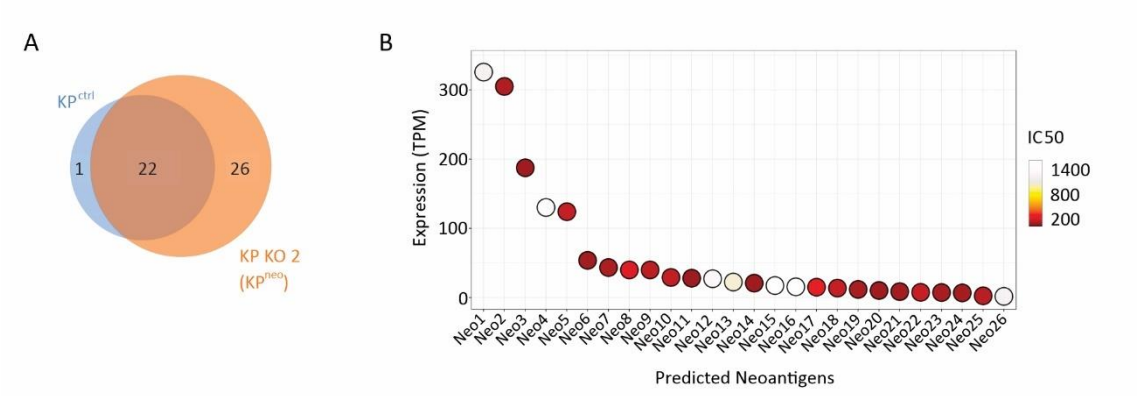

Figure 4.6| *Mlh1* deletion induces accumulation of neoantigens in KP tumors. A) Coding variants identified by whole exome sequencing were sorted by expression levels. Venn diagram from RNA-seq data shows the number of expressed neoantigens in KP^{ctrl} and KP KO 2 cell line. Data represent mean from three RNA-seq replicates. **B)** Expressed neoantigens in KP KO 2 (KP^{neo}) were plotted according to their expression levels (TPM). Color depicts the predicted IC_{50} value for each peptide-MHC class-I complex (n=3).

Importantly, we checked if the deletion of *Mlh1* altered biological process that could impact in cancer cell proliferation or alter the inflammatory response against KP^{neo}. For this, we performed a pathway enrichment analysis using gene sets representing relevant biological processes from Reactome and Hallmark database on the RNA-seq data from KP^{ctrl} and KP^{neo}. This analysis revealed that no gene pathways related to metabolism, inflammatory responses or antigen processing were differentially expressed in KP^{neo} versus KP^{ctrl} (Figure 4.7 B).

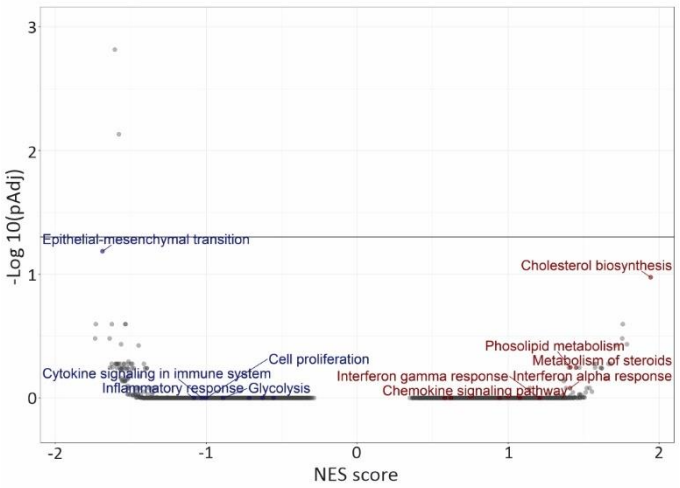

Figure 4.7| Key biological processes between KP^{ctrl} and KP^{neo}. Volcano plot of gene pathways related to cell proliferation, metabolism, inflammatory responses, and antigen processing in KP^{neo} vs KP^{ctrl} cell lines, obtained from RNA-seq data.

In summary, the deletion of Mlh1 in KP cells leads to the *in vitro* accumulation of non-synonymous mutations that generate putative neoantigens. Moreover, the genome editing did not affect biological processes that could affect neoantigen presentation, proliferative capacities, metabolism, or inflammatory responses. On this basis, we have selected KP^{ctrl} and KP^{neo} cells with similar features in terms of growth rate and MHCI expression, for further *in vivo* experiments.

Chapter 3. KP^{neo} tumors induce CD8 T cells activation and partial tumor containment. Subcutaneous model

To explore the impact of neoantigen accumulation in KP cells during the generation of the tumor immunity, KP^{ctrl} and KP^{neo} were implanted *in vivo* in mice. To this aim, KP^{ctrl} and KP^{neo} were inoculated subcutaneously into immunocompetent mice to establish flank tumors. The tumor volume was measured at day 10, 12, 15, 18 and 21 after tumor inoculation. The endpoint for KP^{ctrl} was earlier than KP^{neo} for ethical reasons because

tumors start to show ulcerous signs. We observed that KP^{ctrl} tumors grew progressively whereas KP^{neo} tumors experienced a tumor growth delay (Figure 4.8 A).

To further understand the role of the tumor microenvironment, in particular the role of the immune system for controlling of tumor harboring neoantigens, we evaluated the immune infiltrated in flank's tumors. To this aim, we have characterized the immune infiltrate by flow cytometry analysis, in which we analyzed the presence of total leucocytes, as $CD45^+$ cells, and in particular T lymphocytes as $CD3^+$, specifically $CD8^+$ T cells. We have observed an increased recruitment of leucocytes $CD45^+$ cells in KP^{neo} tumors in comparison with KP^{ctrl} (Figure 4.8 B). These immune infiltrate was characterized by an increased number of $CD3^+$ T cells (Figure 4.8 C), in particular $CD8^+$ T cells (Figure 4.8 E). Moreover, immunofluorescence staining of tumor sections confirmed the presence of $CD8^+$T cells deeply infiltrating KP^{neo} tumors (Figure 4.8 E).

To directly assess the role of cDC1 in $CD8^+$ T cells recruitment, KP^{neo} tumors were implanted in $Batf3^{ko}$ animals. These mice have a deletion in the transcription factor *Batf3* that ablates the development of cDC1[243]. By using this model, we have observed that the number of $CD8^+$ T cells per gram of tumor tissue was strongly inhibited in $Batf3^{ko}$ mice in comparison with immunocompetent animals (Figure 4.8 F). Moreover, $CD8^+$ immunostaining in tumor sections showed very few cells infiltrating KP^{neo} tumors on $Batf3^{ko}$ mice (Figure 4.8 D), suggesting that cDC1 are required to process neoantigens for T cell activation.

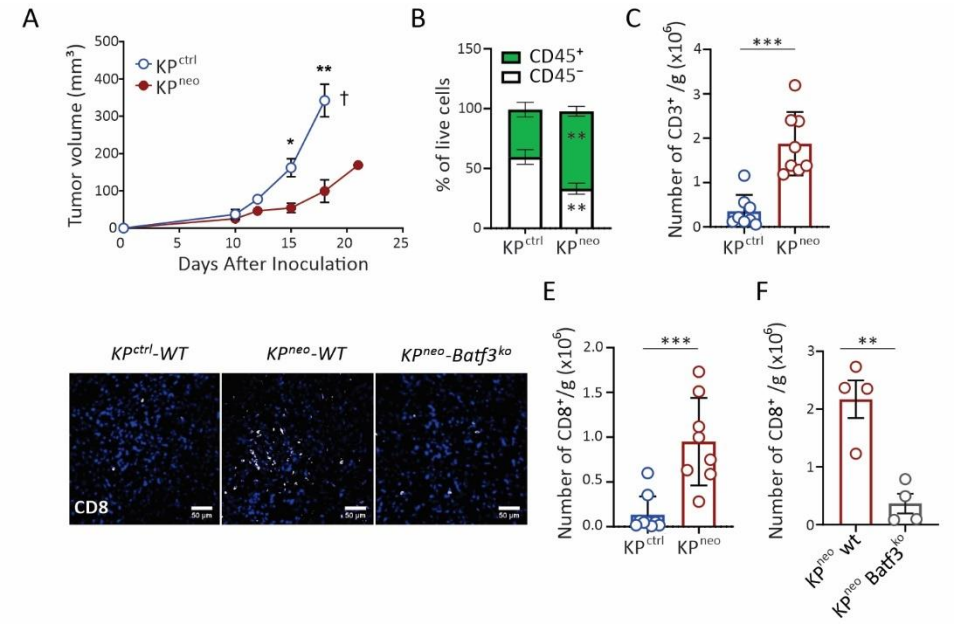

Figure 4.8| | Hypermutated KP tumor induces cDC1-dependent CD8 T cell responses and delayed tumor growth. **A)** Outgrowth of subcutaneous KP^{ctrl} or KP^{neo} tumors in WT mice. KP^{ctrl} group was harvested at day 18 for ethical reasons (†). Statistical analysis was conducted by two-ways ANOVA followed by Sidak's posttest *p<0.05, **p<0.01. **B)** Relative frequencies of $CD45^+$ or $CD45^-$ cells in tumor mass (n=9). Statistical analysis was conducted by two-ways ANOVA followed by Sidak's posttest **p<0.01. **C)** Absolute numbers of $CD3^+$ T cells per gram of tumor (n=8). Statistical analysis was conducted by t-test ***p<0.001. **D)** Representative immunofluorescence images of CD8 T cell distribution in tumor mass from KP^{ctrl} or KP^{neo} in WT mice, or KP^{neo} tumors in $Batf3^{ko}$ mice. Scale bar represents 50 µm. **E)** Absolute numbers of $CD8^+$ T cells per gram of tumor (n=8). Statistical analysis was conducted by t-test ***p<0.001. **F)** Absolute numbers of $CD8^+$ T cells per gram of tumor (n=8) in Wt and $Batf3^{ko}$ mice. Statistical analysis was conducted by t-test **p<0.01. **(A-F)** Data represent mean ± SEM.

To further characterize the immune infiltrate, we have analyzed the phenotype of intratumoral T cells by flow cytometry; particularly, we analyzed the frequencies of effector-memory and PD-1^+ $CD8^+$ T cells. We noticed that 75% of $CD8^+$ T cell infiltrating KP^{neo} tumors expressed markers of effector-memory T cells ($CD44^+CD62L^-$) (Figure 4.9 A), and strongly upregulated PD-1 expression (Figure 4.9 B), indicating antigen exposure.

To complement the immunophenotyping performed by flow cytometry we have analyzed the gene expression of effector-cytotoxic molecules in tumors by quantitative PCR (RT-qPCR). We measured the expression levels of *GzmB* that is directly involved during tumor-killing, *IFNγ* that is expressed in activated-effector CD8 T cells and *Cxcr3* that is the receptor for T cell chemoattraction and it is expressed in effector T cells[68]. Gene expression analysis showed a significant induction of *GzmB*, *IFNγ* and *Cxcr3* in KP^{neo} tumors with respect to KP^{ctrl} (Figure 4.9 C). Additionally, we observed that expression of these genes was significantly reduced in KP^{neo} tumors from $Batf3^{ko}$ mice, indicating that cDC1 were crucial during the CD8 T cell differentiation upon antigen recognition (Figure 4.9 C).

In addition, we have evaluated the frequencies of IFNγ^{+} cells in the tumor draining lymph node after restimulation. Thus, total draining lymph node cells were *ex vivo* restimulated with PMA/Iono, production of IFNγ cells was labeled with a specific antibody and relative frequencies of positive cells were quantified using flow cytometry. We detected an increase frequency of IFNγ^{+}CD8^{+} T cells KP^{neo} tumor draining lymph node cells, where around 12% of CD8^{+} T cells produced high levels of IFNγ in comparison with 5% of CD8^{+} T cells from KP^{ctrl} tumors, indicating effector functions (Figure 4.9 D). This result shows that neoantigens induce effector-cytotoxic CD8^{+} T cells in the TME and also in the draining lymph nodes.

In order to evaluate the role of adaptive immunity during the delay tumor growth of KP^{neo} tumors, we performed a CD8 T cell depletion in established KP^{neo} tumors. To this aim KP^{neo} cells were injected subcutaneously in the flank of immunocompetent mice. Tumor-bearing mice were treated intraperitoneally with a depleting antibody against CD8 T cells every four days. We noticed that the absence of CD8 T cells increased the tumor growth rate in KP^{neo} tumors (Figure 4.9 E), indicating that this subset has an active role during tumor growth control.

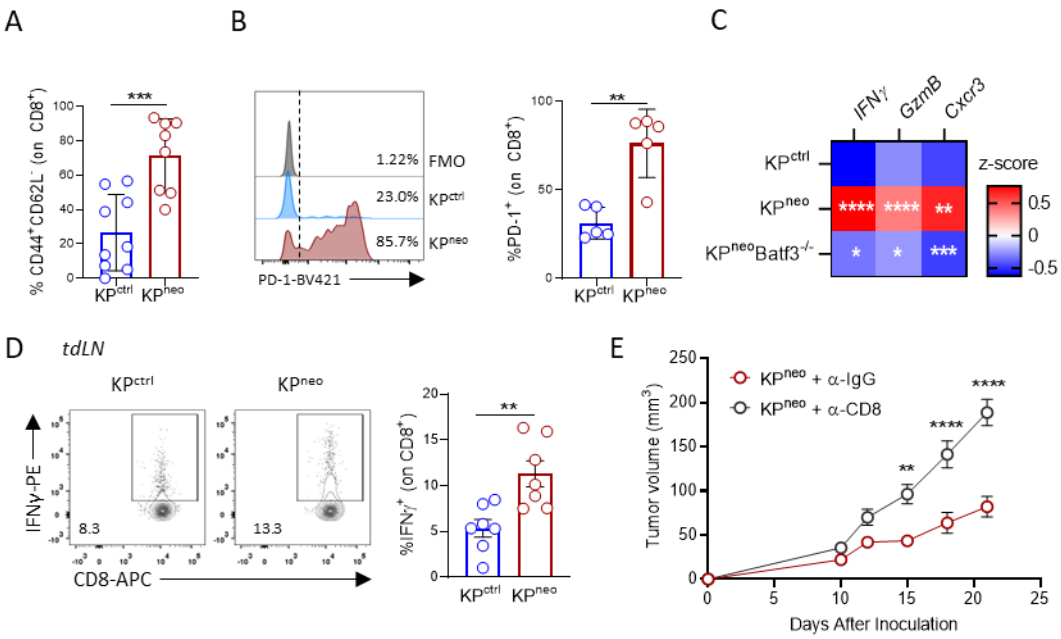

Figure 4.9| Tumor-infiltrating CD8⁺ T cells recruited in KP^{neo} tumors acquire effector functions and show antigen exposure. A) Frequencies of effector memory CD8⁺ T cells (CD44+CD62L-) (n=9). Statistical analysis was conducted by t-test p<0.001. **B)** Frequencies of PD-1⁺ CD8⁺ T cells (n=5). Statistical analysis was conducted by t-test p<0.01. **C)** Gene expression analysis by RT-qPCR of KP^{ctrl} and KP^{neo} tumor mass in WT mice, and KP^{neo} in Batf3^{ko} mice. Data are shown as z-score for each gene (n=7 for KP^{ctrl} and KP^{neo}, and n=4 for KP^{neo} in Batf3^{ko} mice). Statistical analysis was done by multiple t-test comparing KP^{ctrl} vs KP^{neo}, and KP^{neo} in WT vs KP^{neo} in Batf3^{ko} mice *p<0.05, **p<0.01, ***p<0.001 ****p<0.0001. **D)** Total cells from tdLN were collected at day 18 after tumor injection and were stimulated *ex vivo* with PMA/Iono. Levels of IFNγ⁺ CD8⁺ T cells were analyzed by flow cytometry (n=7). Statistical analysis was conducted by t-test **p<0.01. **E)** Tumor growth of subcutaneous KP^{neo} tumors, mice were treated either with α-CD8 or control isotype (α-IgG). Statistical analysis was conducted by two-ways ANOVA followed by Sidak's posttest *p<0.05, **p<0.01, ***p<0.001. **(A-E)** Unless it is mentioned data represent mean ± SEM.

Altogether, the results summarized above show that increasing neoantigens content generates recruitment of functional CD8 T cells in the TME that contribute to partially restrain tumor growth. The immune infiltrate of KP^{neo} was enriched in CD8⁺ T cells with effector-memory phenotype and cytotoxic features whose recruitment actively depended on cDC1.

Having observed that cDC1 are critical to support CD8 T cell activation we sought to directly analyze recruitment of cDC1 in the TME. To identify rare cDC1 in the TME we employed an exclusion mix including antibodies to T cell, NK and B cell markers (CD3, NK1.1 and B220) and macrophages (F4/80). After exclusion, CD11c⁺ MHCII⁺ double positive cells were gated, and XCR1⁺CD11b⁻ were considered as cDC1 (Figure 4.10 A). Surprisingly, we observed recruitment of cDC1 exclusively in KP^{neo} flank tumors, in which, ~4% of the CD11c⁺MHCII⁺ cells were cDC1. This subset was almost absent in KP^{ctrl} tumors where we detected only 0.5% of the CD11c⁺MHCII⁺ expressing XCR1 (Figure 4.10 A).

To understand molecular changes underlying cDC1 recruitment we analyzed expression of chemokines related to cDC1 recruitment such as *Ccl4* and *Ccl3*[244]; and cytokines and chemokines produced by cDCs such as *Cxcl9*, *Cx3cl1*, *Il-12* and *Ccl22*[125,126] that are involved in T cell chemoattraction, in KP^{ctrl} and KP^{neo} tumors. We noticed that KP^{neo} tumors showed higher expression of *Ccl4*, *Cx3cl1* and *Ccl22* than KP^{ctrl} (Figure 4.10 B). These results indicate that the TME of KP^{neo} tumors is enriched in chemoattractant signals for cDC1 such as *Ccl4* and in chemokines produced by mature/activated cDCs such as *Cx3cl1* and *Ccl22*.

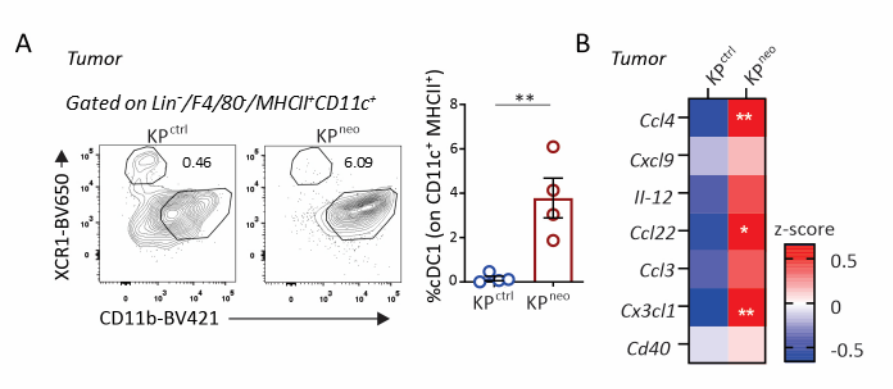

Figure 4.10| Neoantigen burden impacts on cDC1 recruitment in tumors. A) Representative flow cytometry of cDC1 in KP^{ctrl} and KP^{neo} tumors (Gated on Lin^{-}CD11c^{+} MHCII^{+}). Relative frequencies of cDC1 in KP^{ctrl} and KP^{neo} tumors (n=4). Data represent mean ± SEM. Statistical analysis was performed by t-test **p<0.01. **B)** Gene expression analysis by RT-qPCR of KP^{ctrl} and KP^{neo} tumor mass in WT mice. Data are shown as z-score for each gene (n=7) Statistical analysis was done by multiple t-test comparing KP^{ctrl} vs KP^{neo}, *p<0.05, **p<0.01.

Previous studies employing *Mlh1* deletion to increase the mutational burden[43,245] in different experimental tumor model had obtained similar results, i.e., increasing TMB can enhance tumor immunogenicity and rejection by CD8 T cells. However, in none of these previous reports, the relation between induced neoAgs and specifity of the CD8 response has been investigated. Having identified neoAgs accumulated in KP^{neo} we therefore set up an assay to assess the specificity of the T cell response induced *in vivo* by KP^{neo}. To this aim, we exposed total cells from tdLNs of tumor bearing mice to restimulation with selective predicted neoantigens. We chose 9 out of the 26 KP^{neo} predicted neoantigens to represent peptides with high or low predicted affinities with a range of expression. In this way we have generated a neoantigen matrix that cover all possible combinations between predicted affinity and expression levels (Figure 4.11). To increase presentation, we pre-loaded BMDCs with the peptides representing neoantigens and the Ova peptide (257-264 SIINFEKL) as a negative control in presence

of LPS, for 3 hours. DCs loaded with peptide were washed and incubated with tdLNs single cell suspensions from KP^{ctrl} or KP^{neo} tumor bearing mice. The co-culture was maintained for 5 days and IFNγ production was measured in the supernatant by ELISA (Figure 4.12 A).

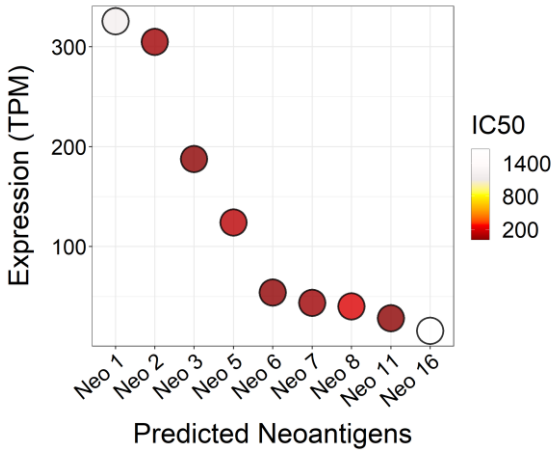

Figure 4.11| Peptides representing putative neoantigens selected to study neoantigen-specificity anti-tumoral response against KP^{neo}. Selected peptides are shown with the respective MHC class-I binding affinity (IC_{50}) and expression levels.

Thus, we found a specific induction of IFN-g to all specific KP^{neo} peptide and not against the control peptide, whereases KP^{ctrl} did not show responses to any on the peptide (Figure 4.12 B). However, we could not yet identify a strong correlation between intensity of the IFNγ signal and peptide features (expression/affinity). As discussed in discussion (page 90) further analysis with a wider peptide range and improving the assay will be needed to draw conclusion on this important aspect.

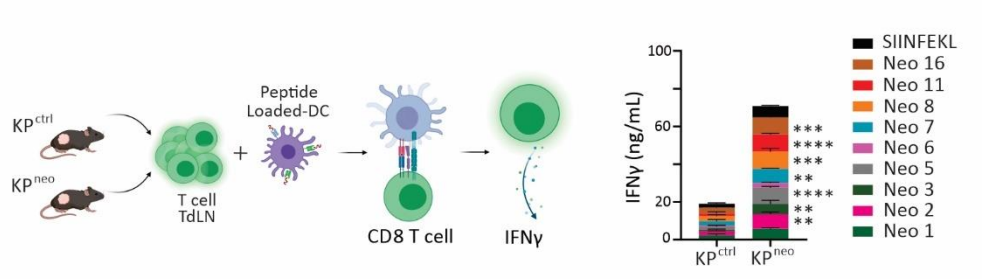

Figure 4.12| KP^{neo} generates tumor-specific T cell responses. A) Experimental setup. **B)** IFNγ levels detected after stimulation of tdLN cells from KP^{ctrl} and KP^{neo} mice with peptide loaded BMDCs. Data show mean ± SEM. Statistical analysis was performed by two-ways ANOVA followed by Sidak´s posttest **p<0.01, *** p<0.001, **** p<0.0001.

Summarizing, the data present across this chapter demonstrated that increasing neoantigen content in KP tumors generates neoantigen specific response that impact in the tumor outgrowth. This immune response comprises effector-memory T cells,

cytotoxic responses, and recruitment of myeloid cell, in particular cDC1, to the TME. Abolishing different components of the immune system as CD8 T cells or cDC1 reverted the immune response against KP^{neo} tumor and the tumor growth control was lost.

All these data suggest that increasing the neoantigens burden in KP cells generated warm tumors that are highly infiltrated by the immune system and the immune cells show signs activation and effector functions.

Orthotopic lung model

Tumor´s strategies to evade the immune system include suppression of priming of tumor-specific T cells and in a tissue specific manner. Recent evidence in NSCLC models and PDAC model showed that the anatomic site influences DC functionality, in particular, priming of tumor specific CD8 T cells[86,246]. Moreover, CD8 T cells showed different differentiation programs between heterotopic and orthotopic models of NSCLC, generating different outcomes to ICB[86].

Therefore, to further validate the potential immunogenicity of KP^{neo} tumor we established orthotopic tumors in lungs. To this aim, KP^{ctrl} or KP^{neo} cells were injected intravenously in the caudal tail vein of immune-competent mice to establish lung tumors. Lungs were collected to measure the tumor engraftment by hematoxilyn and eosin (H&E) (Figure 4.13 A). We noticed that development of KP^{neo} nodules was reduced in comparison with KP^{ctrl}.

In addition, we also studied the infiltration of T cells, in particular, $CD8^+$ T cells in the nodules. To this aim paraffin-embedded lungs sections were stained using specific antibodies to label CD8 T cells, and their abundance was normalized to the tumor area. We observed that KP^{neo} nodules were highly infiltrated by $CD8^+$ T cells whereas these cells were almost absent in KP^{ctrl} nodules (Figure 4.13 B). We noticed a 3-fold increase in infiltrating CD8 T cells in KP^{neo} in comparison to KP^{ctrl}. This result is in line with similar evidence found by independent groups in which increased neoantigen burden led to the accumulation of intratumoral $CD8^+$ T cells[43,126].

We then explored whether tumor growth containment was limited to the grafting period or was also maintained in well-established tumors. To this aim, we intravenously injected KP^{ctrl} and KP^{neo} and we harvested tumor bearing lungs at later endpoints. We

observed that the growth delay was maintained at later stages and CD8$^+$ T cells depletion rescued tumor progression (Figure 4.13 C). Altogether, these results showed that increasing the neoantigen burden KP^{neo} tumors becomes warm and highly infiltrated by CD8 T cells, and tumors are controlled in their growth by the immune system.

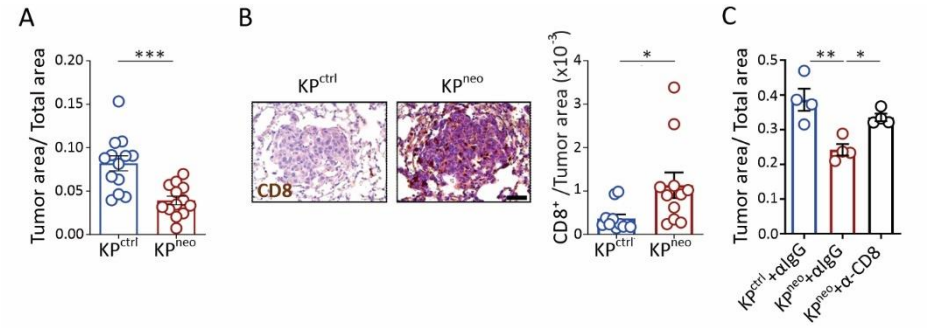

Figure 4.13| Orthotopic lung KP^{neo} tumor induces neoantigen specific CD8 responses and partial tumor containment. A) Quantification of lung tumor burden on day 7. Lung sections were stained with haematoxylin and eosin (n=12). Data from combined experiments and statistical analysis was conducted by t-test ***p<0.001. **B)** Quantification of CD8$^+$ T cells by immunohistochemistry in lung nodules (n=11). Data from combined experiments and statistical analysis was conducted by t-test **p<0.01. **C)** Quantification of lung tumor burden at day 14 after treatment either with α-CD8 or control isotype (α-IgG) (n=4). Data represents mean ± SEM and statistical analysis was conducted by one-way ANOVA followed by Tukey's posttest *p<0.05 **p<0.01. Unless noted, data represent mean ± SEM.

The phenotype of intratumoral T cells by flow cytometry showed increased frequencies of effector-memory CD8$^+$ T cells (CD44^{high}CD62L$^-$) and PD-1$^+$ in CD8$^+$ T cells. This result unveiled that CD8$^+$ T cell had an effector-memory phenotype (Figure 4.14 A) and expressed PD-1 in KP^{neo} tumor-bearing lungs (Figure 4.14 B). Neoantigens bearing tumors increased 2.5-fold the frequencies of effector-memory CD8$^+$ T cells and PD-1$^+$ CD8$^+$ T cells, indicating antigen exposure.

To examine the capacity of CD8 T cells to produce cytotoxic cytokines after *ex vivo* restimulation, total cells from lung and the mediastinal tumor draining LNs were restimulated with PMA/Iono and IFNγ production was detected by intracellular staining (ICS). We observed that CD8$^+$ T cells derived from KP^{neo} tumor bearing mice showed 2.5-fold increase in the frequencies of IFNγ producing cells, indicating induction of cytotoxic functions (Figure 4.14 C-D).

Effector-cytotoxic functions were confirmed by gene expression in isolated CD8 T cells from tumor bearing lungs. We analyzed cytokines gene expression by RT-qPCR. CD8 T

cells isolated from KP^{neo} showed significantly higher levels of IFNγ and Granzyme B (GzmB) in comparison to those isolated from KP^{ctrl} tumor-bearing lungs (Figure 4.14 E).

Taken together these results demonstrated that increasing neoantigens burden in KP cells lead to an increased immunogenicity characterized by higher intratumoral infiltration of lymphocytes and these cells showed effector-cytotoxic phenotypes, also in the native tissue: the lung. In addition, the increased neoantigen burden leads to a high tumor growth control, in part, by CD8$^+$ T cells.

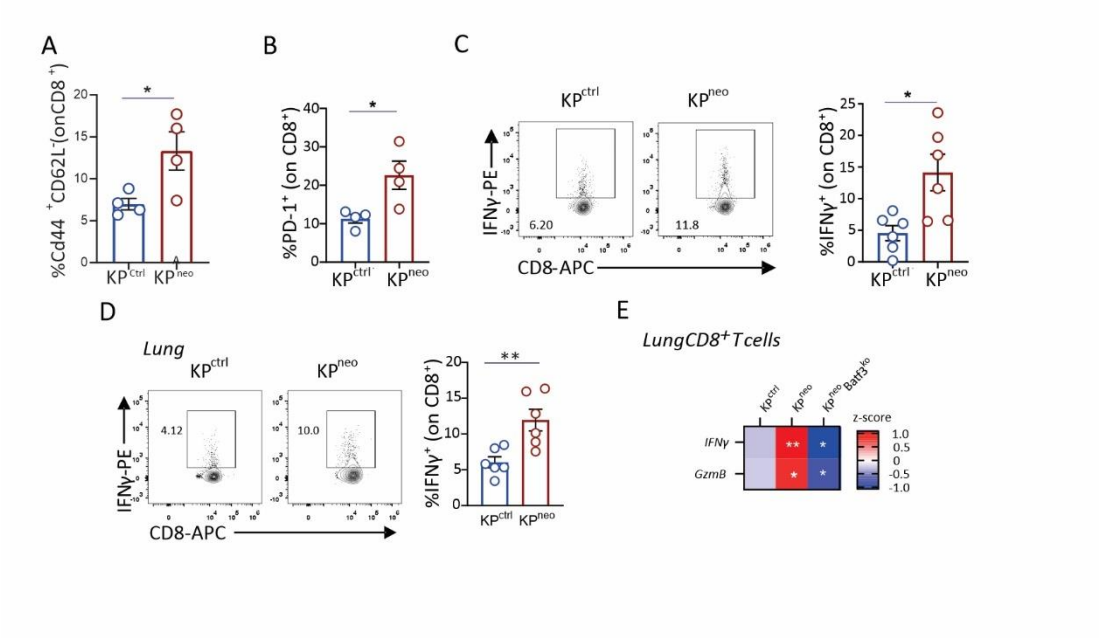

Figure 4.14| Tumor-infiltrating CD8$^+$ T cells recruited in orthotopic KP^{neo} tumors acquire effector functions and show antigen exposure. A) Frequencies of effector memory CD8$^+$ T cells (CD44$^+$CD62L$^-$) (n=4). Statistical analysis was conducted by t-test *p<0.05. **B)** Frequencies of PD-1$^+$ CD8$^+$ T cells (n=4). Statistical analysis was conducted by t-test *p<0.05. **C-D)** Total cells from tdLN **(C)** or lung **(D)** were collected at day 7 after tumor injection and were stimulated *ex vivo* with PMA/Iono. Levels of IFNγ$^+$ CD8$^+$ T cells were analyzed by flow cytometry (n=6). Statistical analysis was conducted by t-test *p<0.05, **p<0.01. **E)** Gene expression analysis by RT-qPCR of isolated CD8 T cells from KP^{ctrl} and KP^{neo} tumor bearing lungs in Wt mice, and KP^{neo} in Batf3^{ko} mice. Data are shown as z-score for each gene (n=4). Statistical analysis was done by multiple t-test comparing KP^{ctrl} vs KP^{neo}, and KP^{neo} in WT vs KP^{neo} in Batf3^{ko} mice *p<0.05, **p<0.01. Unless noted, data represent mean ± SEM.

According to the active role of cDC1 during antigen processing, presentation and trafficking necessary for CD8 priming, we explored their impact in the context of *bona-fide* neoantigen. KP^{neo} were implanted orthotopically in immunocompetent and in Batf3^{ko} mice and tumor bearing lungs were harvested after 14 days. We have analyzed the infiltration of CD8 in tumor nodules. For this purpose, paraffin-embedded lung sections were stained with antibodies specific for labeling CD8 T cells. We have observed that CD8 T cell recruitment was halved in Batf3^{ko} mice compared to their immunocompetent counterpart (Figure 4.15 A). Also, we analyzed gene expression of

molecules related with cytotoxicity and effector functions in isolated CD8 T cells from KP^{neo} tumor bearing mice in Wt and Batf3^{ko} mice. Using RT-qPCR we observed that *GzmB* and *IFNγ* expression was significantly reduced in CD8^{+} T cell isolated in Batf3^{ko} lungs harboring KP^{neo} tumors (Figure 4.14 E). H&E staining to assess tumor burden showed that tumor control was lost in absence of cDC1 (Figure 4.15 B), suggesting a major role of this subset during the generation of tumor immunity and tumor growth control.

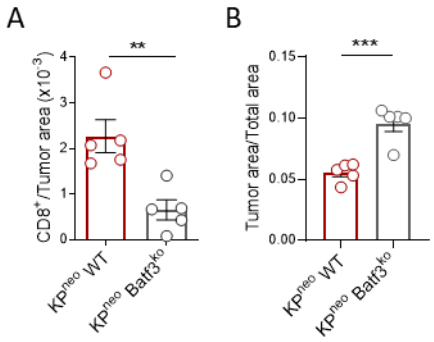

Figure 4.15| Tumor-specific CD8 T cell responses against KP^{neo} depend on cDC1. A) Quantification of CD8^{+} T cells by immunohistochemistry in lung nodules of KP^{neo} tumor-bearing lungs in Wt and Batf3^{ko} mice (n=5). Statistical analysis was conducted by t-test **p<0.01. **B)** Quantification of lung tumor burden at day 15 in KP^{neo} tumor bearing lungs in Wt and Batf3^{ko} mice. Lung sections were stained with haematoxylin and eosin (n=5). Statistical analysis was conducted by t-test ***p<0.001. Unless noted, data represent mean ± SEM.

Moreover, we wanted to address the specificity of the T cell response against neoantigens in the native tissue of the tumor. We have performed a T cell restimulation with the selected peptides described in the figure 4.11. Restimulation of cells from mediastinal tdLN confirmed reactivity to KP^{neo} specific neoAgs. We observed that 4 out of 9 of the tested peptides reached a significant increase over KP^{ctrl}, indicating a slightly reduced activation in the lung as compared to the subcutaneous model.

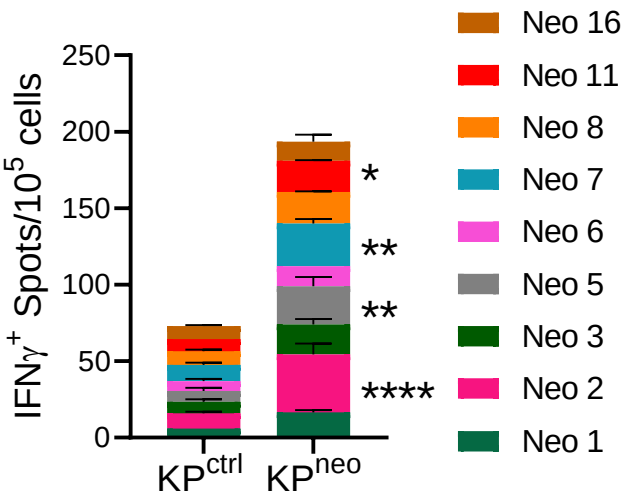

Figure 4.16| KP^{neo} generates neoantigen specific T cell responses. Number IFNγ producing cells from tdLN assessed by IFNγ ELISpot of lung KP^{ctrl} or KP^{neo}-bearing mice on day 7 post tumor injection. Data represent mean ± SEM and statistical analysis was performed by two ways ANOVA followed by Sidak's postttest. *p<0.05,**p<0.01,****p<0.0001.

In conclusion, likewise in the subcutaneous model increased neoantigen burden in KP^{neo} lung orthotopic tumor led to the accumulation of effector-memory CD8 T cells with cytotoxic capacities delaying the tumor growth. Also, in lung tissue neoantigens have generated T cells responses cDC1-dependent. We can conclude that increased neoantigen content generates warm tumors with higher immunogenicity.

Chapter 4. Increased mutational burden is not sufficient to improve ICB response in KP tumor.

During the previous sections it has been demonstrate that increasing neoantigenicity in KP tumors shapes the tumor immunity and slightly affect disease progression. Boosting neoantigen content leads to T cell-mediated immunity and disease containment in two different anatomic sites. Since neoantigen burden is one of the parameters that correlates with better responses to ICB we wanted to explore its efficacy in KP^{neo} tumors.

To this purpose, immunocompetent mice were injected subcutaneously in the right flank with KP^{neo} tumors and treated intratumorally either with control isotype or anti-PD-L1 monoclonal antibody, every four days.

The tumor growth was monitored at day 10, 12, 15, 18 and 21 and the CD8 T cell response was analyzed at the endpoint the day 21. KP^{neo} tumors grew slowly in both

groups, and no significant differences were observed between control and treated groups (Figure 4.17 A).

Analysis of the immune infiltrated by flow cytometry, showed a slightly increase in the recruitment of immune cells ($CD45^+$), and CD8 T after therapy (Figure 4.17 B-C), but no statistically significant differences were found. The frequencies of effector memory ($CD44^+CD62L^-$) (Figure 4.17 D) and $PD1^+$ $CD8^+$ T cells (Figure 4.17 E) was high and remained unchanged after therapy (around the 90% of $CD8^+$ T cells for effector-memory and 60% for $PD\text{-}1^+CD8^+$ T cells). In addition, no differences were detected in the IFNγ production by $CD8^+$ T cells from the tdLN after *ex-vivo* PMA/Iono stimulation (Figure 4.17 F).

Altogether, the results showed that despite the higher neoantigen burden of KP^{neo} in comparison with the parental line, the increased immunogenicity acquired was not sufficient to benefit from ICB therapy.

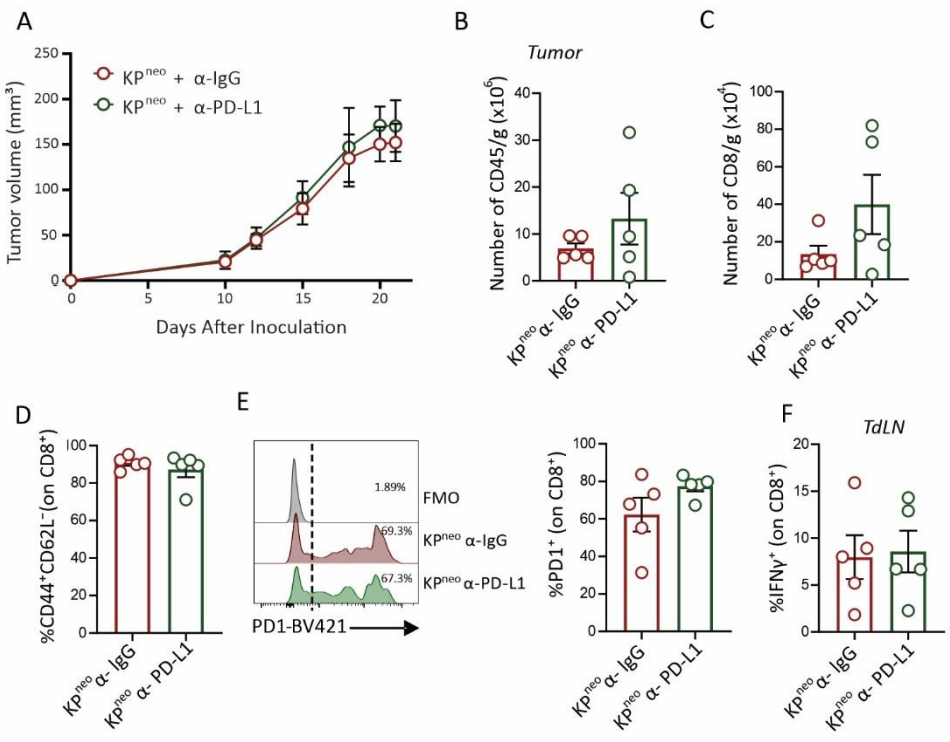

Figure 4.17| Tumor antigenicity is not sufficient to generate responses after ICB. A) Tumor outgrowth of KP^{neo} tumor treated either with control isotype (αIgG) or anti-PDL1 (α-PDL1) (n=5 per group). **B-E)** Absolute number of $CD45^+$ (n=5) **(B)**, $CD8^+$ T cells (n=5) **(C)**, effector memory $CD8^+$ T cells (n=5) **(D)**, $PD\text{-}1^+$ $CD8^+$ T cells (n=5) **(E)**, in KP^{neo} tumors after treatments (n=5). **F)** Total cells from tdLN were stimulated with PMA/Iono and frequencies of IFNγ $CD8^+$ T cells were measured by flow cytometry (n=5). Unless noted, data represent mean ± SEM.

Due to the importance of the anatomic site on the orchestration of the specific tumor immune response presented in the previous section, the efficacy of ICB was tested also using the orthotopic model. KP^{neo} tumor were injected intravenously in the tail vein of immunocompetent mice, and we have treated intraperitoneally either with control isotype or anti-PDL1. After 9 days tumor bearing lungs were collected to measure CD8 infiltration and tumor area by IHC. No differences were found in the number of $CD8^+$ T cells nor in the size of tumor nodules cells between the two groups (Figure 4.18 A-B).

Furthermore, we wanted to explore whether ICB, despite not increasing the number of intratumoral CD8 T cells, could affect their phenotype. We observed that the treatment with ICB significantly increased the frequencies of effector memory CD8 T cells, from 15% in control group to 25% in treated group (Figure 4.18 C). Moreover, the frequencies of $CD8^+$ T cell producing IFNγ was significantly increased (2-fold) in mice that have received anti-PD-L1, suggesting that anti-PD-L1 improves T cell responses increasing cytotoxic and effector-memory phenotypes. In conclusion, ICB boost effector-memory and cytotoxic phenotype in intratumoral $CD8^+$ T cells in KP^{neo} tumor bearing lungs. However, induction of anti-tumoral CD8 T cells is not sufficient to impact on initial progression of tumor nodules.

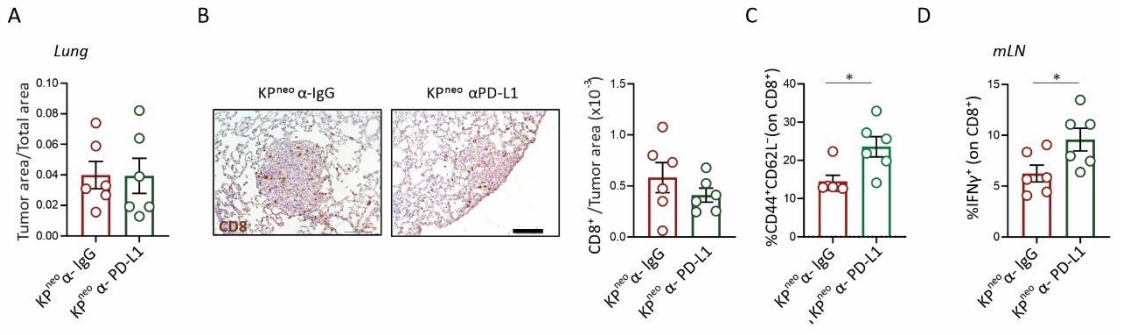

Figure 4.18| Tumor antigenicity is not sufficient to generates responses after ICB in orthotopic tumors. A) Quantification of lung tumor burden on day 9. Lung sections were stained with haematoxylin and eosin (n=6). **B)** Quantification of $CD8^+$ T cells by immunohistochemistry in lung nodules (n=6). **C)** Frequencies of effector memory CD8+ T cells ($CD44^+CD62L^-$) (n=6). **D)** Total cells from tdLN were stimulated with PMA/Iono and frequencies of IFNγ $CD8^+$ T cells were measured by flow cytometry (n=6). Unless noted, data represent mean ± SEM.

In conclusion, we can see a mild effect on the intratumoral CD8 T cell activation state, but not sufficient to inhibit tumor progression. These data are congruent with results found in other murine cancer models as pancreas or colorectal tumors encoding strong

neoantigens, in which the main strategy to evade the immune system remain the impairment of priming of neoantigen-specific T cell[43,246,247].

Chapter 5. Combination of Flt3L and anti PD-L1 blockade promotes DC1-dependent anti-tumor immunity.

In many cancer models, the longer the disease progresses cDC1 become dysfunctional and systematically decrease in number in tissues[146,188,203,218]. DCs are required for the recruitment of effector T cells into the TME and are a major component of the establishment of the T cell-inflamed tumor phenotype[150]. Therapeutic strategies to boost and activate DCs, in particular, cDC1 have been explored successfully in melanoma, pancreas, NSCLC and breast tumor models[144–147,218]. Predominantly, all these studies reported that cDC1 mobilization in the TME unblocks tumor immunity, leading to an improved tumor control by the adaptive immunity. Expression of a range of endogenous *bona-fide* neoantigens that induce partial tumor immunity via a cDC1/CD8 axis, provides a context to formally explore the correlation between neoantigens density and therapies that boost antigen presentation, that so far have been tested with strong-surrogate antigens.

In this context we have tested a combinatorial DC-based therapy in KP tumors, this therapy includes FLT3L, Poly (I:C) and anti-PD-L1. To assess the impact of the therapy in KP tumors we moved back to the subcutaneous model to facilitate testing. In fact, this anatomical localization represents many advantages: it allows to directly treat the tumor avoiding systemic effects and side effects and to track tumor progression.

To this purpose, KP^{ctrl} and KP^{neo} cells were injected subcutaneously in the right flank of immunocompetent mice. Mice harboring tumors were treated intratumorally either with control isotype or the combinatorial therapy (FL/p(I:C) + αPD-L1) at day 3, 6, 9, 12 and 15 after tumor inoculation (Figure 4.19 A). Tumor volume was monitored and measured at day 10, 12, 15 and 18, at this last point tumor and tdLNs were collected and analyzed.

Surprisingly, our first observation was that KP^{ctrl} tumor volume remain unchanged after therapy indicating that DC boost and checkpoint inhibitors are not sufficient to trigger protective responses at low neoantigen load (Figure 4.19 B). In contrast, KP^{neo} tumors

were highly controlled by therapy (Figure 4.19 C). The therapy reduced 3-fold the tumor volume in comparison with control isotype treated mice, with lesions that remained smaller than 50 mm^3 at the latest time point of analysis. In KP^{neo} the tumor reduction was significant suggesting that cDC1 mobilization into the TME benefits from neoantigens to improve the clinical benefits of the therapy.

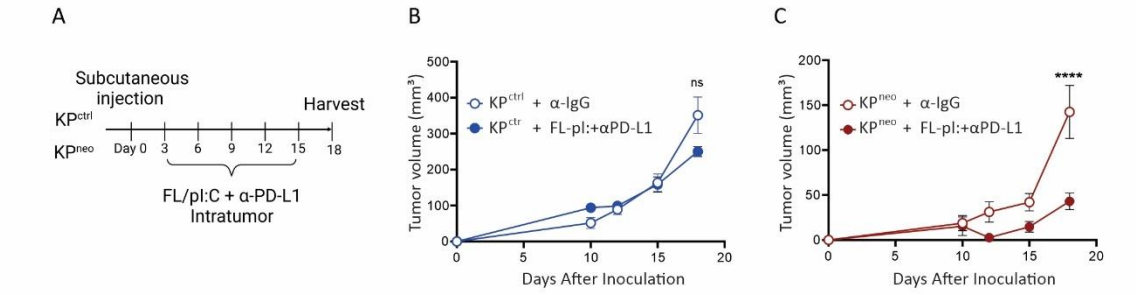

Figure 4.19| Enhancing cDC1 leads to improved tumor growth control of tumors harboring neoantigens. A) Experimental setup. B-C) Outgrowth of KP^{ctrl} (B) or KP^{neo} (C) tumors treated either with control isotype or FL/p(I:C)+αPD-L1. Data represent ± SEM and statistical analysis was performed by two-ways ANOVA followed by Sidak's postest ****p<0.0001.

We next sought to characterize the cellular immune response accounting for tumor control. KP^{neo} tumor treated with therapy were highly infiltrated by $CD45^+$, whereas the recruitment of leucocytes was unchanged in KP^{ctrl} tumors after the therapy. In KP^{neo} tumors the combinatorial therapy led to 4-fold increase in the number of immune cells infiltrating tumors in comparison to untreated group (Figure 4.20 A). Moreover, the combinatorial therapy led to a 5-fold increase of $CD8^+$ T cells in KP^{neo} tumors. In contrast, KP^{ctrl} remained poorly infiltrated by $CD8^+$ T cells even after therapy (Figure 4.21 B).

These observations were further confirmed by immunofluorescence in tumor sections, in which we observed that CD8 T cells deeply infiltrated the tumor core of KP^{neo} tumors, whereas KP^{ctrl} remained deserted of $CD8^+$ T cells (Figure 4.21 C). These results showed that tumors with increased neoantigen burden benefit from combinatorial therapies that boost and activate cDC1 in the TME. Moreover, the therapy significantly enhanced the recruitment of leucocytes in particular of CD8 T cells into the TME.

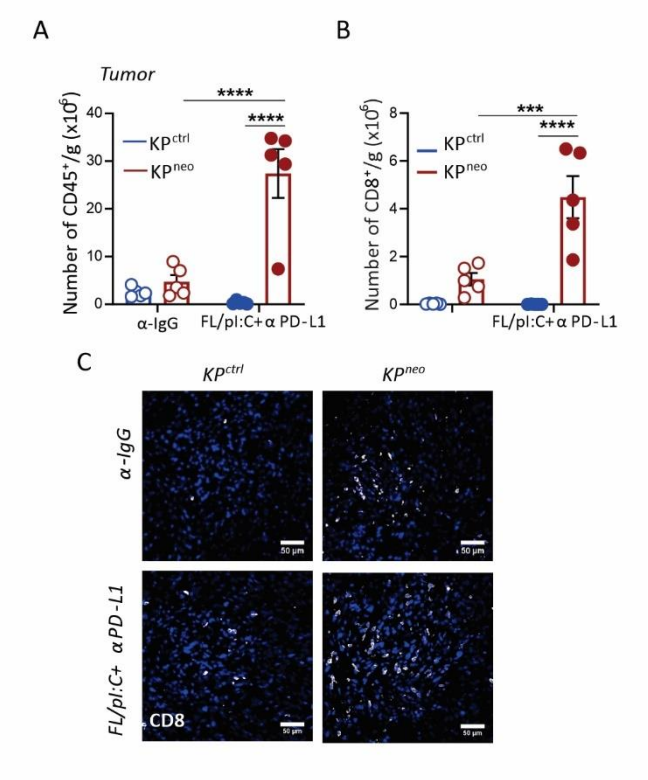

Figure 4.20| Neoantigen content improves responses to therapies enhancing cDC1. A-B) Absolute number of CD45$^+$ **(A)** or CD8$^+$ T cells **(B)** per gram of tumor in KP^{ctrl} or KP^{neo} tumors treated either with control isotype (αIgG) or FL/pI:C+αPD-L1. Statistical analysis was performed by two-ways ANOVA followed by Sidak's posttest ***p<0.001, ****p<0.0001. **C)** Representative immunofluorescence images of CD8 T cell distribution in tumor mass from KP^{ctrl} or KP^{neo} in WT mice, treated either control isotype (αIgG) or FL/pI:C+αPD-L1. Scale bar represents 50 µm.

We further analyzed the functional features of CD8$^+$ T cells in KP^{neo} tumors in control and treated groups. Given the paucity of CD8 T cells infiltrating KP^{ctrl} even after therapy, further analysis in the tumor mass was limited to KP^{neo}. The expression *GzmB* in CD8$^+$ T cells was significantly increased after therapy (Figure 4.21 A).

Additionally, we have analyzed the phenotypical characteristic of CD8$^+$ T in the tdLN of KP^{ctrl} and KP^{neo} tumor bearing mice, by flow cytometry. Thus, we have analyzed the frequencies of TCF1$^-$GzmB$^+$ CD8$^+$ T cells and effector-memory CD8$^+$ T cells in the tdLN. We noted that TCF1$^-$GzmB$^+$ CD8$^+$ T cells were almost absent in KP^{ctrl} and KP^{neo} tdLN treated with control isotype. Despite their low abundance the combinatorial therapy slightly increased their frequencies in KP^{ctrl} tdLN, and significantly increased their abundance in KP^{neo} tdLN (Figure 4.21 B). This result suggested that the combinatorial therapy induced the differentiation of CD8$^+$ T cells into TCF1$^-$GzmB$^+$. This subset has been associated with the direct tumor killing in preclinical models of melanoma[248].

Moreover, the therapy increased the frequencies of effector memory $CD8^+$ T cells in both KP^{ctrl} and KP^{neo} tdLN; however, the increment in KP^{neo} was significantly higher than in KP^{ctrl} (Figure 4.21 C), suggesting that neoantigen content influence the CD8 T cell differentiation in the LNs.

In addition, short *ex-vivo* restimulation showed a dramatic expansion of IFNγ producing $CD8^+$ T cells post therapy in KP^{neo} tumors, whereas no increase was observed in KP^{ctrl} tumors (Figure 4.21 D), indicating higher cytotoxic capacity in $CD8^+$ T cells from KP^{neo} exposed to the therapy.

In conclusion, we have tested a combinatorial therapy that induced the activation and mobilization of cDC1 in the TME. Using this therapy, we have demonstrated that neoantigen content dictates the tumor growth control and that, boosting DCs and checkpoint inhibitors are not sufficient to trigger protective responses at low neoantigen load, indicating that a minimal threshold of neoantigens is needed to achieve benefits from the DC-based therapy. Moreover, we observed that the presence of neoantigens drives T cell differentiation in the tdLN after therapy, indicating their major role during antitumor immunity.

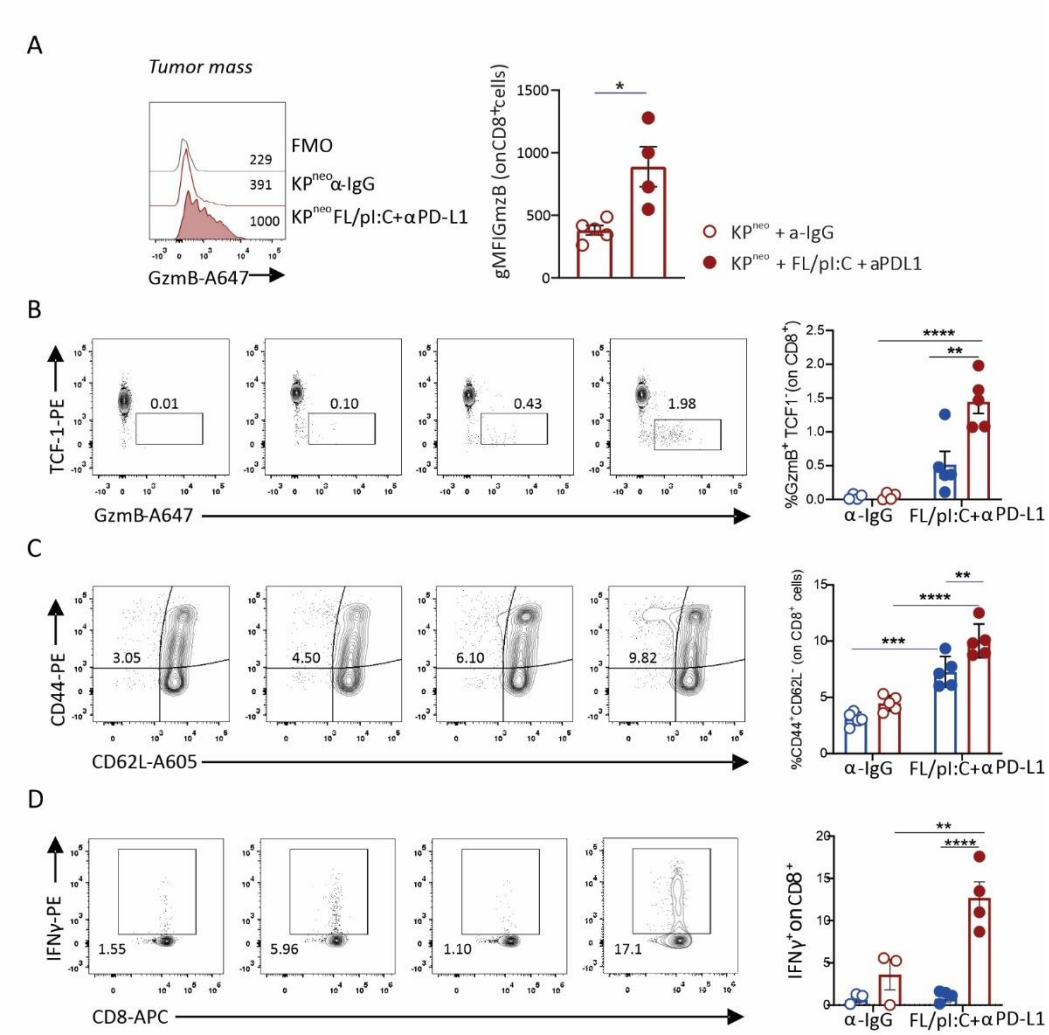

Figure 4.21| Boosting DCs activates CD8⁺ T cells and overcomes resistance to PD-L1 blockade in KP^{neo} tumors. A) Geometric mean of fluoresce of GzmB in CD8⁺ T cells in KP^{neo} tumors treated either with control isotype (αIgG) or FL/pI:C+αPD-L1 (n=5). Statistical analysis was performed by t-test *p<0.05. **B-C)** Frequencies of GzmB⁺TCF1⁻ (B) or CD44⁺CD62L⁻ **(C)** CD8⁺ T cells in KP^{ctrl} and KP^{neo} tumor treated as indicated (n=5). Statistical analysis was performed by two-ways ANOVA followed by Sidak's posttest **p<0.05, ****p<0.0001. **D)** Total cells from tdLN from KP^{ctrl} or KP^{neo} tumors treated as indicated were stimulated with PMA/Iono and frequencies of IFNγ CD8⁺ T cells were measured by flow cytometry (n=5). Unless noted, data represent mean ± SEM.

Chapter 6. Tumor control induced by the theraoy depends on cDC1

Since Flt3L may have bystander effects acting on cell subset different than DCs, it was important to assess the contribution of cDC1 during the generation of neoantigen-specific immune responses after the combinatorial therapy. To this purpose we have used XCR1^{DTA} mice, in which XCR1-Cre-driven activation of cytotoxic diphtheria toxin A (DTA) allows to specifically deplete differentiated cDC1[225]. This model offers substantial advantages in comparison with other available models lacking cDC1; first, the expression of the DTA remains confined to the cell avoiding side effects generated during the systemic administration of the toxin; second, this model does not delete the expression

of transcription factors such as Batf3 which is involved in the development of different immune subsets; third, these mice were shown to specifically lack cDC1 without involvement of any other immune subset.

Thus, to study the role of cDC1 during the generation of tumor immunity after the therapy, KP^{neo} tumors were subcutaneously injected in the right flank of $XCR1^{DTA}$ or WT mice. KP^{neo} tumor were subsequently treated *in situ* with the combinatorial therapy described in previous paragraphs. Tumor volume was monitored and tdLN and tumor masses were collected 21 after tumor challenge.

Notably, the growth of KP^{neo} tumors in in $XCR1^{DTA}$ mice was significantly faster that in Wt animals and lesions grew progressively starting from day 10 after challenge (Figure 4.22 A), indicating the cDC1 are required for tumor control after therapy. Consistently, flow cytometry and immunofluorescence in tumor slices showed that recruitment of CD8 T cells in the tumor mass was significantly blunted in $XCR1^{DTA}$ mice (Figure 4.22 B-C).

In addition, we analyzed the gene expression of molecules associated with activated-cytotoxic $CD8^{+}$ T cells such as *IFNγ*, *GzmB* and *Cxcr3*. We noticed that these molecules showed a significant decrease in their expression in $XCR1^{DTA}$ mice (Figure 4.22 D), indicating the crucial role of cDC1 during the CD8 T cell activation.

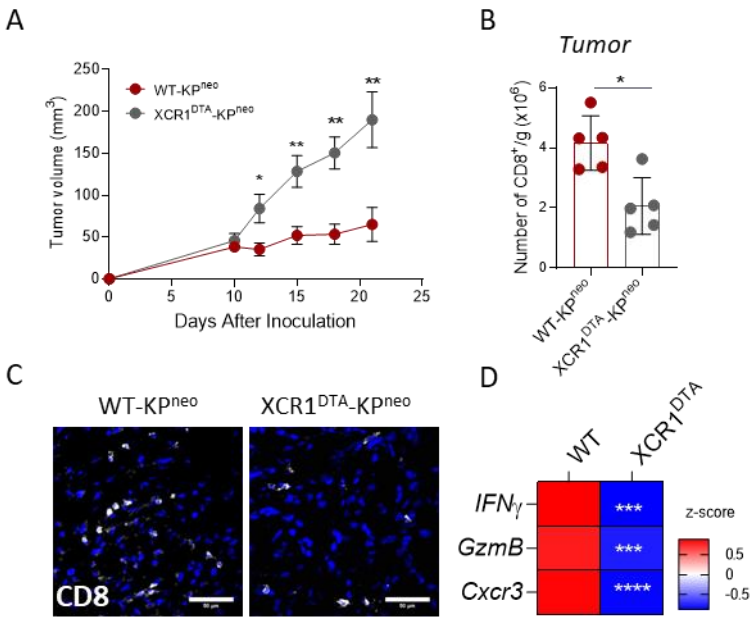

Figure 4.22| Therapeutic immunity and CD8 T cells responses to neoAgs requires cDC1. A) Outgrowth of KP^{neo} tumors in Wt or $XCR1^{DTA}$ mice treated with FL/pI:C+αPD-L1. Statistical analysis was conducted by two-ways ANOVA followed by Sidak's posttest *p<0.05, **p<0.01 (n=5). **B)** Absolute numbers of $CD8^+$ T cells per gram of tumors (n=4). Statistical analysis was performed by t-test *p<0.05. **C)** Representative immunofluorescence images of CD8 T cell distribution in tumor mass from KP^{neo} in WT or $XCR1^{DTA}$ mice, treated with FL/pI:C+αPD-L1. Scale bar represents 50 µm. **D)** Gene expression analysis by RT-qPCR of KP^{neo} tumor in Wt or $XCR1^{DTA}$ mice. Data are shown as z-score for each gene (n=4). Statistical analysis was done by multiple t-test comparing KP^{neo} in WT vs $XCR1^{DTA}$ mice ***p<0.001, ****p<0.0001. Unless noted, data represent mean ± SEM.

Also, we analyzed the frequencies of effector-memory $CD8^+$ T cells in the tdLN. We noted that this subset was diminished in $XCR1^{DTA}$ mice (Figure 4.23 A). Moreover, the frequencies of $IFN\gamma^+$, $TNF\alpha^+$ and double-positive cells after short *ex vivo* restimulation in $XCR1^{DTA}$ in comparison with Wt mice (Figure 4.23 B) was reduced. The results presented in the last two figures demonstrated the fundamental role of cDC1 during tumor immunity generation, because its ablation led to the loss of effector and activated CD8 T cell subsets.

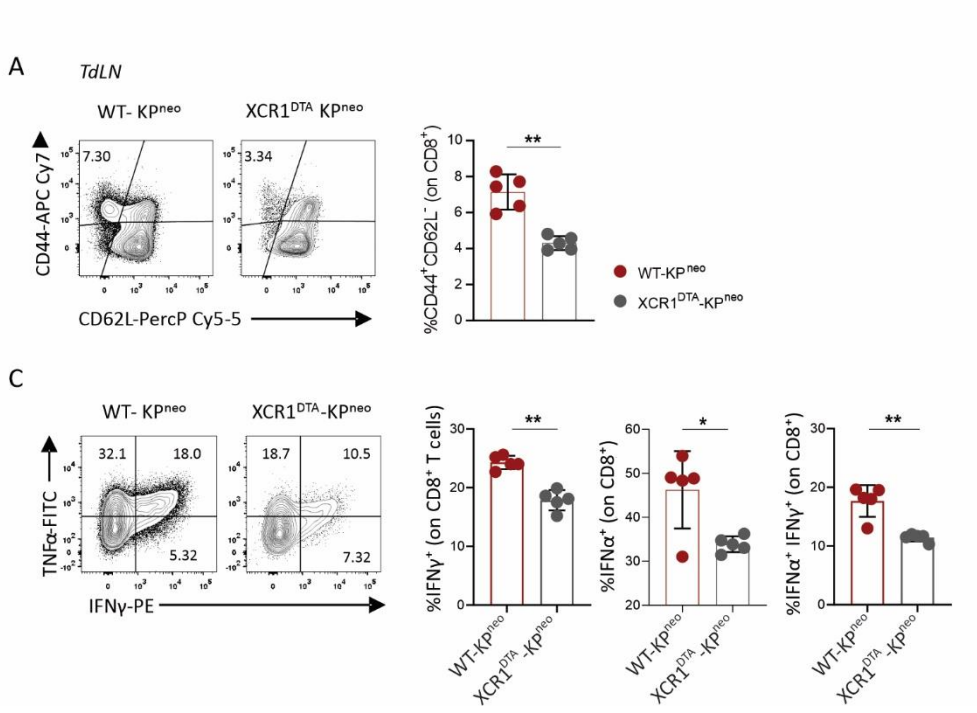

Figure 4.23| cDC1 are required to efficiently activate CD8 T cells against neoantigens. A) Relative frequencies of effector-memory CD8$^+$ T cells (CD44$^+$CD62L$^-$) (n=5). Statistical analysis was performed by t-test **p<0.01. **B)** Total cells from tdLN from KP^{neo} tumors in Wt or XCR1^{DTA} treated with FL/pI:C+αPD-L1 were stimulated with PMA/Iono and frequencies of IFNγ CD8$^+$ T cells were measured by flow cytometry (n=5). Statistical analysis was performed by t-test *p<0.05, **p<0.01. Unless noted, data represent mean ± SEM.

To explore the role of cDC1 during the neoantigen cross-presentation *in vivo,* we have performed *ex vivo* restimulation of total cell from the tdLN with the selected peptides, presented in the figure 4.11. Thus, BMDCs were loaded with the neoantigen peptides and co-cultured with cells derived from tdLN either from XCR1^{DTA} or Wt mice. After 5 days of co-culture, IFNγ accumulation was measured by ELISA in the supernatant as a sign of specific activation.

In general, we observed a decreased production of IFNγ in almost all the peptides but only Neo 2 or Neo7 showed a significant decrease (Figure 4.24). This evidence indicated the decisive role of cDC1 during neoantigen capture, processes and presentation to activate specific CD8 T cells.

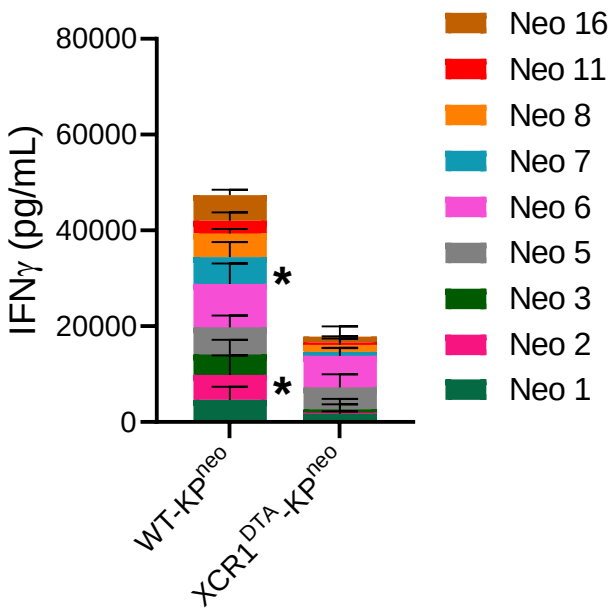

Figure 4.24| cDC1 are necessary to orchestrate neoantigen-specific T cell responses. IFNγ levels detected after stimulation of tdLN cells from KP^{neo} in Wt or $XCR1^{DTA}$ mice with peptide loaded BMDCs (n=5). Data show mean ± SEM. Statistical analysis was performed by two-ways ANOVA followed by Sidak´s posttest **p<0.01, *** p<0.001, **** p<0.0001.

In summary, we have tested a DC-based therapy in the context of increased neoantigen burden. We found that therapy is effective in tumors expressing a consistent level of neoAgs, whereas poorly immunogenic tumors remain resistant to the treatment. The therapy leads to an increased immune infiltrate in KP^{neo} tumors and particularly by effector memory and activated CD8 T cells. The therapeutic effect and the impact in the immune response against neoantigens was lost in cDC1 deficient background, demonstrating the role of this subset during the orchestration of neoantigen specific T cell response.

Chapter 7. FLT3L+aCD40 therapy is sufficient to expand neoantigen specific CD8 T cells and tumor control in the lung.

Previous studies in our lab have shown that KP undergoes progressive depletion and functional suppression of cDC1 in lung tumor tissues[182]. Recently, Westcott *et al.,* have demonstrated that suboptimal T cell responses against neoantigens can be reverted by improving CD8 T priming. Thus, therapeutic rescue of priming rendered T cells fully capable of controlling tumors[247].

In addition, migratory cDC1 were found to be reduced in the LNs of KP tumors[218]. A combination of Flt3L+αCD40 rescued the number of migratory cDC1 in tdLNs and

promoted presentation of a surrogate model antigen in lymph nodes, leading to expansion of a subpopulation of not exhausted tumor-specific CD8 T cell in tdLNs in a NSCLC model[218]. This combinatorial therapy was also tested in others tumor models as PDAC, showing and increased number of cDC1 in the tumor and the reduction of apoptosis in this subset[146].

Based on the observations collected in flank tumors and the evidence reported in the literature, here we employed the orthotopic KP^{neo} model to examine the effect of Flt3L+αCD40 (FL/pI:C+αPD-L1), and a combination of this therapy and anti PD-L1 blockade in the context of tumors expressing a known amount of neoantigens. KP^{neo} cells were injected intravenously to establish lung tumors and different groups were treated intraperitoneally with the therapies described in Figure 4.1. A control group received control isotype antibody (α-IgG).

In order to evaluate the mobilization of cDC1 into tumor bearing lungs we took advantage of the $XCR1^{Venus}$ mouse model. This strain specifically encoded the sequence of the fluorescent protein Venus under the *Xcr1* promoter, thus cDC1 population can be tracked either by flow cytometry of immunofluorescent microscopy. By using this model, we have observed an increased infiltration by cDC1 in KP^{neo} nodules after FL/αCD40 therapy in comparison with the control group (Figure 4.25).

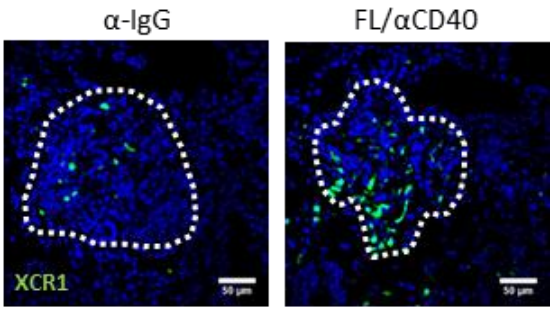

Figure 4.25| FL/αCD40 mobilizes cDC1 in KP^{neo} nodules. Representative lung sections showing cDC1 infiltrating KP^{neo} tumors in mice treated either with control isotype or FL/αCD40. Scale bar 50 µm.

In order to quantify the recruitment and increase of cDC1 in KP^{neo} lung-tumor bearing mice after the treatments described above, a rigorous gating strategy was used to identify cDC1 (Figure 4.26 A). This gating strategy excluded lymphocytes, monocytes, and macrophages in the lineage as possible contaminants. The first observation was the influx of a $Lin^{-}CD11c^{+}$ population with low expression of MHC class II after FL/αCD40

therapy alone or in combination with αPD-L1 (Figure 4.26 B). Deeper analysis are needed to further characterize and identify this population; however, we might suppose that they are pre-DCs based on their low expression of MHCII and, also because it has been reported that FLT3L is involved in the recruitment of this subset into the TME in melanoma mouse models[168].

Regarding cDC1, we have observed that the combination FL/αCD40 led to a significant increase in the frequencies and absolute numbers of this subset in KP^{neo} tumor bearing lungs (Figure 4.26 C). Surprisingly, the addition of anti-PD-L1 to DC-based therapy did not improve the effect, on the contrary, cDC1 frequencies in this group were comparable to those found for the untreated group.

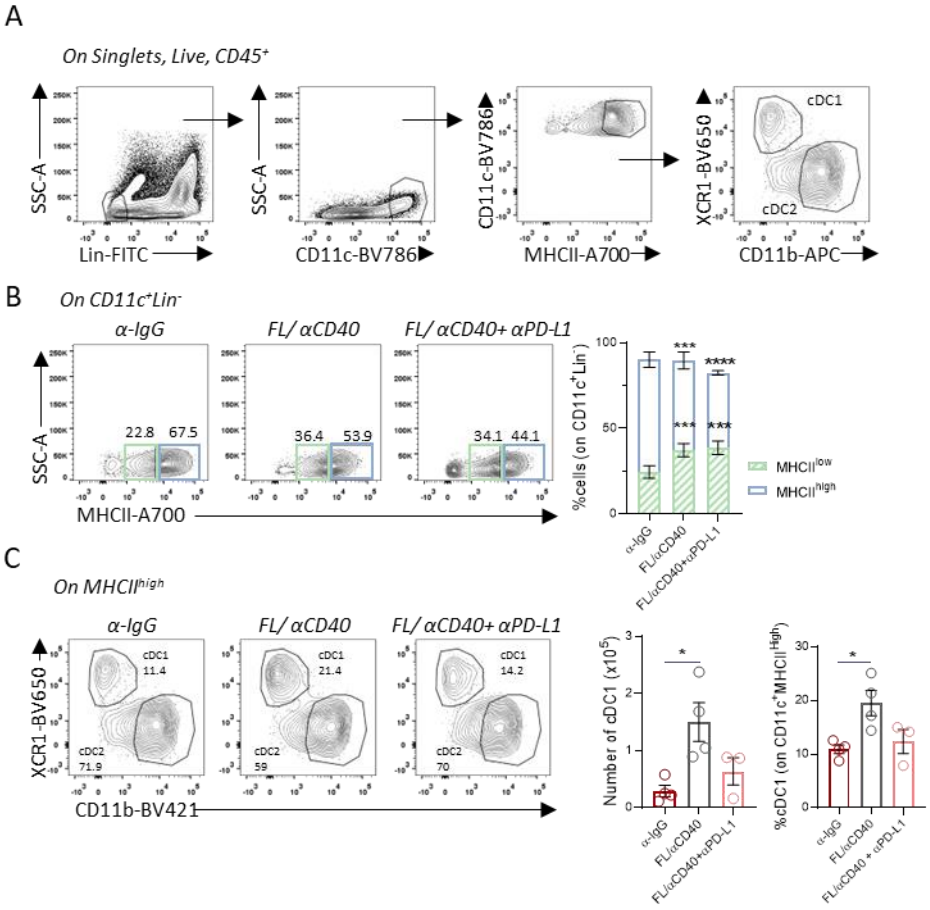

Figure 4.26| FL/αCD40 leads to the accumulation of myeloid subsets as cDC1. A) Gating strategy used for identifying cDC1 in total lung tissue. Lin (lineage) includes B220, CD3ε, CD19, F4/80, Ly6C, Ly6G and NK1.1. **B)** Relative frequencies of MHCII^{low} and MHCII^{high} cells in lungs of tumor bearing mice (n=4). Statistical analysis was performed by one-way ANOVA followed by Tukey's posttest ***p<0.001, ****p<0.0001. **C)** Relative frequencies and absolute numbers of cDC1 cells in lungs of tumor bearing mice (n=4). Statistical analysis was performed by one-way ANOVA followed by Tukey's posttest *p<0.05. Unless noted, data represent mean ± SEM.

Based on the previous results, we wondered whether the therapy could also impact on the enrollment of CD8 T cells in tumor bearing lungs. To this purpose we analyzed tumor baring lungs by flow cytometry and specific immunostaining in lung sections. We observed that the impact of DCs therapy (FL/αCD40) includes an increased frequency of $CD8^+$ T cells infiltrating lungs (Figure 4.27 A-B). The higher infiltration of CD8 T cells was also evident by immunofluorescence in tissue section, where in lungs treated with DC therapy nodules were highly infiltrated by CD8 T cells (Figure 4.27 A).

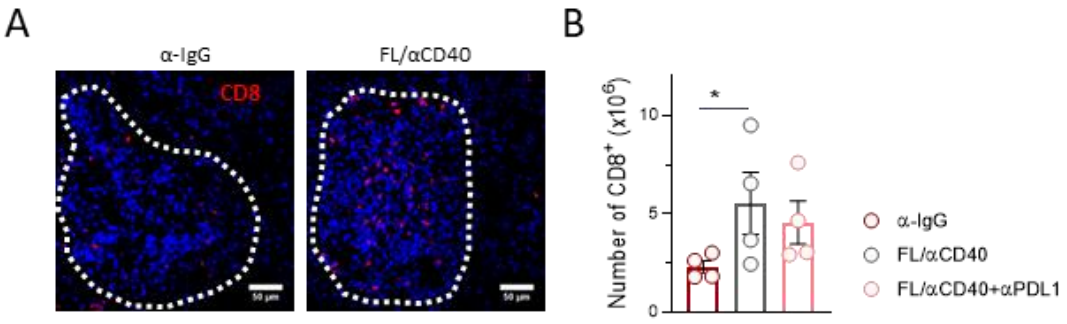

Figure 4.27| FL/αCD40 mobilizes CD8 T in KP^{neo} nodules. A) Immunostaining of CD8 T cells in tissue sections in control and treated mice. Scale bar 50 µm. **B)** Absolute number of $CD8^+$ T cell infiltrating KP^{neo} tumor bearing mice (n=4). Data represent mean ± SEM and statistical analysis was performed by one-way ANOVA followed by Tukey's posttest *p<0.05.

To further investigate the impact of the therapies on the $CD8^+$ T cell phenotype, we performed flow cytometry analysis. Thus, we have quantified the relative frequencies of effector-memory CD8 T cells, the proliferative capacity characterized by the intranuclear expression of Ki-67, and the frequency of $TCF1^+PD1^+$ $CD8^+$ T cells. This subset has been proposed to have stem-like progenitors[82] with proliferative capacities and to promote tumor control. Moreover, $TCF1^+PD1^+$ $CD8^+$ T cells were associated with improved responses to ICB in murine models[248].

In our setting we observed an increased fraction of effector-memory CD8 T cells (Figure 4.28 A) in mice treated with both therapies in comparison with the control group. We noted a 2-fold increment in the frequencies of $CD44^+CD62L^-$ $CD8^+$ T cells. Moreover, the fraction of proliferating ($Ki\text{-}67^+$) $CD8^+$ T cells, was significantly induced by FL/αCD40 therapy, with no addictive effect of PD-L1 blockade (Figure 4.28 B). Additionally, FL/αCD40 produced a 2-fold expansion of $TCF\text{-}1^+PD\text{-}1^+$ $CD8^+$ T cells (Figure 4.28 B), with potential to differentiate into effector cells[248] and addition of anti-PDL1 to the DC

therapy did not improve the observed effect, suggesting a major contribution of the DC-based components.

Taken together, these results showed that the DC-based therapy mobilized cDC1 to the TME counteracting their depletion during tumor progression and their increased number remodeled the CD8 T differentiation by favoring effector and pre-dysfunctional phenotypes.

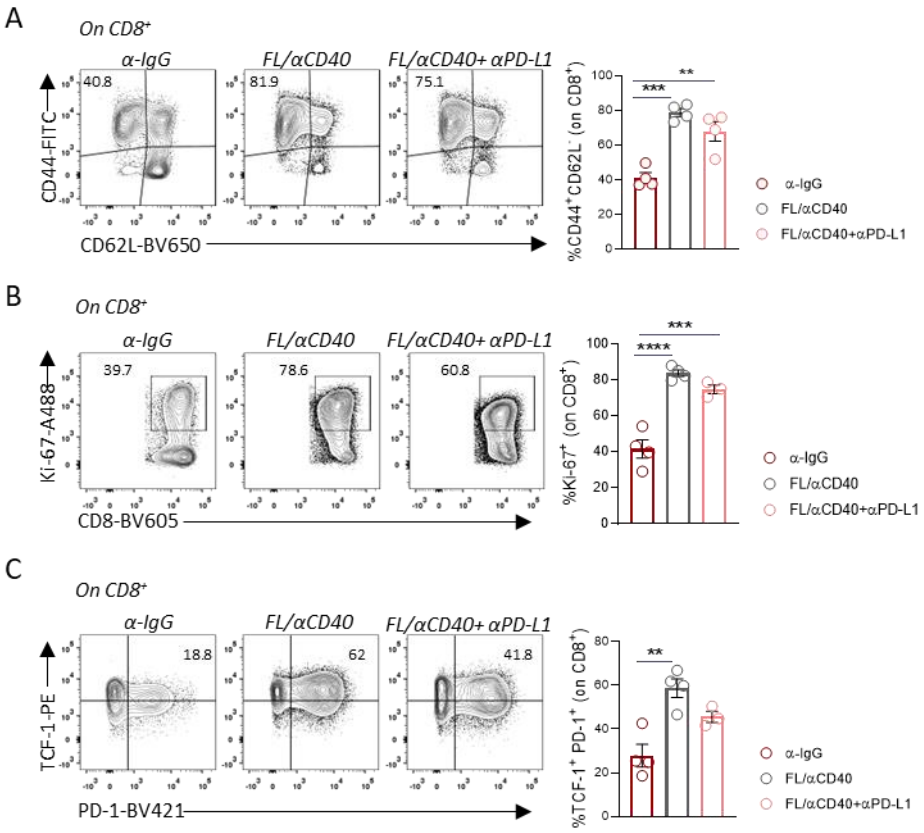

Figure 4.28| DCs therapy is sufficient to expand progenitor exhausted and proliferating CD8 T cells. A) Flow cytometry analysis and relative frequencies of effector memory $CD8^+$ T cells (n=4). **B)** Flow cytometry analysis and relative frequencies of proliferating ($KI\text{-}67^+$) $CD8^+$ T cells (n=4). **C)** Flow cytometry analysis and relative frequencies of progenitor exhausted ($TCF1^+PD1^+$) $CD8^+$ T cells (n=4). **(A-C)** Data represent mean ± SEM and statistical analysis was performed by one-way ANOVA followed by Tukey's posttest **p<0.01, ***p<0.001, ****p<0.0001.

DC-based therapy not only generated a remodeling of the tumor microenvironment but also impacted on tumor growth at early stages. FL/αCD40 led to a delay during the tumor engraftment process of KP^{neo} tumors, the addition of anti-PDL1 did not improve the therapeutic effect observed for the DC therapy alone (Figure 4.49 A-B).

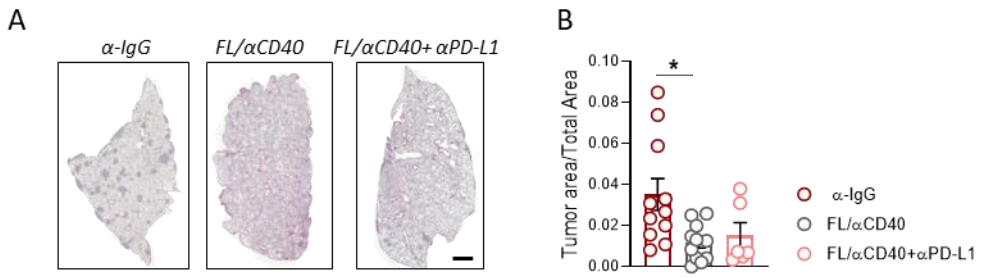

Figure 4.29| DCs targeting is more effective than checkpoint blockade to promote therapeutic immunity to KP^{neo} in lung tissues. A) Representative images of KP^{neo} tumor bearing lung sections. Scale bar represents 1 mm. **B)** Quantification of KP^{neo} lung tumor burden on day 9. Lung sections were stained with haematoxylin and eosin (n=11). Data represent mean ± SEM and statistical analysis was performed by one-way ANOVA followed by Tukey's posstest. *p<0.05.

Collectively these data show that boosting the DCs compartment is necessary and sufficient to unleash reactivity to neoantigens encoded by KP^{neo} tumors that instead remain refractory to anti PD-L1 therapy.

Chapter 8. FL/αCD40 therapy induces remodeling of the cDC compartment and CD8 subsets in the orthotopic model.

In the previous chapters the collected data showed the impact of FL/αCD40 therapy during the recruitment of myeloid cells, in particular cDC1 and pre-DC like cells, and proliferating CD8 T cells with an effector phenotype. To perform an in-depth analysis during immune compartment remodeling in the TME, scRNAseq analysis was used.

To this purpose, KP^{neo} cells were injected intravenously in immunocompetent mice to generate lungs tumors. KP^{neo} tumor bearing mice were treated either with control isotype or FL/αCD40 according to the scheme presented in the Figure 4.1. Thus, CD45^{+} cells were sorted from KP^{neo} tumor bearing lungs treated with FL/αCD40 or control isotype antibody (α-IgG). For both condition 1x10^{4} cells were loaded to generate the barcoded single-cell gel beads and 8861 or 6762 cells were obtained for control and treated groups, respectively, with a coverage of 100.000 reads/cell. After sequencing and quality checks, data from both groups were computationally integrated and after unsupervised analysis, groups of different cell subsets were identified.

This analysis identified 11 clusters of immune related subsets based on signatures from the IMMGEN consortium (Figure 4.30 A) and consistent with the structure of immune populations previously identified in the same tumor model (Zilionis 2019). These 11 clusters were characterized by the expression of specific genes listed in Figure 4.30 C. The main impact of therapy was observed in NK cells, monocytes, neutrophils and

dendritic cells (Figure 4.30 B). NK cells, monocytes and dendritic cells clusters have higher frequencies in the treated group, whereas γδ T cells, and T regs were enriched in the control group. Similar observations were obtained by Hegde *et al.,* using a PDAC model treated with FLT3L and anti-CD40, they observed an increase in the numbers of NK cells infiltrating tumors. These results indicate that the combinatorial therapy generated a general remodeling of the immune subsets that are infiltrating KP^{neo} tumors in the lung.

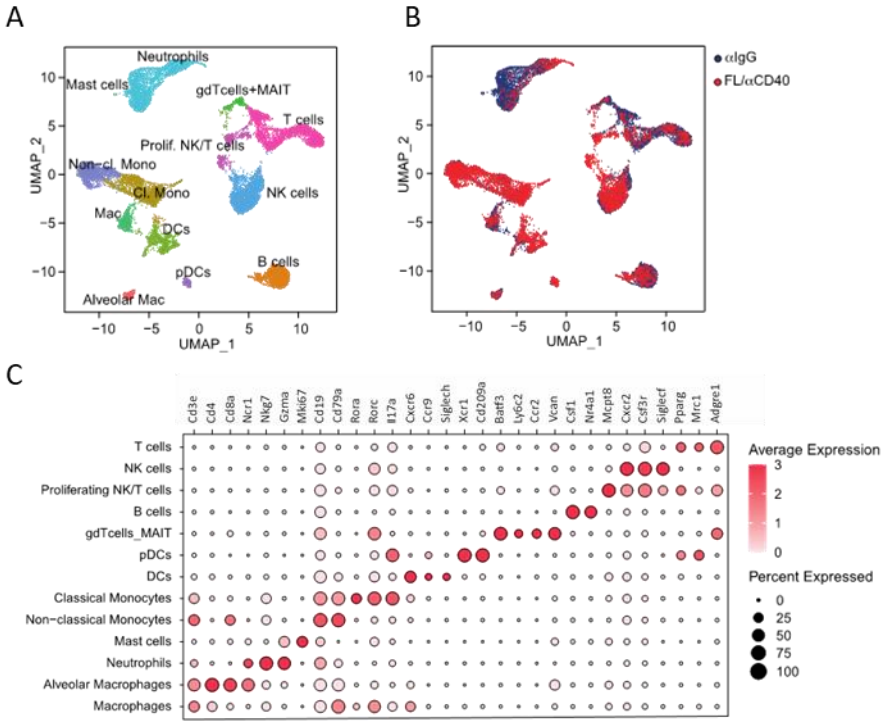

Figure 4.30| Immune subsets present in KP^{neo} tumors in control and treated groups. A) UMAP plot of curated DCs clusters integrating treated and not treated conditions. **B)** UMAP showing treatment dependent changes in clusters distribution/abundance**. C)** Bubble plot map showing genes used to identify clusters.

Section A. FL/αCD40 therapy induces remodeling of the cDC subsets

In order to further explore the changes generated by therapy in the dendritic cells, this cluster was re-clustered. Thus, 4 major cluster were identified (C0-C3) based in their gene expression (Figure 4.31 A). The first observation was that the general cluster distribution was maintained upon therapy.

These clusters represented the main DCs subsets described for lung tissue in mice[124] and each cluster was characterize by a specific gene signature that is summarized in the figure 4.32 B. In this sense, C0 expresses cDC2 markers like *Igam, CD209* and *Sirpα*; C1

represents cDC1 based on the expression of *Xcr1, Clecl9* and *Camd1*; C2 showed lower expression of cDC1 markers and strongly expression of cell proliferation genes such as *Mik67* and *Topa2*. These two clusters were named cDC1a (C1) and cDC1b (C2).

Startlingly, C3 shows the expression of cDC1 and cDC2 markers. This clusters segregates from the others, and it is characterized by the expression of *Ccr7*, *Fscn1* and *Socs2K* (Figure 4.31 B). Similar characteristic to those observed for C3 were described previously by independent groups. Thus, Maier *et al.,* have named them as mregDCs[125], whereas other groups have focused in the migratory phenotype and they name these cells as migDCs[249].

Further analysis of expression of selected genes across all cDC clusters revealed that cDC1a shows high expression of genes related to the vesicular trafficking and antigen presentation, whereas cDC1b genes related to the proliferation (Figure 4.31 C). In that regard, cDC1a showed expression of *Wdfy4*, *Vamp3*, *Vamp4* and *Tap1*, all genes related to vesicular trafficking and antigen presentation indicating that this subset correspond to differentiated cDC1.

Regarding to cDC1b, this subset showed expression of genes related to proliferation such as *MKi-67*, *Top2*a and genes for different cyclins indicating high proliferative capacity (Figure 4.31 C). Moreover, this subset showed low expression levels of maturation markers. Based on its high proliferative capacity and immature phenotype, we suggest that this subset may correspond to pre-committed cDC1, that has been described as a target of FLT3L recruitment.

Furthermore, C3 shows high expression of maturation markers as *Cd40*, *CD80* and *Cd86*, migratory related genes as *Ccr7* and *Fscn1*, and regulatory molecules as *Cd276*. As mentioned above the gene expression analysis indicated that this cluster correspond to migDCs.

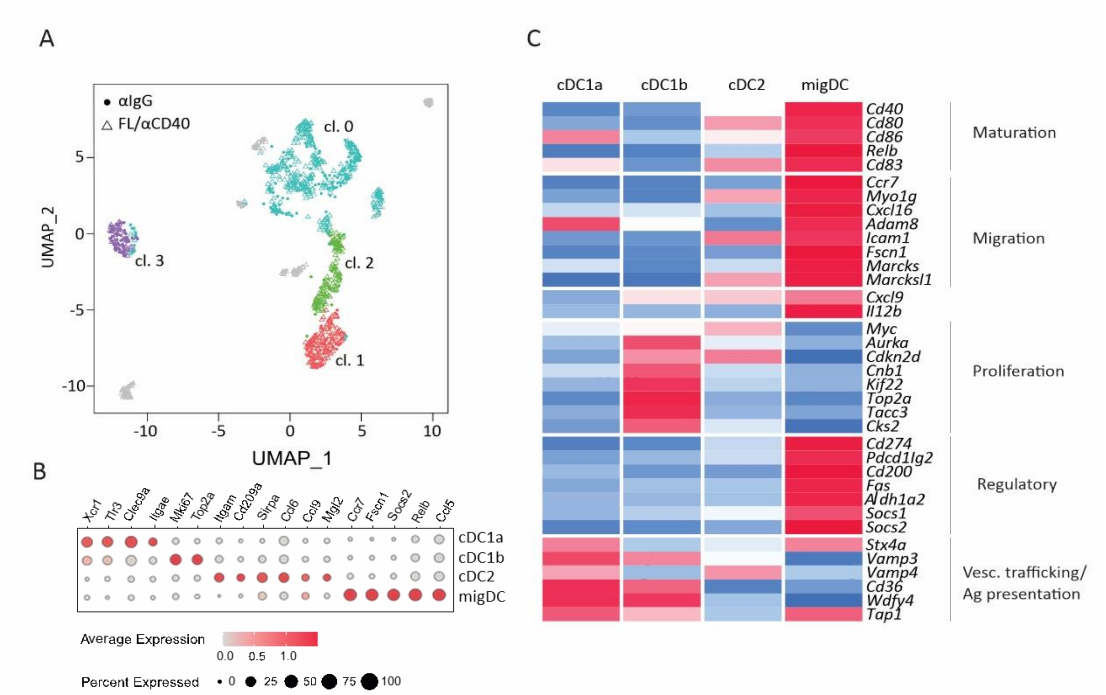

Figure 4.31| FL/CD40 therapy induces remodeling of the cDC compartment in lung tissues. A) UMAP plot of curated DCs clusters integrating treated and not treated conditions. **B)** Bubble plot map showing genes used to identify DCs clusters. **C)** Heat map showing the expression of selected genes across the different DC clusters and association of individual genes to the indicated processes.

Then, we asked if the therapy affects only the DC phenotype or also the frequencies of these subsets. Thus, analyzing the composition of the subsets we have observed that before therapy cDC2 is the main subset representing almost 50% of the cells and remained almost unchanged after therapy (Figure 4.32 A); the second subset according to the frequencies were the migDCs that had a considerable reduction after therapy (Figure 4.32 B). cDC1 represent the least frequent groups before therapy, but were the main subsets increased by therapy (Figure 4.32 A-B), suggesting the specificity of FLT3L during the recruitment of cDC1-like cells.

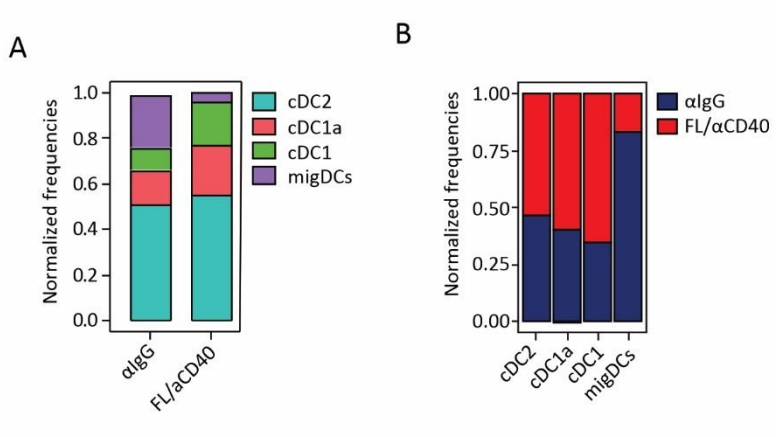

Figure 4.32| Combinatorial therapy boosts specifically cDC1 clusters. A) Bars represent the composition of each cluster based on treatment and the proportion of the clusters in the two treatment conditions. **B)** Stack charts of contribution of each cluster in control and treated groups.

As mentioned above, we wanted to address the phenotypical changes driven by the therapy. Therefore, we analyzed differentially expressed genes (DEGs) and biological processes in cDCs. migDCs were excluded from the analysis due to the scarce number upon therapy.

DEGs analysis showed that the therapy modulated gene expression profiles within each cluster, with shared gene modules as well as specific patterns (Figure 4.33 A). Thus, *Klf2* (a transcription factor involved in self-renewal of myeloid cells) was upregulated in all cDCs subsets, also, genes related proliferation such as Plac8 and histones were increased in all cDC clusters. Moreover, *Ramp1* (a co-receptor for calcitonin-gene related peptide) a protein that was recently associated to innate lymphoid cell differentiation in the lung[250] was significantly expressed in all cDC clusters after therapy.

Specificaly, cDC1 showed specific overexpression of genes related cross-presentation (*Rac2)*[251], metabolism (*C1qbp*), cholesterol metabolism (*Pycard)* and *Sell* an integrin described in pre-DCs entering in the lung[152]. Regarding cDC2 the most prominent genes were related to the NF-κB dependent proinflammatory cytokine *Ccl5*. Interestingly, many genes related to the regulatory program defined by Maier *et al.,* (including, *Axl*, *Ccl22*, *Ccl17*, *Il4ra* and *Mgl2*)[125] were downregulated in all subsets.

Regarding the biological processes, GSEA analysis in cDC1a showed an increase in pathways related to metabolic changes associated to activation such as aerobic respiration, oxidative phosphorylation, and protein synthesis (mRNA processing, tRNA metabolism and ribosome biogenesis). Moreover, genes controlling responses to type I

interferon responses were upregulated in cDC1a which may reflect the specialization of this lung subset in sensing type-I IFNs. cDC1b and cDC2 were enriched mainly in processes related to cell proliferation (Figure 4.33 B).

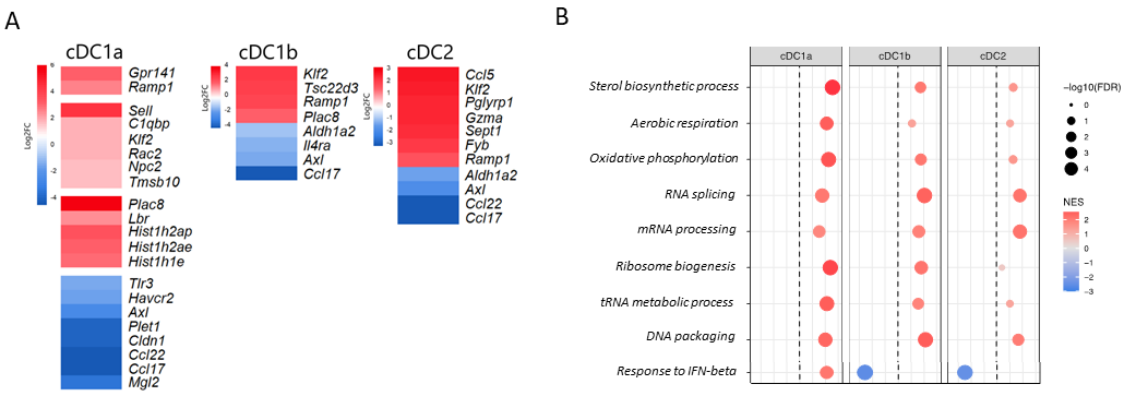

Figure 4.33| FL/αCD40 produce metabolic reprograming and increased proliferation in cDC subsets. A) Heatmap of DEGs in cDC clusters. Data represent Log_2FC. **B)** GSEA analysis of biological processes significantly regulated in cDC clusters. Data represent normalized expression score (NES).

In summary, scRNAseq unveiled the changes generated by FLT3L and agonist for CD40 in tumor bearing lungs. We detected 4 clusters of cDCs that were conserved after therapy. The combinatorial therapy modified the frequencies and the phenotype of dendritic cells increasing the frequencies of cDC1 and their proliferative capacities. Moreover, the therapy decreased regulatory programs in cDC and reduced the frequencies of migDCs.

Section B. FL/αCD40 therapy induces remodeling of the CD8⁺ T cells.

Dendritic cells play a critical role in generating anti-tumor T cell immunity. Due to the remodeling on the DC subset induced by the therapy we wanted to analyze whether or not the therapy impacts on the T cell subsets.

Thus, T cells cluster was re-clustered and 10 new clusters were identified (C0-C9); where, C0 and C2 corresponded with CD4 T cells, C9 with Tregs, C7 with γδ T cells, C8 with MAIT cells and C1, C3, C5 and C6 with CD8 T cells (Figure 4.34 A).

Then, we analyzed the frequencies of these subsets in control and therapy groups, and we observed that C5 and C6 were increased after therapy whereas C7 and C8 were reduced in frequencies (Figure 4.34 B).

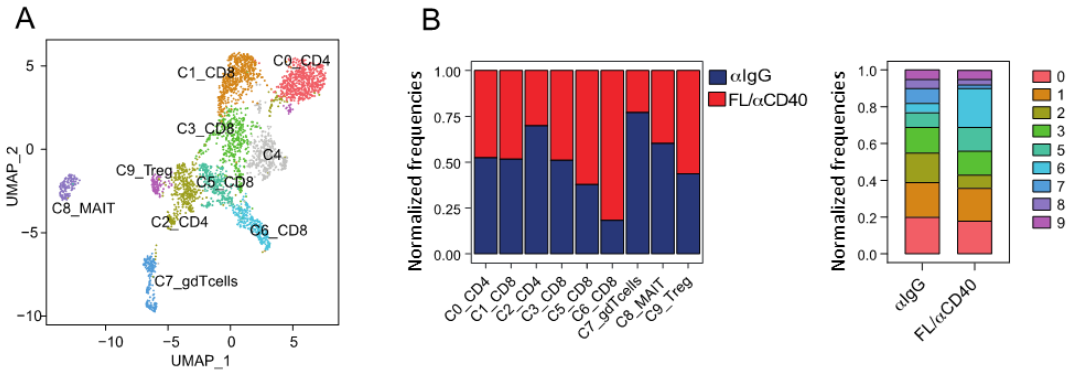

Figure 4.34| DC-therapy promotes expansion CD8⁺ T cells in KP^{neo} lung tumors. A) UMAP plot of curated T lymphocytes clusters integrating treated and not treated conditions. **B)** (Left) Stack charts of contribution of each cluster in control and treated groups. (Right) Bars represent the composition of each cluster based on treatment and the proportion of the clusters in the two treatment conditions

In this study we mainly focused on CD8 T cells consequently we analyzed C1, C3, C5 and C6 in more depth. C1 showed an enrichment in genes related to naïve T cells such as *Sell, Lef1* and *Ccr9*. C3 presented gene expression of a broad number of genes associated to T cells activation such as *Cxcr3* and short-lived effector T cells marker (*Ifit1, Ifit2, Eomes*). C5 was enriched in genes associated to conventional T cell activation and exhaustion (*Gzmb, Gzmk, Cxcr3, Ccl5, Itga1, Lag3, Pdcd1*) and C6 highly expressed proliferation markers (*Top2a, Mki67*) and effector function genes (*Klrg1, Gzma*) (Figure 4.35).

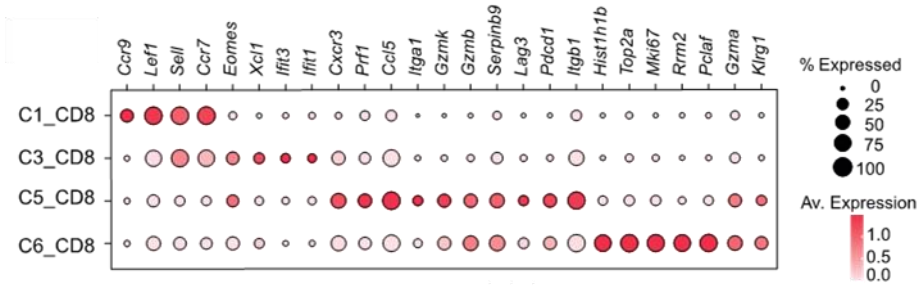

Figure 4.35| FL/αCD40 promotes expansion effector and proliferating CD8⁺ T cells in KP^{neo} lung tumors. Bubble plot map showing genes used to identify CD8 T cell clusters.

To address the molecular changes driven by the therapy we analyzed the DEGs and biological processes after therapy for the non-naïve CD8 T cell clusters. DEGs analysis showed an enhanced effector/cytotoxic function in C3 and C5 with an increase in the expression of *Gzma*, *Ctla2* and *Serpina3g*. Also, C6 showed an increased in cytotoxic genes such as *Gzma*, *GzmK* and *Klrg1* (Figure 4.36 A).

To further analyze the cytotoxic and exhaustion phenotype we have combined selected genes in a signature of cytotoxicity and in a second one associated to exhaustion. The signatures associated to cytotoxicity showed a significant increase in all non-naïve CD8 T cells. Concomitantly a signature including genes defining negative regulation and exhaustion were downregulated in C5 and C6. These results indicated that the therapy favored activated-effector phenotypes rather than exhausted even in presence of chronic exposure to neoantigen (Figure 4.36 B).

The biological pathway analysis showed a metabolic reprograming with increased aerobic respiration and oxidative phosphorylation related pathways in all non-naïve CD8 T cells. This analysis also showed an increased in proliferation pathways such as cell division and DNA replication in C6. Response to TGF-β signalling and bone morphogenetic protein were consistently lost across subsets (Figure 4.36 C).

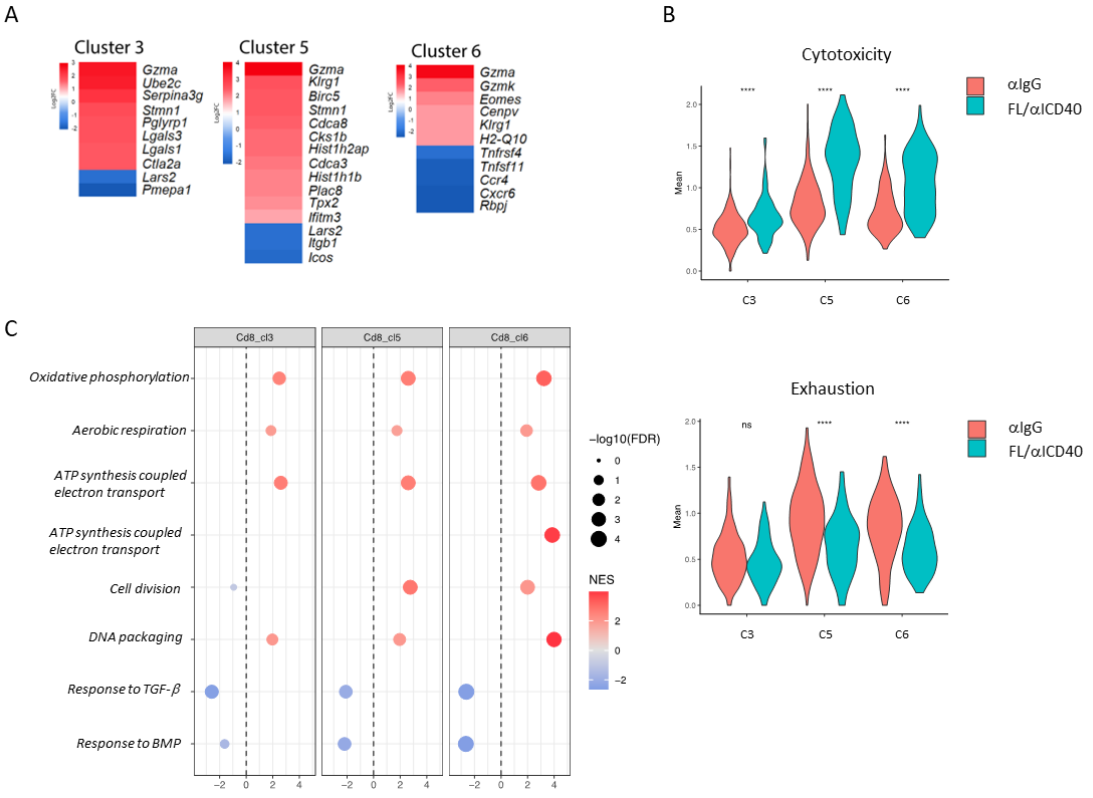

Figure 4.36. FL/αCD40 promotes expansion effector and proliferating CD8⁺ T cells in KP^{neo} lung tumors. A) Heatmap of DEGs in non-naïve CD8 T cells. Data represent Log2FC. **B)** Violin plot representing the mean of expression of selected genes involved with cytotoxicity (upper panel) or exhaustion programs (lower panel) in non-naïve CD8⁺ T cells. **C)** GSEA analysis of biological processes significantly regulated in non-na¨ve CD8 T cells clusters. Data represent normalized expression score (NES).

In summary, the results presented above showed that the therapy not only impacted the DC compartment but that its effects also encompassed CD8 T cells. The therapy

modified their phenotype, amplifying more cytotoxic groups and with greater proliferative capacity, as well as modifying their metabolism, favoring energy production to support these processes.

5. Discussion

The results presented in this study have shown that CD8 T cell responses generated against neoAgs depend on cDC1. Furthermore, cDC1 enhancement generates reprogramming in CD8 T cells in tumor-bearing lungs, and their expansion is sufficient to generate therapeutic effects in mice with hypermutated tumors. This study shows that cDC1 expansion in the tumor overcomes ICB resistance and it is in line with emerging evidence found in other preclinical models for tumors[144–147,218]. Moreover, as proposed in the aim of this report we have generated a hypermutated model of lung cancer that overtakes the limitations of preclinical model harboring a single strong antigen. This model allowed us to show the importance of varied and multiple neoAgs during the generation of the tumor immunity. Thus, the KP^{neo} model permitted us to show that:

- Multiple and varied neoAgs are required to generate tumor-specific CD8 T cell responses and lead to control of tumor growth.
- Increasing the neoantigen burden was not enough to overcome ICB resistance in this context.
- cDC1s are essential during the orchestration of the immune response against neoAgs, and when this subset is missing, the CD8 T-cell response and control of tumor growth is lost.
- Mobilizing cDC1 to the TME by FLT3L to the TME increases and reinvigorates CD8 T cells.

5.1 Neoantigens matter, but what kind and how many are needed to make the difference?

Currently it is well established that somatic mutations in the tumor lead to the accumulation of neoAgs capable of eliciting significant tumor immune responses[10,16,252,253]. Yet, neoantigen content is moderately associated with significant responses[253,254] to ICB and only 20% of patients with solid tumors, and 53% of patients with MMRd obtain durable benefits from ICB[106]. Patients who benefit from ICB have cancers with high TMB and, in addition, strongly associated with environmental carcinogens such as chronic exposure to tobacco or ultraviolet radiation[252]. In this context, understanding the biological basis that leads to the generation of the immune

response against neoAgs and its nature is crucial to better stratify patients before deciding on therapeutic options.

Mouse preclinical model of cancers have provided invaluable insights related to the mechanisms of the immune response against cancer[37]. However, in majority of them single model antigens were used to track the immune response, and only a few of these preclinical models recapitulate features of human cancers. In this report we have used the KP cell line as a lung cancer model because when implanted in the lung, it develops an adenocarcinoma that resembles the histopathology of human NSCLC[241].

This model was used to study the impact of a baseline neoantigen load generated by genomic instability due to p53 loss, on ICB outcome. We found that this model is resistant to ICB, it does not show tumor growth control in early or late endpoints and the treatment does not enhance the T cell response against the tumor. These observations are in line with published data wherein independent laboratories found KP resistance to ICB[43,86,125,255,256]. However, none of these studies addressed the content of neoAgs as one of the axes to increase tumor immunogenicity.

Mandal *et al.*, have addressed this question using two preclinical models and by studying the impact of the neoantigen burden on the response to ICB. They used B16F10 mouse melanoma model and CT26 mouse colorectal carcinoma cell line. Using CRISPR Cas9 technology they targeted a mismatch repair gene (MSH2) generating MMRd cell lines with different degrees of MSI. They observed that the CT26 parental cell line and cells carrying an intermediate mutational burden remained refractory to ICB whereas high MSI scores led to control of tumor growth paralleled by an increase number of immune cells infiltrating the tumors[257]. These data suggest that a threshold in neoantigen content determines the immune response generated against tumors and the responsiveness to ICB.

In our report, we have generated a KP model with an increment in the neoantigen content as compared to the parental line. The deletion of Mlh1 led to the accumulation of somatic mutations, as single nucleotide variants and frameshifts, giving place to a 2-fold increase in putative neoAgs. Such an increase in neoantigen load in the KP model was sufficient to turn it into a *"warm"* tumor infiltrated by CD8 T cells in both

subcutaneous and orthotopic environments and to induce expression of genes reflecting immune activation. These data are consistent with other groups using the KP model. Martinez-Usatorre *et al.*, have shown that deletion of MSH2 in the autochthonous KP model led to the accumulation of mutations in tumors. They also observed that after 4 weeks from the tumor induction, tumor nodules were more infiltrated by CD4 and CD8 T cells in comparison with MMR sufficient tumors[43].

We have analyzed the neoantigen-specific CD8 T cell response against a pool of predicted neoAgs, covering a varied range of expression and affinity to bind MHC class I complex. We noticed that according to the anatomic sites the response generated against neoAgs was different. In subcutaneous model, CD8 T cells were responding to a broad number of neoAgs, whereas in the orthotopic model CD8 T cell responses were restricted to neoAgs with high predicted affinity for MHC class I.

Recent studies have addressed the role of both parameters: neoantigen expression and predicted affinity to MHCI during the generation of neoantigen-specific immune responses. Westcott *et al.*, have used SIINFEKL as a single antigen in a system that allowed to modulate its expression. They observed that low neoantigen expression prevents productive priming and drives a tolerogenic T-cell response characterized by reduced magnitude, effector commitment, and per-cell functionality. In parallel, Burger *et al.*, have addressed the role of neoantigen MHC affinity during the generation of distinct neoantigen-specific CD8 T cell responses in the context of an antitumor response. Using two different surrogate antigens of varying affinity to the MHCI complex under the same viral promoter, they found that antigens with higher affinity generated dominance over suboptimal antigens, with high-affinity neoAgs limiting the diversity and differentiation from progenitor to exhausted CD8 T cells[258] of suboptimal CD8 T-cell. These two reports provided initial formal hints on how neoantigen features drive different responses and the interplay between multiple antigens. In the context of KP^{neo}, as far as we could assess in our assay, the immune response is not dominated by a single neoantigen. However, in the more suppressive microenvironment of the lung, dominance by the highest affinity antigen seem to emerge.

Moreover, Fessenden *et al.*, have addressed the role of DCs during cross-presentation of neoAgs. They have shown that cross-presentation of neoAgs by DCs is biased towards peptides derived from cytoplasmic proteins, while peptides originating from proteins located in the plasma membrane are underrepresented[259].

Altogether these previous studies showed that neoAgs' features as expression levels, binding affinity for MHCI and the location in different subcellular compartment, dictate the immune response generated against the neoantigen.

In our report we have generated a preclinical model harboring real and varied neoAgs (regulated by their endogenous promoter and with different binding affinities) capable of generating neoantigen-specific CD8 T cell responses. Using this model, we did not observe a hierarchical dominance of strong neoAgs in subcutaneous tumors, but in lung, we observed that the specific responses were restricted to strong antigens. This model offers a precious tool to study the generation of neoantigen-specific responses and can be exploited for further analyses.

5.2 Are neoantigens sufficient to overcome ICB resistance?

One of the best predictors for ICB is the T cell infiltration in tumor nests[32,260]. KP^{neo} tumor showed an increased T cell infiltration in both subcutaneous and orthotopic settings. CD8 T cells infiltrating KP^{neo} tumors showed higher expression of effector/cytotoxic molecules in comparison with those found in KP^{ctrl} tumors. Moreover, increased neoantigen burden led to the accumulation of effector-memory with high expression of PD-1 in $CD8^+$ T cells in KP^{neo} tumor bearing mice. This evidence showed that by increasing neoantigen content, KP tumor becomes warmer.

Despite an objective increase in T cell infiltration and activation, KP^{neo} tumor remained resistant to ICB therapy. In line with our observations, Martinez-Usatorre *et al.,* have generated a KP model with deficiency in the MMR machinery. Using this model, they demonstrated that MMRd tumor accumulates somatic mutations and increased neoantigen burden increased T cell infiltrating tumor[43]. Although the increase in infiltrating CD8 T cells in MMRd tumors remained refractory to ICB. The authors suggested that progressive KP tumors harbor suppressed CD8 T cells, which cannot be rescued by potential endogenous neoAgs[261,262]. It has been shown that the progression

of KP tumors led to accumulation of exhausted CD8$^+$ T cells that expressed increasing number of inhibitory molecules[218]. The terminally exhausted CD8$^+$ T cells are not rescued by anti-PD1 therapy due to the loss of their stem-like properties, but progenitor exhausted CD8$^+$ T cells that have expansion capacities can respond to this therapy[85]. Thus, the balance between these two subsets could dictate the responsiveness to ICB in our model. A second possibility to explain the resistance to ICB could be a suboptimal activation of CD8$^+$ T cells. Westcott *et al*,. have shown that poor T cell priming led to resistance to ICB in a preclinical model of colorectal cancer. Furthermore, they have shown that the rescue of CD8$^+$ T cell priming by anti-CD40 treatment renders T cells fully capable of tumor control after ICB.

Thus, we hypothesize that a combination of factors such as unbalanced frequencies of different exhausted subsets and poor CD8 T cell priming could explain the resistance to ICB in our model. Additional analysis is needed to further investigate the T cell exhaustion status in tumor infiltrating CD8$^+$ T cells and remains as an open question from this report.

5.3 cDC1s are essential during the orchestration of the immune response against neoantigens

The data presented in this report showed that neoantigen-specific CD8 T cell responses depended on cDC1 for its orchestration. Signs of immune activation, such as activation-related gene expression, CD8 T cell infiltration, and tumor growth control in KP^{neo} tumor, were shown to be lost in mice lacking cDC1, establishing this subset as the major determinant of the immunogenicity of tumors expressing neoAgs.

Due to the importance of cDC1 during antigen presentation and lymphocyte activation[148], cDC1 abundance has been suggested to correlate with immune-mediated tumor control and favorable outcome in both human and mice[17,144,150,180]. However, the elements that control the accumulation of cDC1 within tumors are still poorly understood.

Our data showed that cDC1s were selectively recruited in KP^{neo} tumors subucutaneous tumors and not in parental KP tumors. We can exclude the possibility of a bias in chemoattractant expression by tumor cells between KP^{ctrl} and KP^{neo}, because RNA-seq data did not show major differential expression of chemokines in the two cell lines.

However, we observed an increased expression of chemokines that recruit dendritic cell[263] as *Ccl4* in the TME of KP^{neo} in comparison to KP^{ctrl} subcutaneous tumors. The sources of CCL4, as other chemokines to recruit DC, are varied- from tumor cells to immune cells as NK cells[244,264]. The role of NK cells during the recruitment of cDC1 in tumors was well documented by Böttcher *et al.*; they have demonstrated that the secretion of CCL5 and XCL1 by intratumoral NK cells lead to the recruitment of cDC1 into tumors[149]. We cannot exclude the role of NK cells during the recruitment of cDC1 in tumors, but it remains unclear why this occurs only in KP^{neo} tumors. Since T lymphocytes are an important source of FLT3L[265] in TME leading to pre-DCs recruitment and expansion, it is reasonable that priming by neoantigen presenting cDC1 could lead to Flt3L secretion in turn providing the signals to augment the recruitment of immune cells including cDC1, creating a positive feedback loop.

5.4 Mobilizing cDC1 to the TME by FLT3L to the TME increases and reinvigorates CD8 T cells.

Therapeutic strategies to boost and activate DCs, in particular, cDC1 have been explored successfully in melanoma and pancreas tumor models[144,146,214,217]. We have tested a combinatorial DC-based therapy in KP tumors, this therapy includes FLT3L, Poly (I:C) and anti-PD-L1. To assess the impact of the therapy on KP tumors we moved back to the subcutaneous tumors in order to administrate the therapy *in situ*. The subcutaneous model represents many advantages: it allows to directly treat the tumor avoiding systemic effects and side effects, and also allow to follow the tumor progression.

We found that promoting DCs expansion and activation triggers extensive infiltration of immune cells, in particular, T lymphocytes in KP^{neo} tumors. $CD8^+$ T cells showed effector memory markers and effector functions after therapy, the therapy led to the generation of a pool of TCF^-Gzmb^+ $CD8^+$ T cells in tumors and significantly inhibited tumor progression. The combinatorial therapy had an impact also on the $CD8^+$ T cells in the tumor draining lymph node leading to an increase in IFNγ production by $CD8^+$ T cells as well an increment in the frequencies of $TCF1^-GzmB^+$ $CD8^+$ T cells.

Similar evidence was found by independent groups using different tumor preclinical models such as pancreatic tumors, melanoma, and colorectal cancer. Lin *et al.*, have shown that FLT3L administration in combination with anti-CD40 led to an increase in the

frequency of effector memory T cells. In addition, they observed that CD8 T cells produced more IFNγ in treated groups[146]. Salmon *et al.*, have shown that a combinatorial therapy containing FLT3L led to a significant tumor control in melanoma model. The therapy also generated a high lymphocyte infiltration in tumors[144]. In parallel, Oba *et al.*, have tested the efficacy of therapy with FLT3L in combination with TLR3 agonist, anti-CD40, radiotherapy and anti-PD-L1 in different preclinical tumor model. They found that FLT3L alone was sufficient to mobilize cDC1 in tumors and the combinatorial therapy led to an influx of $TCF1^+$ CD8 T cell infiltrating the tumors[214]. Evidence from human data extracted from a clinical trial (NCT02129075) testing FLT3L in a combinatorial therapy to treat high risk melanoma patients showed that FLT3L administration increased peripheral monocytes, cDCs and plasmacytoid DCs. Also, therapy in humans suggests an increase in humoral and T-cell responses and activation of DCs and natural killer cells. All these studies support the data reported in our model demonstrating the ability of cDC1 to enhance antitumor responses.

Surprisingly, KP^{ctrl} tumors were completely refractory to the concomitant boost in antigen presentation and T cell activation. In this line, AT-3 tumors treated with FLT3L, TLR3 agonist and anti-CD40 showed a slight tumor delay; however, when tumors were also treated with radiotherapy (to generate DNA damage and neoAgs[266,267]) tumor size was significantly reduced and had a substantial impact on the survival in treated mice[214]. This result formally proves that a minimal threshold of neoAgs is an essential prerequisite for strategies that aim to empower antigen specific anti-tumoral responses.

5.5. Combinatorial therapy specifically enhances neoantigen cross-presentation

In this thesis we have demonstrated that cDC1s have a non-dispensable role for the generation of anti-tumor response in neoantigen-rich tumors. To investigate whether therapeutic immunity observed with the combinatorial therapy depends on cDC1 we employed $XCR1^{DTA}$ mice; in which the expression of the Diphtheria toxin subunit A (DTA) under the *Xcr1* promoter generates the specific ablation of cDC1 without affecting other immune subsets in different tissues[225,268].

We observed that specific depletion of cDC1 abolishes the advantages conferred by therapy, i.e., tumor growth control and recruitment of $CD8^+$ T cells was lost in $XCR1^{DTA}$ mice. In addition, effector memory and cytotoxic subsets were reduced in $XCR1^{DTA}$ hosts,

demonstrating that cDC1 are required for the recruitment and optimal priming of CD8 T cells.

In addition, we observed that neoantigen-specific T cell responses were weaker in XCR1^{DTA} than Wt mice. The overall response against neoAgs was lower in XCR1^{DTA} and two neoAgs lost statistically significant increment. These data showed that cDC1s are crucial during neoantigen cross-presentation and specific CD8 T cell priming; moreover, cDC1 were necessary to potentiate the response against Neo2 and 7. In line with these observations, Fesseden *et al.*, have shown that cross-presentation of neoAgs by cDC1s is biased towards peptides derived from cytoplasmic proteins[259]. In our case, Neo 2 is derived from a ubiquitin C-terminal hydrolase 3 situated in cytosol, supporting the hypothesis that cDC1 preferentially present cytosolic proteins. Instead, Neo 7 derived from and the Integrin beta 1 (Itgβ1) protein, a transmembrane protein and it represents one of the neoAgs with highest expression. NeoAgs derived from Itgβ1 were shown to be potent MHC-II neoAgs that shape tumor immunity and dictate responses to immunotherapy in preclinical model of sarcoma[269]. Recently, the same group has shown that cDC1s are licensed by CD4$^+$ T cells to induce neoantigen-specific antitumor immunity[46]. Taken together this evidence we might suggest that cDC1 preferentially presented Neo 2 due to its nature and Neo7 by the licensing from CD4$^+$ T cells. However, how the nature of the neoantigen dictate the quality of the cancer immunity and in particular the role of cDC1 during the selection of peptides to present to CD8 T cell remain unclear.

5.6 FLT3L+aCD40 therapy is sufficient to expand dendritic cells in the TME and to increase CD8$^+$ T cells in lungs

Previous studies in our lab have shown that KP tumors progressively deplete and functionally suppress cDC1 in lung tumor tissues. Based on the collective evidence in the previous sections we evaluated the impact of DC enhancement in orthotopic KP^{neo} tumors. We shelved KP^{ctrl} based on the lack of response to therapy that we had observed in the subcutaneous setting, reasoning that responses to this non-immunogenic variant would be even more difficult to detect in the suppressive lung environment.

We dissected the therapy into two main parts in order to evaluate the impact of boosting cDC subsets and inhibition of immune checkpoint molecules. Thus, one group

received FLT3L and anti-CD40 and a second group received anti-PD-L1 in addition to the DC-based therapy. We observed that the therapies led to an influx of $Lin^{-}CD11c^{+}MHCII^{low}$ cells in tumor-bearing lungs, based on the low expression of MHCII and the absence of XCR1[270] we might suggest that this subset could be preDCs. Using cDC1 reporter mice XCR1-Venus we have documented the recruitment of cDC1 in KP^{neo} nodules and the incremented influx after FL/αCD40 therapy. Flow cytometry data showed that FL/αCD40 is mainly responsible of the recruitment of cDC1 in tumor bearing lung whereas the addition of anti-PD-L1 countered the effect of FL/αCD40. Previous reports have shown that FL/αCD40 rescued cDC1 abundance and boosted their maturation in preclinical model of pancreatic cancer. A similar therapy was shown to reduce the frequencies of apoptotic cDC1[146], an aspect that we have not directly investigated.

The increased abundance of cDC1 in KP^{neo} tumors after the therapy generated an enhanced recruitment of $CD8^{+}$ T cells on the nodules. Interestingly, boosting cDC1 generated a 2-fold increase in frequencies of proliferating and effector memory $CD8^{+}$ T cells. Moreover, FL/αCD40 largely expanded progenitor exhausted $TCF1^{+}PD\text{-}1^{+}$ $CD8^{+}$ T cells in lung tissues. This subset was reported by Schenkel *et al.*, to accumulate in the mediastinal lymph node in tumor bearing mice after FL/αCD40 therapy in the autochthonous KP model harboring SIINFEKL as antigens and the authors suggested that are the cDC1 responsible for the propagation of this subset of $CD8^{+}$ T cells. Previous reports have shown that in a melanoma preclinical model, intratumoral of $TCF1^{+}PD\text{-}1^{+}$ $CD8^{+}$ T cells mediate tumor control in response to immunotherapy. The authors associated this subset to memory-like $CD8^{+}$ T cells, as they persist even under chronic exposure to antigens and display considerable phenotypic differences compared to conventional central memory cells[85]. This subset was also identified in mice under viral infection and recently its was demonstrated that cDC1s maintained this subset by sequestrating them within specific anatomical niches, and limiting their activation and thereby balancing the immune response[271]. Our results suggest that a similar behavior can occur in tumor bearing lungs, where the restored cDC1 may lead to accumulation of $TCF1^{+}PD\text{-}1^{+}$ CD8 T cells in lung tissues.

The fact that in our setting we observed little, null, or sometimes a negative effect of anti-PD-L1 in lungs bearing KP^{neo} tumors suggested that the bottleneck during tumor

engraftment and generation of anticancer immunity, is the scarcity of cDC1. We cannot exclude a beneficial effect of anti-PD-L1 treatment in KP tumors in the overall survival of tumor bearing mice. The long-term effects of anti-PD-L1, as well as a different scheme for the administration of therapy, remains an open question in this work.

5.7 FLT3L+aCD40 therapy reshapes molecular networks in the immune compartment in tumor-bearing lungs

Based on the remodeling observed in the immune compartment after FL/αCD40 treatment and the null effect of additional anti-PD-L1, we wanted to further analyze the remodeling in immune cells after FL/αCD40 therapy. Therefore, we have performed scRNAseq analysis on KP^{neo} tumors treated with FL/αCD40 or control isotype.

The major changes observed in the immune subsets were in NK cells, monocytes, neutrophils, dendritic cells and T cells. We observed a reduction in neutrophils and an increased in NK and monocytes. Previous data from our group have shown that recruitment of $SiglecF^{high-}$Neutrophils guided by the tumor secretion of CXCL5 in KP-OVA tumor bearing mice, impairs CD8 T differentiation and acquisition of cytolytic functions[178]. In addition, they have shown that depletion of intratumoral neutrophils promoted the expansion of anti-tumor CD8 T cells[178]. Previous reports using pancreatic cancer models treated with the same combination of FL/αCD40, showed augmented number of NK cells in tumors in comparison with the untreated group[147]. The NK-cDC1 axis mediated by FLT3L was very well documented by Barry *et al.*, in a preclinical model of melanoma, showing that FLT3L production by NK cells dictates the recruitment of cDC1s into the tumors[265]. Moreover, NK cells make frequent and stable interactions with cDC1 that increases their survival levels[265]. Besides, NK cells are recruited into the TME by the expression of several chemokine receptors, including CXCR3 that binds to the chemokine ligands CXCL9 and CXCL10 produced by dendritic cells[272]. This data suggested that a close interplay between NK and cDCs generates a positive feedback loop during their recruitment into the TME. Although we show that KP^{neo} elicits neoantigen-specific T-cell responses, and $CD8^{+}$ T cells are responsible for tumor containment, we cannot rule out the contribution of NK cells during tumor containment.

To further explore the remodeling in the dendritic cell cluster we re-clustered it into 4 sub-clusters, representing the main DC subsets reported for lungs[124,125]. We found a

cluster for cDC2, one for migDCs and two clusters with gene signatures of cDC1. cDC2 represents half of the DCs present in tumor-bearing lungs, and it remained unchanged after the therapy. At transcriptional levels, key pathway analysis revealed that cDC2 actively replicate based on significant upregulation of genes related to the cell cycle and DNA replication. migDC was the most affected subset getting a significant reduction after therapy. These cells are characterized by the expression of maturation, regulatory marker and molecules related to migration. This genetic signature has been described under different names in the TME of preclinical mouse models. Their role during tumor progression or during immunotherapy is still debated. Maier *et al.*, found a similar program in KP tumor bearing lungs and they defined this subset as "mature DCs enriched in immunoregulatory molecules" (mregDCs) due to the expression of maturation markers (*Cd40*, *Il12b* and *Ccr7*) and immunoregulatory molecules (*Cd274* and *Axl*). They defined the mregDCs as a program since they could not assign an identity between cDC1 or cDC2. They proposed that this subset restrains the threshold of the T cell responses; in addition, mregDCs are able to capture antigens and the antigen-loaded DC migrates to the draining lymph node to shape tumor-specific immunity[125]. Also, using the KP model, Li *et al.*, have shown that systemic targeting of AXL unlocks the production of type I interferon by dendritic cells, a key signaling pathway for priming and activating anti-tumor CD8 T cells. They found that inactivation of AXL increased the abundance of $TCF1^{+}PD\text{-}1^{+}$ $CD8^{+}$ T cells the key mediator for therapeutic response to ICB[273]. In our data we observed that not only migDCs are reduced in numbers, but genes characterizing the regulatory side of the mReg program such as *Axl*, *Ccl22* and *Ccl17* appeared in the list of DEGs downregulated in all cDCs clusters, suggesting that the therapy prevent cDCs from acquiring this phenotype. Conversely, *Ccl5* is upregulated, indicating a shift toward immunostimulatory properties. Accordingly, a gene process linked to IFN-I response is among the ones upregulated in therapy treated cDC1. Moreover, therapy may enhance the migration of migDCs to the draining lymph node, reducing their number in lung tissues.

Additionally, we have identified two clusters of cDC1 in KP^{neo} tumor bearing lungs, these two subsets (cDC1a and cDC1b) shared the expression of *Xcr1* and *Clec9a,* but the expression of these markers was lower in cDC1b. This subset showed higher expression

of genes related to the cell proliferation such as cyclins and histones and has lower levels of maturation markers. Looking at the DEGs and the biological processes significantly regulated, we observed that processes such as DNA replication and cell cycle were upregulated. The high proliferative state was reported for cDC1 and pre-DCs in the lung where 30%-40% of cells are Ki-67^{+} [270]. We might suppose that this group corresponded to committed pre-DC1. Pre-DCs do not express *Xcr1*, but as the differentiation process begins, the expression of this molecule increases. In addition, pre-DCs express FLT3 and can be recruited to the TME by FLT3L[265]. However, further analysis using flow cytometry analysis of surface markers is needed to better characterize committed pre-Dcs precursors in the lung.

The cluster we named cDC1a showed high expression of genes related to antigen presentation and vesicular trafficking according to its functions in antigen processing and presentation. DEGs analysis showed an upregulation in genes related to cell replication and a downregulation of immunoregulatory genes related to migDCs. Key biological processes analysis showed that cDC1a upregulated the type I interferon pathway, in line with the concept proposed by *Li et al.,*[273] that Axl inhibition correspond to induction of type I interferons. Based on these data we can propose that in KP^{neo} tumors FL/αCD40 led to the accumulation of restored cDC that have downregulated (or not yet acquired) the regulatory program. These cDCs are able to activate type I interferon pathways and their presence coincides with an increase in TCF1^{+}PD-1^{+} CD8^{+} T cells. The analysis of the biological programs modulated in cDC1a showed that these cells experienced a metabolic reprogramming. These cells showed an increase in aerobic respiration and oxidative phosphorylation showing high ATP synthesis and demand. The maturation process in DCs results in upregulation of MHC complexes, costimulatory molecules and secretion of cytokines[274]. DCs must adapt their metabolic programs to cover the energy demands associated with transcriptional and biosynthetic pathways[275] required for DC survival such as migration, and effective T cell priming[276]. Most of the studies of metabolism in dendritic cells have been done *in vitro* using mouse BMDCs that do not recreate the TME; however, using this simple model, most of the reports showed that DCs become glycolytic after TLR activation[277]. Moreover, when growth factors stimulate cells to proliferate, cells take up more glucose than they require, excess of

glycolytic intermediates are redirected into pathways that support the production of non-essential amino acids, nucleotides and lipids necessary for cell growth[278]. All these three anabolic processes were found to be upregulated in cDC1a after the therapy suggesting that the administration of FLT3L led to the induction of proliferation in cDC1a generating a metabolic change in the cell.

Additionally, we observed that FL/αCD40 generated changes in the frequencies of T lymphocytes clusters. To analyze the changes in this cluster more in depth, T cells cluster was re-clustered into 10 sub-clusters including: CD4 and CD8T cells, γδ T cells and MAIT. The main observations were the reduction of γδ T cells and the increase in proliferating and effector $CD8^+$ T cells. Previous studies in KP tumor-bearing lungs shown that the activation γδ T cells by microbiota stimulated the production of IL-17 by this subsets promoting tumor growth[279]. Therefore, the reduction in the frequencies of γδ T cells might contribute with the tumor control after therapy.

In this study we mainly focused on CD8 T cells. Consequently, we analyzed clusters associated to non-naïve $CD8^+$ T cells, such as short-lived effector, effector and proliferating $CD8^+$ T cells. Short-live effector $CD8^+$ T cells were represented in the C3 and were characterized by the expression of *Eomes* and *Ifit1*. The DEGs analysis showed that this cluster acquired cytotoxic functions after the therapy by the induction of cytotoxic genes such as *Gzma* and *Serpina3g*. Biological processes analysis suggested that these clusters experienced, as cDC1a, rewiring of metabolic pathways related to cellular proliferation and oxidative phosphorylation. Cluster 5 was defined by the expression of activation/exhaustion markers such as *Gzmb*, *Gzma*, *Prf1*, *Lag3* and *Pdcd1*. This subset could represent depleted progenitor CD8 T cells that still maintain some stem cell-like function, while displaying effector functions. The frequency of this cluster increased upon therapy and the DEGs analysis showed enhanced expression of cytotoxic genes and genes related to cell cycle. C3 and C5 displayed a metabolic change that favors oxidative phosphorylation. Werry *et al*., have shown using a model of viral infection that chronic exposure to antigen generates a particular phenotype in $CD8^+$ T cells characterized by the expression of inhibitory, memory and effector molecules. In this subset, that they called exhausted T cells (Tex), they found a metabolic change from glycolysis to oxidative phosphorylation[280]. In our model these short-lived cells and

TCF1^{+}PD1^{+} CD8^{+} T cells could follow the metabolic changes that the Tex cells experienced, but without the expression of inhibitory molecules on the surface. The most affected cluster by the therapy was cluster 6 that is characterized by genes related to DNA replication and cell cycle. This group increased in frequency 3-fold and DEG analysis showed that these CD8^{+} T cells increased genes related to effector/cytotoxic function, such as *GzmK*, *Gzma* and *Eomes*. The pathway analysis showed that DNA replication and cell cycle were the most upregulated processes, showing that the therapy with FL/αCD40 not only remodeled the myeloid compartment but also reshaped adaptive cancer immunity.

6. Conclusions

In conclusion our work shows that cDC1 are crucial during the orchestration of neoantigen-specific T cell responses in a hypermutated murine lung cancer model. Also, we demonstrated that boosting DCs activity in ICB-resistant mutated lung tumors is critical to leverage neoantigen content for therapeutic advantage.

While published studies characterized the role of cDC1 during antigen presentation in cancer using strong surrogate antigens, our model contributes to the field by reflecting a more physiological model harboring *bona-fide* neoAgs generated endogenously in the tumor cell by a deficiency in mismatch repair system.

By increasing the neoantigen burden, tumors turned from cold into warm tumors with enhanced T cell responses. Despite the increased neoantigen burden and the enhanced cancer immunity, tumors harboring neoAgs remain resistant to ICB.

We showed that boosting cDC1 in the TME by a combinatorial therapy including FLT3L led to an enhanced immune response against tumors that controlled tumor growth, and this effect was unique to tumors with a higher neoantigen load.

Moreover, DC-therapy (FLT3L in combination with anti-CD40) generated a remodeling of the immune infiltrate in tumor bearing lungs. The remodeling included: increased number of cDC1 with high proliferative capacities, reduction of an immunoregulatory program on cDC, increased number of NK cells and CD8 T cells. Single-cell RNA sequencing uncovered the molecular changes in the CD8 T cell subsets. These subsets were reprogrammed by the therapy inducing high proliferative phenotypes with effector/cytotoxic functions and reducing exhaustion programs.

However, I would also like to highlight some limitations of this study and to list those that in my opinion represent critical open questions and opportunities offered by this work.

7. Limitations and future perspectives

A major limitation during this study has been, expectedly, the COVID pandemic that has caused delay in progression of *in vivo* experiments and has obliged us to restructure some of the aims. Technical challenges and limited resources have also imposed a choice on some of the approaches.

The assay to study the specificity of the T cell response to neoAgs need to be improved and combined to other analysis. First the assay of restimulation using peptides should be optimized and the role of the full spectrum of neoAgs should be conducted using all the 26 predicted KP^{neo} neoAgs and those encoded by the parental KP line. This will help to understand how the nature of the neoAgs (expression levels, binding affinity to MHCI or their subcellular localization) dictates the immune response against the tumor, possibly at different time points. In particular, exploring what determine their immunogenicity the characteristics of CD8 T cells.

Furthermore, a deeper description of the diversity and phenotype of neoantigen-specific CD8 T cells would add invaluable information regarding the characteristics of CD8 T cells against genuine neoAgs. This can be achieved by the analysis of the TCR repertoire. We have demonstrated that CD8 are expanded after therapy; however, we ignore how the therapy modulates the frequencies and diversity of their TCRs. A further valuable tool would be to generate tetramers against selected neoAgs to screen and isolate specifically CD8 T cells against neoAgs, Extensive studies using tools to label specifically CD8 against different neoAgs in KP and KP^{neo} will help to reveal the features of CD8 T cells generated against a variety of neoAgs.

An additional area of improvement is to study the long-term consequences of therapy (DC and combinatorial) on survival in longer tumor challenge experiments. In fact, our analysis was limited to the analysis of the early events of CD8 T cell activation and initial tumor progression. However, we cannot exclude that the addition of ICB would synergize with DC therapy to prolong the survival.

Lastly, we are currently trying to translate our proof of concept into the human system. In this regard the efforts are being taken to search the available datasets for possible (positive) correlations between ICB, density of cDC1 and TMB.

8. Bibliography

1. Organization, W. health. Cancer. (2022). Available at: https://www.who.int/news-room/fact-sheets/detail/cancer. (Accessed: 29th September 2022)

2. Barta, J. A., Powell, C. A. & Wisnivesky, J. P. Global Epidemiology of Lung Cancer. *Ann. Glob. Heal.* **85**, (2019).

3. Osmani, L., Askin, F., Gabrielson, E. & Li, Q. K. Current WHO guidelines and the critical role of immunohistochemical markers in the subclassification of non-small cell lung carcinoma (NSCLC): Moving from targeted therapy to immunotherapy. *Semin. Cancer Biol.* **52**, 103–109 (2018).

4. Herbst, R. S., Morgensztern, D. & Boshoff, C. The biology and management of non-small cell lung cancer. *Nature* **553**, 446–454 (2018).

5. Dunn, G. P., Old, L. J. & Schreiber, R. D. The immunobiology of cancer immunosurveillance and immunoediting. *Immunity* **21**, 137–148 (2004).

6. Kunimasa, K. & Goto, T. Molecular Sciences Immunosurveillance and Immunoediting of Lung Cancer: Current Perspectives and Challenges. doi:10.3390/ijms21020597

7. Chen, D. S. & Mellman, I. Oncology meets immunology: The cancer-immunity cycle. *Immunity* **39**, 1–10 (2013).

8. E Verdegaal, E. M. *et al.* Neoantigen landscape dynamics during human melanoma-T cell interactions. (2016). doi:10.1038/nature18945

9. Schumacher, T. N. & Schreiber, R. D. Realising the promise: neoantigens in cancer immunotherapy. *Science* **348**, 69–74 (2015).

10. Schumacher, T. N., Scheper, W. & Kvistborg, P. Cancer Neoantigens. *Annu. Rev. Immunol.* **37**, 173–200 (2019).

11. Schumacher, T. N. & Hacohen, N. Neoantigens encoded in the cancer genome. *Curr. Opin. Immunol.* **41**, 98–103 (2016).

12. Le, D. . *et al.* PD-1 Blockade in Tumors with Mismatch-Repair Deficiency. *new engl J. Med. Orig.* **372**, 2509–2520 (2015).

13. Binnewies, M. *et al.* Understanding the tumor immune microenvironment (TIME) for effective therapy. *Nat. Med.* **24**, 541–550 (2018).

14. Pardoll, D. M. The blockade of immune checkpoints in cancer immunotherapy. *Nat. Rev. Cancer* **12**, 252–264 (2012).

15. Leach, D. R., Krummel, M. F. & Allison, J. P. Enhancement of antitumor immunity by CTLA-4 blockade. *Science (80-.).* **271**, 1734–1736 (1996).

16. Rizvi, N. A. *et al.* Mutational landscape determines sensitivity to PD-1 blockade in non-small cell lung cancer. *Science (80-.).* **348**, 124–128 (2015).

17. Mayoux, M. *et al.* Dendritic cells dictate responses to PD-L1 blockade cancer immunotherapy. *Sci. Transl. Med.* **12**, 1–12 (2020).

18. Siegel, R. L., Miller, K. D. & Jemal, A. Cancer statistics, 2019. *CA. Cancer J. Clin.* **69**, 7–34 (2019).

19. Ribas, A. & Wolchok, J. D. Cancer immunotherapy using checkpoint blockade. *Science* **359**, 1350–1355 (2018).

20. Alexandrov, L. B. *et al.* Signatures of mutational processes in human cancer. *Nature* **500**, 415–421 (2013).

21. Rosenthal, R. *et al.* Neoantigen-directed immune escape in lung cancer evolution. *Nature* **567**, 479–485 (2019).

22. Wang, C. *et al.* Reprogramming NK cells and macrophages via combined antibody and cytokine therapy primes tumors for elimination by checkpoint blockade. *Cell Rep.* **37**, (2021).

23. Connolly Kelly *et al.* Conneolly_2021_Tyler.pdf. *Sci. i* **6**, (2021).

24. Hellmann, M. D. *et al.* Tumor Mutational Burden and Efficacy of Nivolumab Monotherapy and in Combination with Ipilimumab in Small-Cell Lung Cancer. *Cancer Cell* **33**, 853-861.e4 (2018).

25. Grout, J. A. *et al.* Spatial positioning and matrix programs of cancer-associated fibroblasts promote T cell exclusion in human lung tumors. *Cancer Discov.* (2022). doi:10.1158/2159-8290.CD-21-1714/708811/SPATIAL-POSITIONING-AND-MATRIX-PROGRAMS-OF-CANCER

26. Patel, S. P. & Kurzrock, R. PD-L1 expression as a predictive biomarker in cancer immunotherapy. *Mol. Cancer Ther.* **14**, 847–856 (2015).

27. Reck, M. *et al.* Pembrolizumab versus Chemotherapy for PD-L1–Positive Non–Small-Cell Lung Cancer. *N. Engl. J. Med.* **375**, 1823–1833 (2016).

28. Chen, S. *et al.* Mechanisms regulating PD-L1 expression on tumor and immune cells. *J. Immunother. Cancer* **7**, 1–12 (2019).

29. Tokito, T. *et al.* Predictive relevance of PD-L1 expression combined with CD8+ TIL density in stage III non-small cell lung cancer patients receiving concurrent chemoradiotherapy. *Eur. J. Cancer* **55**, 7–14 (2016).

30. Herbst, R. S. *et al.* Predictive correlates of response to the anti-PD-L1 antibody MPDL3280A in cancer patients. *Nature* **515**, 563–567 (2014).

31. Chen, D. S. & Mellman, I. Elements of cancer immunity and the cancer-immune set point. *Nature* **541**, 321–330 (2017).

32. Duan, Q., Zhang, H., Zheng, J. & Zhang, L. Turning Cold into Hot: Firing up the Tumor Microenvironment. *Trends in Cancer* **6**, 605–618 (2020).

33. Govindan, R. *et al.* Genomic landscape of non-small cell lung cancer in smokers and never-smokers. *Cell* **150**, 1121–1134 (2012).

34. Kang, J. *et al.* Tumor Mutation Load: A Novel Independent Prognostic Factor in Stage IIIA-N2 Non-Small-Cell Lung Cancer. *Dis. Markers* **2019**, (2019).

35. Meng, G., Liu, X., Ma, T., Lv, D. & Sun, G. Predictive value of tumor mutational burden for immunotherapy in non-small cell lung cancer: A systematic review and meta-analysis. *PLoS One* **17**, e0263629 (2022).

36. Hurkmans, D. P. *et al.* Tumor mutational load, CD8+ T cells, expression of PD-L1 and HLA class I to guide immunotherapy decisions in NSCLC patients. *Cancer Immunol. Immunother.* **69**, 771–777 (2020).

37. Landgraf, M., McGovern, J. A., Friedl, P. & Hutmacher, D. W. Rational Design of Mouse Models for Cancer Research. *Trends Biotechnol.* **36**, 242–251 (2018).

38. Kersten, K., Visser, K. E. de, Miltenburg, M. H. van & Jonkers, J. Genetically engineered mouse models in oncology research and cancer medicine. *EMBO Mol. Med.* **9**, 137 (2017).

39. DuPage, M., Dooley, A. L. & Jacks, T. Conditional mouse lung cancer models using adenoviral or lentiviral delivery of Cre recombinase. *Nat. Protoc.* **4**, 1064 (2009).

40. Marjanovic, N. D. *et al.* Emergence of a High-Plasticity Cell State during Lung Cancer Evolution. *Cancer Cell* **38**, 229-246.e13 (2020).

41. DuPage, M. *et al.* Endogenous T cell responses to antigens expressed in lung adenocarcinomas delay malignant tumor progression. *Cancer Cell* **19**, 72–85 (2011).

42. Fitzgerald, B. *et al.* A mouse model for the study of anti-tumor T cell responses in Kras-driven lung adenocarcinoma. *Cell Reports Methods* **1**, 100080 (2021).

43. Martinez-Usatorre, A. *et al.* Overcoming microenvironmental resistance to PD-1 blockade in genetically engineered lung cancer models. *Sci. Transl. Med.* **13**, (2021).

44. Poncette, L., Bluhm, J. & Blankenstein, T. The role of CD4 T cells in rejection of solid tumors. *Curr. Opin. Immunol.* **74**, 18–24 (2022).

45. Cachot, A. *et al.* Tumor-specific cytolytic CD4 T cells mediate immunity against human cancer. (2021).

46. Ferris, S. T. *et al.* cDC1 prime and are licensed by CD4+ T cells to induce anti-tumour immunity. *Nature* **584**, 624–629 (2020).

47. Murphy, T. L. & Murphy, K. M. Dendritic cells in cancer immunology. *Cell. Mol. Immunol.* **19**, 3–13 (2022).

48. Todaro, M. *et al.* Efficient killing of human colon cancer stem cells by gammadelta T lymphocytes. *J. Immunol.* **182**, 7287–7296 (2009).

49. Couzi, L. *et al.* Antibody-dependent anti-cytomegalovirus activity of human γδ T cells expressing CD16 (FcγRIIIa). *Blood* **119**, 1418–1427 (2012).

50. Li, Y., Li, G., Zhang, J., Wu, X. & Chen, X. The Dual Roles of Human γδ T Cells: Anti-Tumor or Tumor-Promoting. *Front. Immunol.* **11**, 3880 (2021).

51. Van Hede, D. *et al.* Human papillomavirus oncoproteins induce a reorganization of epithelial-associated γδ T cells promoting tumor formation. *Proc. Natl. Acad. Sci. U. S. A.* **114**, E9056–E9065 (2017).

52. Zhou, B. Y. *et al.* An imbalance between stellate cells and γδT cells contributes to hepatocellular carcinoma aggressiveness and recurrence. *Hepatol. Int.* **13**, 631–640 (2019).

53. Welte, T. & Zhang, X. H. F. Interleukin-17 Could Promote Breast Cancer Progression at Several Stages of the Disease. *Mediators Inflamm.* **2015**, (2015).

54. Jin, C. *et al.* Commensal Microbiota Promote Lung Cancer Development via γδ T Cells. *Cell* **176**, 998-1013.e16 (2019).

55. Pace, L. & Amigorena, S. Epigenetics of T cell fate decision. *Curr. Opin. Immunol.* **63**, 43–50 (2020).

56. Franco, F., Jaccard, A., Romero, P., Yu, Y. R. & Ho, P. C. Metabolic and epigenetic regulation of T-cell exhaustion. *Nat. Metab. 2020 210* **2**, 1001–1012 (2020).

57. Sen, D. R. *et al.* The epigenetic landscape of T cell exhaustion. *Science* **354**, 1165–1169 (2016).

58. Montacchiesi, G. & Pace, L. Epigenetics and CD8+ T cell memory*. *Immunol. Rev.* **305**, 77–89 (2022).

59. Chen, Z. *et al.* TCF-1-Centered Transcriptional Network Drives an Effector versus Exhausted CD8 T Cell-Fate Decision. *Immunity* **51**, 840-855.e5 (2019).

60. Dolina, J. S., Van Braeckel-Budimir, N., Thomas, G. D. & Salek-Ardakani, S. CD8+ T Cell Exhaustion in Cancer. *Front. Immunol.* **12**, 2880 (2021).

61. Zhou, X. *et al.* Differentiation and persistence of memory CD8(+) T cells depend on T cell factor 1. *Immunity* **33**, 229–240 (2010).

62. Ando, M., Ito, M., Srirat, T., Kondo, T. & Yoshimura, A. Memory T cell, exhaustion, and tumor immunity. *Immunol. Med.* **43**, (2020).

63. Khan, O. *et al.* TOX transcriptionally and epigenetically programs CD8+ T cell exhaustion. *Nat. 2019 5717764* **571**, 211–218 (2019).

64. Yu, B. *et al.* Epigenetic landscapes reveal transcription factors that regulate CD8+ T cell differentiation. *Nat. Immunol. 2017 185* **18**, 573–582 (2017).

65. Allis, C. D. & Jenuwein, T. The molecular hallmarks of epigenetic control. *Nat. Rev. Genet. 2016 178* **17**, 487–500 (2016).

66. Pace, L. *et al.* The epigenetic control of stemness in CD8+ T cell fate commitment. *Science* **359**, 177–186 (2018).

67. Russ, B. E. *et al.* Regulation of H3K4me3 at Transcriptional Enhancers Characterizes Acquisition of Virus-Specific CD8+ T Cell-Lineage-Specific Function. *Cell Rep.* **21**, 3624–3636 (2017).

68. Guo, X. *et al.* Global characterization of T cells in non-small-cell lung cancer by single-cell sequencing. *Nat. Med.* **24**, 978–985 (2018).

69. Montacchiesi, G. & Pace, L. Epigenetics and CD8+ T cell memory. *Immunol. Rev.* **305**, 77–89 (2022).

70. Wherry, E. J. T cell exhaustion. *Nat. Immunol.* **12**, 492–499 (2011).

71. Blank, C. U. *et al.* Defining 'T cell exhaustion'. *Nat. Rev. Immunol. 2019 1911* **19**, 665–674 (2019).

72. van der Leun, A. M., Thommen, D. S. & Schumacher, T. N. CD8+ T cell states in human cancer: insights from single-cell analysis. *Nat. Rev. Cancer* **20**, 218–232 (2020).

73. Spranger, S. *et al.* Mechanism of tumor rejection with doublets of CTLA-4, PD-1/PD-L1, or IDO blockade involves restored IL-2 production and proliferation of CD8+ T cells directly within the tumor microenvironment. *J. Immunother. Cancer* **2**, 3 (2014).

74. Krummel, M. F. & Allison, J. P. CTLA-4 engagement inhibits IL-2 accumulation and cell cycle progression upon activation of resting T cells. *J. Exp. Med.* **183**, 2533–2540 (1996).

75. Zhang, L. *et al.* Lineage tracking reveals dynamic relationships of T cells in colorectal cancer. *Nat. 2018 5647735* **564**, 268–272 (2018).

76. Azizi, E. *et al.* Single-Cell Map of Diverse Immune Phenotypes in the Breast Tumor

Microenvironment. *Cell* **174**, 1293-1308.e36 (2018).

77. Sade-Feldman, M. *et al.* Defining T Cell States Associated with Response to Checkpoint Immunotherapy in Melanoma. *Cell* **175**, 998-1013.e20 (2018).

78. Andreatta, M. *et al.* Interpretation of T cell states from single-cell transcriptomics data using reference atlases. *Nat. Commun.* **12**, 1–19 (2021).

79. Zarour, H. M. Reversing T-cell Dysfunction and Exhaustion in Cancer. *Clin. Cancer Res.* **22**, 1856–1864 (2016).

80. Wei, S. C. *et al.* Distinct Cellular Mechanisms Underlie Anti-CTLA-4 and Anti-PD-1 Checkpoint Blockade. *Cell* **170**, 1120-1133.e17 (2017).

81. Chow, M. T. *et al.* Intratumoral Activity of the CXCR3 Chemokine System Is Required for the Efficacy of Anti-PD-1 Therapy. *Immunity* **50**, 1498-1512.e5 (2019).

82. D'Alise, A. M. *et al.* Adenoviral-based vaccine promotes neoantigen-specific CD8+ T cell stemness and tumor rejection. *Sci. Transl. Med.* **14**, eabo7604 (2022).

83. Gubin, M. M. *et al.* High-Dimensional Analysis Delineates Myeloid and Lymphoid Compartment Remodeling during Successful Immune-Checkpoint Cancer Therapy. *Cell* **175**, 1014-1030.e19 (2018).

84. Gubin, M. M. *et al.* Checkpoint blockade cancer immunotherapy targets tumour-specific mutant antigens. *Nature* **515**, 577–581 (2014).

85. Siddiqui, I. *et al.* Intratumoral Tcf1 + PD-1 + CD8 + T Cells with Stem-like Properties Promote Tumor Control in Response to Vaccination and Checkpoint Blockade Immunotherapy. *Immunity* **50**, 195-211.e10 (2019).

86. Horton, B. L. *et al.* Lack of CD8+T cell effector differentiation during priming mediates checkpoint blockade resistance in non-small cell lung cancer. *Sci. Immunol.* **6**, (2021).

87. Galon, J. & Bruni, D. Approaches to treat immune hot, altered and cold tumours with combination immunotherapies. *Nat. Rev. Drug Discov.* **18**, 197–218 (2019).

88. Budhu, S. *et al.* CD8+ T cell concentration determines their efficiency in killing cognate antigen–expressing syngeneic mammalian cells in vitro and in mouse tissues. *J. Exp. Med.* **207**, 223–235 (2010).

89. Herbst, R. S. *et al.* Pembrolizumab versus docetaxel for previously treated, PD-L1-positive, advanced non-small-cell lung cancer (KEYNOTE-010): A randomised controlled trial. *Lancet* **387**, 1540–1550 (2016).

90. Camus, M. *et al.* Coordination of intratumoral immune reaction and human colorectal cancer recurrence. *Cancer Res.* **69**, 2685–2693 (2009).

91. Spranger, S. Mechanisms of tumor escape in the context of the T-cell-inflamed and the non-T-cell-inflamed tumor microenvironment. *Int. Immunol.* **28**, 383–391 (2016).

92. Hegde, P. S., Karanikas, V. & Evers, S. The Where, the When, and the How of Immune Monitoring for Cancer Immunotherapies in the Era of Checkpoint Inhibition. *Clin. Cancer Res.* **22**, 1865–1874 (2016).

93. Camus, M. *et al.* Coordination of intratumoral immune reaction and human colorectal cancer recurrence. *Cancer Res.* **69**, 2685–2693 (2009).

94. Tran, E., Robbins, P. F. & Rosenberg, S. A. 'Final common pathway' of human cancer

immunotherapy: targeting random somatic mutations. *Nat. Immunol. 2017 183* **18**, 255–262 (2017).

95. Chae, Y. K. *et al.* Mutations in DNA repair genes are associated with increased neoantigen burden and a distinct immunophenotype in lung squamous cell carcinoma. *Sci. Rep.* **9**, 1–10 (2019).

96. Bräunlein, E. & Krackhardt, A. M. Identification and Characterization of Neoantigens As Well As Respective Immune Responses in Cancer Patients. *Front. Immunol.* **8**, 1702 (2017).

97. Jiricny, J. Postreplicative mismatch repair. *Cold Spring Harbor Perspectives in Biology* **5**, 1–23 (2013).

98. Kunkel, T. A. & Erie, D. A. Dna Mismatch Repair. *Annu. Rev. Biochem.* **74**, 681–710 (2005).

99. Vilar, E. & Gruber, S. B. Microsatellite instability in colorectal cancerthe stable evidence. *Nature Reviews Clinical Oncology* **7**, 153–162 (2010).

100. McGrail, D. J. *et al.* Proteome Instability Is a Therapeutic Vulnerability in Mismatch Repair-Deficient Cancer. *Cancer Cell* **37**, 371-386.e12 (2020).

101. Chang, L., Chang, M., Chang, H. M. & Chang, F. Microsatellite Instability: A Predictive Biomarker for Cancer Immunotherapy. *Appl. Immunohistochem. Mol. Morphol.* **26**, e15–e21 (2018).

102. Hause, R. J., Pritchard, C. C., Shendure, J. & Salipante, S. J. Classification and characterization of microsatellite instability across 18 cancer types. *Nat. Med.* **22**, 1342–1350 (2016).

103. Bonneville, R. *et al.* Landscape of Microsatellite Instability Across 39 Cancer Types. *JCO Precis. Oncol.* 1–15 (2017). doi:10.1200/po.17.00073

104. Cortes-Ciriano, I., Lee, S., Park, W. Y., Kim, T. M. & Park, P. J. A molecular portrait of microsatellite instability across multiple cancers. *Nat. Commun.* **8**, (2017).

105. Takamochi, K. *et al.* DNA mismatch repair deficiency in surgically resected lung adenocarcinoma: Microsatellite instability analysis using the Promega panel. *Lung Cancer* **110**, 26–31 (2017).

106. D.T., L. *et al.* Mismatch repair deficiency predicts response of solid tumors to PD-1 blockade. *Science (80-.).* **357**, 409–413 (2017).

107. Germano, G. *et al.* Inactivation of DNA repair triggers neoantigen generation and impairs tumour growth. *Nature* **552**, 1–5 (2017).

108. Turajlic, S. *et al.* Articles Insertion-and-deletion-derived tumour-specific neoantigens and the immunogenic phenotype: a pan-cancer analysis. *Lancet Oncol.* **18**, (2017).

109. Hu, H. *et al.* Aberrant methylation of mutL homolog 1 is associated with increased risk of non-small cell lung cancer. *J. Clin. Lab. Anal.* **32**, 1–7 (2018).

110. Takamochi, K. *et al.* DNA mismatch repair deficiency in surgically resected lung adenocarcinoma: Microsatellite instability analysis using the Promega panel. *Lung Cancer* **110**, 26–31 (2017).

111. Chae, Y. K. *et al.* Mutations in DNA repair genes are associated with increased neo-antigen load and activated T cell infiltration in lung adenocarcinoma. *Oncotarget* **9**,

7949–7960 (2018).

112. Au, L. *et al.* Determinants of anti-PD-1 response and resistance in clear cell renal cell carcinoma. *Cancer Cell* **39**, 1497-1518.e11 (2021).

113. Veglia, F. & Gabrilovich, D. I. Dendritic cells in cancer: the role revisited. doi:10.1016/j.coi.2017.01.002

114. Belderbos, R. A., Aerts, J. G. J. V. & Vroman, H. Enhancing Dendritic Cell Therapy in Solid Tumors with Immunomodulating Conventional Treatment. *Mol. Ther. - Oncolytics* **13**, 67–81 (2019).

115. Trombetta, E. S. & Mellman, I. Cell biology of antigen processing in vitro and in vivo. *Annu. Rev. Immunol.* **23**, 975–1028 (2005).

116. Steinman, R. M., Hawiger, D. & Nussenzweig, M. C. Tolerogenic Dendritic cells*. *Annu. Rev. Immunol.* **21**, 685–711 (2003).

117. Nace, G., Evankovich, J., Eid, R. & Tsung, A. Dendritic cells and damage-associated molecular patterns: Endogenous danger signals linking innate and adaptive immunity. *Journal of Innate Immunity* **4**, 6–15 (2011).

118. Sabado, R. L., Balan, S. & Bhardwaj, N. Dendritic cell-based immunotherapy. *Cell Research* **27**, 74–95 (2017).

119. Audsley, K. M., McDonnell, A. M. & Waithman, J. Cross-Presenting XCR1+ Dendritic Cells as Targets for Cancer Immunotherapy. *Cells* **9**, 565 (2020).

120. Asano, K. *et al.* CD169-Positive Macrophages Dominate Antitumor Immunity by Crosspresenting Dead Cell-Associated Antigens. *Immunity* **34**, 85–95 (2011).

121. Steinman, R. M. & Cohn, Z. A. IDENTIFICATION OF A NOVEL CELL TYPE IN PERIPHERAL LYMPHOID ORGANS OF MICE I. MORPHOLOGY, QUANTITATION, TISSUE DISTRIBUTION. *J. Exp. Med.* **137**, 1142–1162 (1973).

122. Broz, M. L. *et al.* Dissecting the Tumor Myeloid Compartment Reveals Rare Activating Antigen-Presenting Cells Critical for T Cell Immunity. *Cancer Cell* **26**, 638–652 (2014).

123. Segura, E. Review of mouse and human dendritic cell subsets. *Methods Mol. Biol.* **1423**, 3–15 (2016).

124. Zilionis, R. *et al.* Single-Cell Transcriptomics of Human and Mouse Lung Cancers Reveals Conserved Myeloid Populations across Individuals and Species. *Immunity* **50**, 1317-1334.e10 (2019).

125. Maier, B. *et al.* A conserved dendritic-cell regulatory program limits antitumour immunity. *Nature* **580**, 257–262 (2020).

126. Ghislat, G. *et al.* NF-kB–dependent IRF1 activation programs cDC1 dendritic cells to drive antitumor immunity. *Sci. Immunol.* **6**, (2021).

127. Villar, J. & Segura, E. Decoding the Heterogeneity of Human Dendritic Cell Subsets. *Trends Immunol.* **41**, 1062–1071 (2020).

128. Merad, M., Sathe, P., Helft, J., Miller, J. & Mortha, A. The dendritic cell lineage: ontogeny and function of dendritic cells and their subsets in the steady state and the inflamed setting. *Annu. Rev. Immunol.* **31**, 563–604 (2013).

129. Guilliams, M. *et al.* Dendritic cells, monocytes and macrophages: A unified

nomenclature based on ontogeny. *Nat. Rev. Immunol.* **14**, 571–578 (2014).

130. Bain, C. C. & Mowat, A. M. I. The monocyte-macrophage axis in the intestine. *Cell. Immunol.* **291**, 41–48 (2014).

131. Reizis, B. Regulation of plasmacytoid dendritic cell development. *Curr. Opin. Immunol.* **22**, 206–211 (2010).

132. Reizis, B., Bunin, A., Ghosh, H. S., Lewis, K. L. & Sisirak, V. Plasmacytoid Dendritic Cells: Recent Progress and Open Questions. *https://doi.org/10.1146/annurev-immunol-031210-101345* **29**, 163–183 (2011).

133. Reizis, B. Plasmacytoid Dendritic Cells: Development, Regulation, and Function. *Immunity* **50**, 37–50 (2019).

134. Sathe, P., Vremec, D., Wu, L., Corcoran, L. & Shortman, K. Convergent differentiation: myeloid and lymphoid pathways to murine plasmacytoid dendritic cells. *Blood* **121**, 11–19 (2013).

135. Kim, C. W., Kim, K. Do & Lee, H. K. The role of dendritic cells in tumor microenvironments and their uses as therapeutic targets. *BMB Rep.* **54**, 31–43 (2021).

136. Bosteels, C. *et al.* Inflammatory Type 2 cDCs Acquire Features of cDC1s and Macrophages to Orchestrate Immunity to Respiratory Virus Infection. *Immunity* **52**, 1039-1056.e9 (2020).

137. Diao, J., Gu, H., Tang, M., Zhao, J. & Cattral, M. S. Tumor Dendritic Cells (DCs) Derived from Precursors of Conventional DCs Are Dispensable for Intratumor CTL Responses. *J. Immunol.* **201**, 1306–1314 (2018).

138. Guilliams, M. *et al.* HHS Public Access. **2**, 147–185 (2015).

139. Cabeza-Cabrerizo, M., Cardoso, A., Minutti, C. M., Pereira Da Costa, M. & Reis E Sousa, C. Dendritic Cells Revisited. *Annu. Rev. Immunol.* **39**, 131–166 (2021).

140. Benvenuti, F. The dendritic cell synapse: A life dedicated to T cell activation. *Front. Immunol.* **7**, 70 (2016).

141. Onai, N. *et al.* Identification of clonogenic common Flt3+M-CSFR+ plasmacytoid and conventional dendritic cell progenitors in mouse bone marrow. *Nat. Immunol.* **8**, 1207–1216 (2007).

142. Meredith, M. M. *et al.* Expression of the zinc finger transcription factor zDC (Zbtb46, Btbd4) defines the classical dendritic cell lineage. *J. Exp. Med.* **209**, 1153–1165 (2012).

143. Merad, M. *et al.* The Dendritic Cell Lineage: Ontogeny and Function of Dendritic Cells and Their Subsets in the Steady State and the Inflamed Setting A BRIEF HISTORY OF THE DENDRITIC CELL LINEAGE. (2013). doi:10.1146/annurev-immunol-020711-074950

144. Salmon, H. *et al.* Expansion and Activation of CD103+ Dendritic Cell Progenitors at the Tumor Site Enhances Tumor Responses to Therapeutic PD-L1 and BRAF Inhibition. *Immunity* **44**, 924–938 (2016).

145. Oba, T. *et al.* Overcoming primary and acquired resistance to anti-PD-L1 therapy by induction and activation of tumor-residing cDC1s. *Nat. Commun.* **11**, (2020).

146. Lin, J. H. *et al.* Type 1 conventional dendritic cells are systemically dysregulated early in pancreatic carcinogenesis. *J. Exp. Med.* **217**, (2020).

147. Hegde, S. *et al.* Dendritic Cell Paucity Leads to Dysfunctional Immune Surveillance in Pancreatic Cancer. *Cancer Cell* **37**, 289-307.e9 (2020).

148. Böttcher, J. P., Reis Sousa, C. & Reis, crickacuk C. The Role of Type 1 Conventional Dendritic Cells in Cancer Immunity. **4**, (2018).

149. Böttcher, J. P. *et al.* NK Cells Stimulate Recruitment of cDC1 into the Tumor Microenvironment Promoting Cancer Immune Control. *Cell* **172**, 1022-1037.e14 (2018).

150. Spranger, S., Dai, D., Horton, B. & Gajewski, T. F. Tumor-Residing Batf3 Dendritic Cells Are Required for Effector T Cell Trafficking and Adoptive T Cell Therapy. *Cancer Cell* **31**, 711-723.e4 (2017).

151. Grajales-Reyes, G. E. *et al.* Batf3 maintains Irf8 autoactivation for commitment of a CD8α+ cDC clonogenic progenitor. *Nat. Immunol.* **16**, 708 (2015).

152. Ginhoux, F. *et al.* The origin and development of nonlymphoid tissue CD103+ DCs. *J. Exp. Med.* **206**, 3115–3130 (2009).

153. Duhen, T. *et al.* Co-expression of CD39 and CD103 identifies tumor-reactive CD8 T cells in human solid tumors. *Nat. Commun. 2018 91* **9**, 1–13 (2018).

154. Guilliams, M. *et al.* Unsupervised High-Dimensional Analysis Aligns Dendritic Cells across Tissues and Species. *Immunity* **45**, 669–684 (2016).

155. Gao, Y. *et al.* Control of T Helper 2 Responses by Transcription Factor IRF4-Dependent Dendritic Cells. *Immunity* **39**, 722–732 (2013).

156. Satpathy, A. T., Wu, X., Albring, J. C. & Murphy, K. M. Re(de)fining the dendritic cell lineage. *Nat. Immunol. 2012 1312* **13**, 1145–1154 (2012).

157. Binnewies, M. *et al.* Unleashing Type-2 Dendritic Cells to Drive Protective Antitumor CD4 + T Cell Immunity In Brief. *Cell* **177**, 556–571 (2019).

158. Duong, E. *et al.* Type I interferon activates MHC class I-dressed CD11b+ conventional dendritic cells to promote protective anti-tumor CD8+ T cell immunity. *Immunity* **55**, 308-323.e9 (2022).

159. Satoh, T. *et al.* Human DC3 Antigen Presenting Dendritic Cells From Induced Pluripotent Stem Cells. *Front. Cell Dev. Biol.* **9**, 1978 (2021).

160. Gerhard, G. M., Bill, R., Messemaker, M., Klein, A. M. & Pittet, M. J. Tumor-infiltrating dendritic cell states are conserved across solid human cancers. *J. Exp. Med.* **218**, (2021).

161. Dixon, K. O. *et al.* TIM-3 restrains anti-tumour immunity by regulating inflammasome activation. *Nat. 2021 5957865* **595**, 101–106 (2021).

162. Lavin, Y. *et al.* Innate Immune Landscape in Early Lung Adenocarcinoma by Paired Single-Cell Analyses. *Cell* **169**, 750-765.e17 (2017).

163. van der Woude, L. L., Gorris, M. A. J., Halilovic, A., Figdor, C. G. & de Vries, I. J. M. Migrating into the Tumor: a Roadmap for T Cells. *Trends in Cancer* **3**, 797–808 (2017).

164. Engblom, C., Pfirschke, C. & Pittet, M. J. The role of myeloid cells in cancer therapies. *Nature Reviews Cancer* **16**, 447–462 (2016).

165. Gabrilovich, D. I., Ostrand-Rosenberg, S. & Bronte, V. Coordinated regulation of myeloid cells by tumours. *Nat. Rev. Immunol.* **12**, 253–268 (2012).

166. Roberts, E. W. *et al.* Critical Role for CD103+/CD141+ Dendritic Cells Bearing CCR7 for Tumor Antigen Trafficking and Priming of T Cell Immunity in Melanoma. *Cancer Cell* **30**, 324–336 (2016).

167. Sluijter, B. J. R. *et al.* Arming the melanoma sentinel lymph node through local administration of CpG-B and GM-CSF: Recruitment and activation of BDCA3/CD141+ dendritic cells and enhanced cross-presentation. *Cancer Immunol. Res.* **3**, 495–505 (2015).

168. Barry, K. C. *et al.* A natural killer–dendritic cell axis defines checkpoint therapy–responsive tumor microenvironments. *Nat. Med.* **24**, 1178–1191 (2018).

169. Truxova, I. *et al.* Mature dendritic cells correlate with favorable immune infiltrate and improved prognosis in ovarian carcinoma patients. *J. Immunother. Cancer* **6**, (2018).

170. Böttcher, J. P. *et al.* NK Cells Stimulate Recruitment of cDC1 into the Tumor Microenvironment Promoting Cancer Immune Control. *Cell* **172**, 1022-1037.e14 (2018).

171. Shen, R. *et al.* DNA Damage and Activation of cGAS/STING Pathway Induce Tumor Microenvironment Remodeling. *Front. Cell Dev. Biol.* **9**, (2021).

172. Christopher Paustian *et al.* Extracellular ATP and Toll-Like Receptor 2 Agonists Trigger in Human Monocytes an Activation Program That Favors T Helper 17. *PLoS One* **8**, (2017).

173. Song, X. *et al.* HMGB1 Activates Myeloid Dendritic Cells by Up-Regulating mTOR Pathway in Systemic Lupus Erythematosus. *Front. Med.* **8**, 1–10 (2021).

174. Tugues, S. *et al.* New insights into IL-12-mediated tumor suppression. *Cell Death Differ.* **22**, 237–246 (2015).

175. Li, M., Knight, D. A., Snyder, L. A., Smyth, M. J. & Stewart, T. J. A role for CCL2 in both tumor progression and immunosurveillance. *Oncoimmunology* **2**, (2013).

176. Wang, N. *et al.* CXCL1 derived from tumor-associated macrophages promotes breast cancer metastasis via activating NF-κB/SOX4 signaling. *Cell Death Dis. 2018 99* **9**, 1–18 (2018).

177. Wang, D. *et al.* Colorectal cancer cell-derived CCL20 recruits regulatory T cells to promote chemoresistance via FOXO1/CEBPB/NF-κB signaling. *J. Immunother. Cancer* **7**, 1–15 (2019).

178. Simoncello, F. *et al.* CXCL5-mediated accumulation of mature neutrophils in lung cancer tissues impairs the differentiation program of anticancer CD8 T cells and limits the efficacy of checkpoint inhibitors. *Oncoimmunology* **11**, (2022).

179. Chow, M. T. & Luster, A. D. Chemokines in Cancer. *Cancer Immunol. Res.* **2**, 1125 (2014).

180. Spranger, S., Bao, R. & Gajewski, T. F. Melanoma-intrinsic β-catenin signalling prevents anti-tumour immunity. *Nat. 2015 5237559* **523**, 231–235 (2015).

181. Bickett, T. E. *et al.* FLT3L release by natural killer cells enhances response to radioimmunotherapy in preclinical models of HNSCC. *Clin. Cancer Res.* **27**, 6235–6249 (2021).

182. Caronni, N. *et al.* TIM4 expression by dendritic cells mediates uptake of tumor-associated antigens and anti-tumor responses. *Nat. Commun. 2021 121* **12**, 1–15 (2021).

183. Ziółkowska-suchanek, I. Mimicking Tumor Hypoxia in Non-Small Cell Lung Cancer

Employing Three-Dimensional In Vitro Models. *Cells* **10**, 1–23 (2021).

184. Reinfeld, B. I. *et al.* Cell-programmed nutrient partitioning in the tumour microenvironment. *Nat. 2021 5937858* **593**, 282–288 (2021).

185. Ahmed, M. S. & Bae, Y.-S. Dendritic cell-based therapeutic cancer vaccines: past, present and future. *Clin. Exp. Vaccine Res.* **3**, 113 (2014).

186. Stoitzner, P. *et al.* Inefficient presentation of tumor-derived antigen by tumor-infiltrating dendritic cells. *Cancer Immunol. Immunother.* **57**, 1665–1673 (2008).

187. Ruffell, B. *et al.* Macrophage IL-10 Blocks CD8+ T Cell-Dependent Responses to Chemotherapy by Suppressing IL-12 Expression in Intratumoral Dendritic Cells. *Cancer Cell* **26**, 623–637 (2014).

188. Caronni, N. *et al.* Downregulation of membrane trafficking proteins and lactate conditioning determine loss of dendritic cell function in lung cancer. *Cancer Res.* **78**, 1685–1699 (2018).

189. Giovanelli, P., Sandoval, T. A. & Cubillos-Ruiz, J. R. Dendritic Cell Metabolism and Function in Tumors. *Trends Immunol.* **40**, 699–718 (2019).

190. Chang, C. H. *et al.* Metabolic Competition in the Tumor Microenvironment Is a Driver of Cancer Progression. *Cell* **162**, 1229–1241 (2015).

191. Wculek, S. K. *et al.* Dendritic cells in cancer immunology and immunotherapy. *Nat. Rev. Immunol.* **20**, 7–24 (2020).

192. Wculek, S. K. *et al.* Effective cancer immunotherapy by natural mouse conventional type-1 dendritic cells bearing dead tumor antigen. *J. Immunother. Cancer* **7**, 1–16 (2019).

193. Anguille, S. *et al.* Dendritic cells as pharmacological tools for cancer immunotherapys. *Pharmacol. Rev.* **67**, 731–753 (2015).

194. Cancel, J. C., Crozat, K., Dalod, M. & Mattiuz, R. Are conventional type 1 dendritic cells critical for protective antitomor immunity and how? *Front. Immunol.* **10**, (2019).

195. Wilgenhof, S. *et al.* Phase II Study of Autologous Monocyte-Derived mRNA Electroporated Dendritic Cells (TriMixDC-MEL) Plus Ipilimumab in Patients With Pretreated Advanced Melanoma. *J. Clin. Oncol.* **34**, 1330–1338 (2016).

196. Van Lint, S. *et al.* Intratumoral delivery of TriMix mRNA results in T-cell activation by cross-presenting dendritic cells. *Cancer Immunol. Res.* **4**, 146–156 (2016).

197. Prestwich, R. J. *et al.* The case of oncolytic viruses versus the immune system: waiting on the judgment of Solomon. *Hum. Gene Ther.* **20**, 1119–1132 (2009).

198. Saxena, M. & Bhardwaj, N. Re-Emergence of Dendritic Cell Vaccines for Cancer Treatment. *Trends in Cancer* **4**, 119–137 (2018).

199. Anguille, S., Smits, E. L., Lion, E., Van Tendeloo, V. F. & Berneman, Z. N. Clinical use of dendritic cells for cancer therapy. *Lancet. Oncol.* **15**, (2014).

200. Okada, M. *et al.* PD-L1 Expression Affects Neoantigen Presentation. *iScience* **23**, 101238 (2020).

201. Oh, S. A. *et al.* PD-L1 expression by dendritic cells is a key regulator of T-cell immunity in cancer. *Nat. Cancer* (2020). doi:10.1038/s43018-020-0075-x

202. Peng, Q. *et al.* PD-L1 on dendritic cells attenuates T cell activation and regulates response to immune checkpoint blockade. *Nat. Commun.* **11**, 1–8 (2020).

203. Mayoux, M. *et al.* Dendritic cells dictate responses to PD-L1 blockade cancer immunotherapy. *Sci. Transl. Med.* **12**, 1–12 (2020).

204. Yokoi, T., Oba, T., Kajihara, R., Abrams, S. I. & Ito, F. Local, multimodal intralesional therapy renders distant brain metastases susceptible to PD-L1 blockade in a preclinical model of triple-negative breast cancer. *Sci. Rep.* **11**, 1–9 (2021).

205. Patel, A. *et al.* Multimodal intralesional therapy for reshaping the myeloid compartment to anti-PD-L1 therapy via Irf8 expression. *J. imm* **207**, 1298–1309 (2021).

206. Lyman, S. D. *et al.* Molecular cloning of a ligand for the flt3 flk-2 tyrosine kinase receptor: A proliferative factor for primitive hematopoietic cells. *Cell* **75**, 1157–1167 (1993).

207. Waskow, C. *et al.* The receptor tyrosine kinase Flt3 is required for dendritic cell development in peripheral lymphoid tissues. *Nat. Immunol.* **9**, 676–683 (2008).

208. Cueto, F. J. & Sancho, D. The flt3l/flt3 axis in dendritic cell biology and cancer immunotherapy. *Cancers (Basel).* **13**, (2021).

209. Lynch, D. H. *et al.* Flt3 ligand induces tumor regression and antitumor immune responses in vivo. *Nat. Med.* **3**, 625–631 (1997).

210. Keyue, C. *et al.* Antitumor activity and immunotherapeutic properties of Flt3-ligand in a murine breast cancer model - PubMed. *Cancer re* **57**, (1997).

211. Esche C, Subbotin V, Maliszewski C, Lotze M & Shurin M. FLT3 ligand administration inhibits tumor growth in murine melanoma and lymphoma - PubMed. *Cancer Res.* **58**, (1998).

212. Anandasabapathy, N. *et al.* Efficacy and safety of CDX-301, recombinant human Flt3L, at expanding dendritic cells and hematopoietic stem cells in healthy human volunteers. *Bone Marrow Transplant.* **50**, 924–930 (2015).

213. Prokopi, A. *et al.* Original research: Skin dendritic cells in melanoma are key for successful checkpoint blockade therapy. *J. Immunother. Cancer* **9**, 832 (2021).

214. Oba, T. *et al.* Overcoming primary and acquired resistance to anti-PD-L1 therapy by induction and activation of tumor-residing cDC1s. *Nat. Commun.* **11**, (2020).

215. Roselli, E. *et al.* TLR3 activation of intratumoral CD103+ dendritic cells modifies the tumor infiltrate conferring anti-tumor immunity. *Front. Immunol.* **10**, 503 (2019).

216. Sánchez-Paulete, A. R. *et al.* Intratumoral immunotherapy with XCL1 and sFlt3L encoded in recombinant semliki forest virus–derived vectors fosters dendritic cell–mediated t-cell cross-priming. *Cancer Res.* **78**, 6643–6654 (2018).

217. Hegde, S. *et al.* Dendritic Cell Paucity Leads to Dysfunctional Immune Surveillance in Pancreatic Cancer. *Cancer Cell* **37**, 289-307.e9 (2020).

218. Schenkel, J. M. *et al.* Conventional type I dendritic cells maintain a reservoir of proliferative tumor-antigen specific TCF-1+ CD8+ T cells in tumor-draining lymph nodes. *Immunity* **54**, 2338-2353.e6 (2021).

219. Lai, J. *et al.* Adoptive cellular therapy with T cells expressing the dendritic cell growth factor Flt3L drives epitope spreading and antitumor immunity. *Nat. Immunol.* **21**, 914–

926 (2020).

220. Ho, W. W. *et al.* Dendritic cell paucity in mismatch repair-proficient colorectal cancer liver metastases limits immune checkpoint blockade efficacy. *Proc. Natl. Acad. Sci. U. S. A.* **118**, e2105323118 (2021).

221. Search of: FLT3L | NSCLC - List Results - ClinicalTrials.gov. Available at: https://clinicaltrials.gov/ct2/results?cond=NSCLC&term=FLT3L&cntry=&state=&city=&dist=. (Accessed: 18th October 2022)

222. Lievense, L. A., Sterman, D. H., Cornelissen, R. & Aerts, J. G. Checkpoint blockade in lung cancer and mesothelioma. *American Journal of Respiratory and Critical Care Medicine* **196**, 274–282 (2017).

223. Liau, L. M. *et al.* Dendritic cell vaccination in glioblastoma patients induces systemic and intracranial T-cell responses modulated by the local central nervous system tumor microenvironment. *Clin. Cancer Res.* **11**, 5515–5525 (2005).

224. Yamazaki, C. *et al.* Critical roles of a dendritic cell subset expressing a chemokine receptor, XCR1. *J. Immunol.* **190**, 6071–6082 (2013).

225. Mattiuz, R. *et al.* Novel Cre-Expressing Mouse Strains Permitting to Selectively Track and Edit Type 1 Conventional Dendritic Cells Facilitate Disentangling Their Complexity in vivo. *Front. Immunol.* **9**, 2805 (2018).

226. Dimitrova, N. *et al.* Stromal expression of miR-143/145 promotes neoangiogenesis in lung cancer development. *Cancer Discov.* **6**, 188–201 (2016).

227. Feoktistova, M., Geserick, P. & Leverkus, M. Crystal violet assay for determining viability of cultured cells. *Cold Spring Harb. Protoc.* **2016**, 343–346 (2016).

228. Corti, G. *et al.* A Genomic Analysis Workflow for Colorectal Cancer Precision Oncology. *Clin. Colorectal Cancer* **18**, 91-101.e3 (2019).

229. Rospo, G. *et al.* Evolving neoantigen profiles in colorectal cancers with DNA repair defects. *Genome Med.* **11**, 1–22 (2019).

230. Wang, K. *et al.* MapSplice: accurate mapping of RNA-seq reads for splice junction discovery. *Nucleic Acids Res.* **38**, (2010).

231. Li, B. & Dewey, C. N. RSEM: Accurate transcript quantification from RNA-Seq data with or without a reference genome. *BMC Bioinformatics* **12**, 1–16 (2011).

232. Rospo, G. *et al.* Evolving neoantigen profiles in colorectal cancers with DNA repair defects. *Genome Med.* **11**, 1–22 (2019).

233. Andreatta, M. & Nielsen, M. Gapped sequence alignment using artificial neural networks: application to the MHC class I system. *Bioinformatics* **32**, 511–517 (2016).

234. Zheng, G. X. Y. *et al.* Massively parallel digital transcriptional profiling of single cells. *Nat. Commun. 2017 81* **8**, 1–12 (2017).

235. Lu, Y. C. *et al.* An Efficient Single-Cell RNA-Seq Approach to Identify Neoantigen-Specific T Cell Receptors. *Mol. Ther.* **26**, 379–389 (2018).

236. Germain, P. L., Robinson, M. D., Lun, A., Garcia Meixide, C. & Macnair, W. Doublet identification in single-cell sequencing data using *scDblFinder*. *F1000Research 2022 10979* **10**, 979 (2022).

237. Haghverdi, L., Lun, A. T. L., Morgan, M. D. & Marioni, J. C. Batch effects in single-cell RNA-sequencing data are corrected by matching mutual nearest neighbors. *Nat. Biotechnol. 2018 365* **36**, 421–427 (2018).

238. Korsunsky, I. *et al.* Fast, sensitive and accurate integration of single-cell data with Harmony. *Nat. Methods* **16**, 1289–1296 (2019).

239. Becht, E. *et al.* Dimensionality reduction for visualizing single-cell data using UMAP. *Nat. Biotechnol.* **37**, 38–47 (2018).

240. Connolly, K. A. *et al.* A reservoir of stem-like CD8+ T cells in the tumor-draining lymph node preserves the ongoing anti-tumor immune response. *Sci. Immunol.* **6**, 1–33 (2021).

241. DuPage, M., Dooley, A. L. & Jacks, T. Conditional mouse lung cancer models using adenoviral or lentiviral delivery of Cre recombinase. *Nat Protoc* **4**, 1064–1072 (2009).

242. Lee, J. H. *et al.* Transcriptional downregulation of MHC class I and melanoma de-differentiation in resistance to PD-1 inhibition. *Nat. Commun. 2020 111* **11**, 1–12 (2020).

243. Hildner, K. *et al.* Batf3 deficiency reveals a critical role for CD8α+ dendritic cells in cytotoxic T cell immunity. *Science (80-.).* **322**, 1097–1100 (2008).

244. Spranger, S., Bao, R. & Gajewski, T. F. Melanoma-intrinsic β-catenin signalling prevents anti-tumour immunity. *Nature* **523**, 231–235 (2015).

245. Germano, G., Amirouchene-Angelozzi, N., Rospo, G. & Bardelli, A. The clinical impact of the genomic landscape of mismatch repair–deficient cancers. *Cancer Discov.* **8**, 1518–1528 (2018).

246. Diamond, M. S., Lin, J. H. & Vonderheide, R. H. Site-dependent immune escape due to impaired dendritic cell cross-priming. *Cancer Immunol. Res.* **9**, 877–890 (2021).

247. Westcott, P. M. K. *et al.* Low neoantigen expression and poor T-cell priming underlie early immune escape in colorectal cancer. *Nat. cancer* **2**, 1071–1085 (2021).

248. Siddiqui, I. *et al.* Intratumoral Tcf1 + PD-1 + CD8 + T Cells with Stem-like Properties Promote Tumor Control in Response to Vaccination and Checkpoint Blockade Immunotherapy. *Immunity* **50**, 195-211.e10 (2019).

249. Conejero, L. *et al.* Lung CD103+ dendritic cells restrain allergic airway inflammation through IL-12 production. *JCI Insight* **2**, (2017).

250. Mikami, N. *et al.* Calcitonin gene-related peptide regulates type IV hypersensitivity through dendritic cell functions. *PLoS One* **9**, (2014).

251. Savina, A. *et al.* The small GTPase Rac2 controls phagosomal alkalinization and antigen crosspresentation selectively in CD8(+) dendritic cells. *Immunity* **30**, 544–555 (2009).

252. Rousseau, B. *et al.* The Spectrum of Benefit from Checkpoint Blockade in Hypermutated Tumors. *N. Engl. J. Med.* **384**, 1168–1170 (2021).

253. Marabelle, A. *et al.* Association of tumour mutational burden with outcomes in patients with advanced solid tumours treated with pembrolizumab: prospective biomarker analysis of the multicohort, open-label, phase 2 KEYNOTE-158 study. *Lancet Oncol.* **21**, 1353–1365 (2020).

254. Samstein, R. M. *et al.* Tumor mutational load predicts survival after immunotherapy

across multiple cancer types. *Nat. Genet.* **51**, 202–206 (2019).

255. Peng, D. H. *et al.* Collagen promotes anti-PD-1/PD-L1 resistance in cancer through LAIR1-dependent CD8+ T cell exhaustion. *Nat. Commun.* **11**, 1–18 (2020).

256. Zhang, M. *et al.* CCL7 recruits cDC1 to promote antitumor immunity and facilitate checkpoint immunotherapy to non-small cell lung cancer. *Nat. Commun.* **11**, 1–17 (2020).

257. Mandal, R. *et al.* Genetic diversity of tumors with mismatch repair deficiency influences anti-PD-1 immunotherapy response. *Science (80-.).* **364**, 485–491 (2019).

258. Burger, M. L. *et al.* Antigen dominance hierarchies shape TCF1+ progenitor CD8 T cell phenotypes in tumors. *Cell* **184**, 4996-5014.e26 (2021).

259. Fessenden, T. B. *et al.* Dendritic cell- - mediated cross presentation of tumor- - derived peptides is biased against plasma membrane proteins. 1–18 (2022). doi:10.1136/jitc-2021-004159

260. Pagès, F. *et al.* In situ cytotoxic and memory T cells predict outcome in patients with early-stage colorectal cancer. *J. Clin. Oncol.* **27**, 5944–5951 (2009).

261. Joshi, N. S. *et al.* Regulatory T Cells in Tumor-Associated Tertiary Lymphoid Structures Suppress Anti-tumor T Cell Responses. *Immunity* **43**, 579–590 (2015).

262. Li, S. *et al.* Characterization of neoantigen-specific T cells in cancer resistant to immune checkpoint therapies. *Proc. Natl. Acad. Sci. U. S. A.* **118**, 1–10 (2021).

263. Williford, J. M. *et al.* Recruitment of CD103+ dendritic cells via tumor-targeted chemokine delivery enhances efficacy of checkpoint inhibitor immunotherapy. *Sci. Adv.* **5**, (2019).

264. Robertson, M. J. Role of chemokines in the biology of natural killer cells. *J. Leukoc. Biol.* **71**, 173–183 (2002).

265. Barry, K. C. *et al.* A natural killer-dendritic cell axis defines checkpoint therapy-responsive tumor microenvironments. *Nat. Med.* **24**, 1178–1191 (2018).

266. McLaughlin, M. *et al.* Inflammatory microenvironment remodelling by tumour cells after radiotherapy. *Nat. Rev. Cancer 2020 204* **20**, 203–217 (2020).

267. Dovedi, S. J. *et al.* Fractionated Radiation Therapy Stimulates Antitumor Immunity Mediated by Both Resident and Infiltrating Polyclonal T-cell Populations when Combined with PD-1 Blockade. *Clin. Cancer Res.* **23**, 5514–5526 (2017).

268. Ohta, T. *et al.* Crucial roles of XCR1-expressing dendritic cells and the XCR1-XCL1 chemokine axis in intestinal immune homeostasis. *Sci. Reports 2016 61* **6**, 1–11 (2016).

269. Alspach, E. *et al.* MHC-II neoantigens shape tumour immunity and response to immunotherapy. *Nat. 2019 5747780* **574**, 696–701 (2019).

270. Cabeza-Cabrerizo, M. *et al.* Tissue clonality of dendritic cell subsets and emergency DCpoiesis revealed by multicolor fate mapping of DC progenitors. *Sci. Immunol.* **4**, (2019).

271. Dähling, S. *et al.* Type 1 conventional dendritic cells maintain and guide the differentiation of precursors of exhausted T cells in distinct cellular niches. *Immunity* **55**, 656-670.e8 (2022).

272. Melaiu, O., Lucarini, V., Cifaldi, L. & Fruci, D. Influence of the Tumor Microenvironment on NK Cell Function in Solid Tumors. *Front. Immunol.* **10**, 3038 (2020).

273. Li, H. *et al.* AXL targeting restores PD-1 blockade sensitivity of STK11/LKB1 mutant NSCLC through expansion of TCF1+ CD8 T cells. *Cell Reports Med.* **3**, (2022).

274. Raker, V. K., Domogalla, M. P. & Steinbrink, K. Tolerogenic Dendritic Cells for Regulatory T Cell Induction in Man. *Front. Immunol.* **6**, (2015).

275. Lelouard, H. *et al.* Regulation of translation is required for dendritic cell function and survival during activation. *J. Cell Biol.* **179**, 1427–1439 (2007).

276. de Lima Thomaz, L. *et al.* The impact of metabolic reprogramming on dendritic cell function. *Int. Immunopharmacol.* **63**, 84–93 (2018).

277. Wculek, S. K., Khouili, S. C., Priego, E., Heras-Murillo, I. & Sancho, D. Metabolic Control of Dendritic Cell Functions: Digesting Information. *Front. Immunol.* **10**, 775 (2019).

278. Zhu, J. & Thompson, C. B. Metabolic regulation of cell growth and proliferation. *Nat. Rev. Mol. Cell Biol. 2019 207* **20**, 436–450 (2019).

279. Jin, C. *et al.* Commensal Microbiota Promote Lung Cancer Development via γδ T Cells. *Cell* **176**, 998-1013.e16 (2019).

280. Wherry, E. J. *et al.* Molecular signature of CD8+ T cell exhaustion during chronic viral infection. *Immunity* **27**, 670–684 (2007).